CHALMERS
UNIVERSITY OF TECHNOLOGY

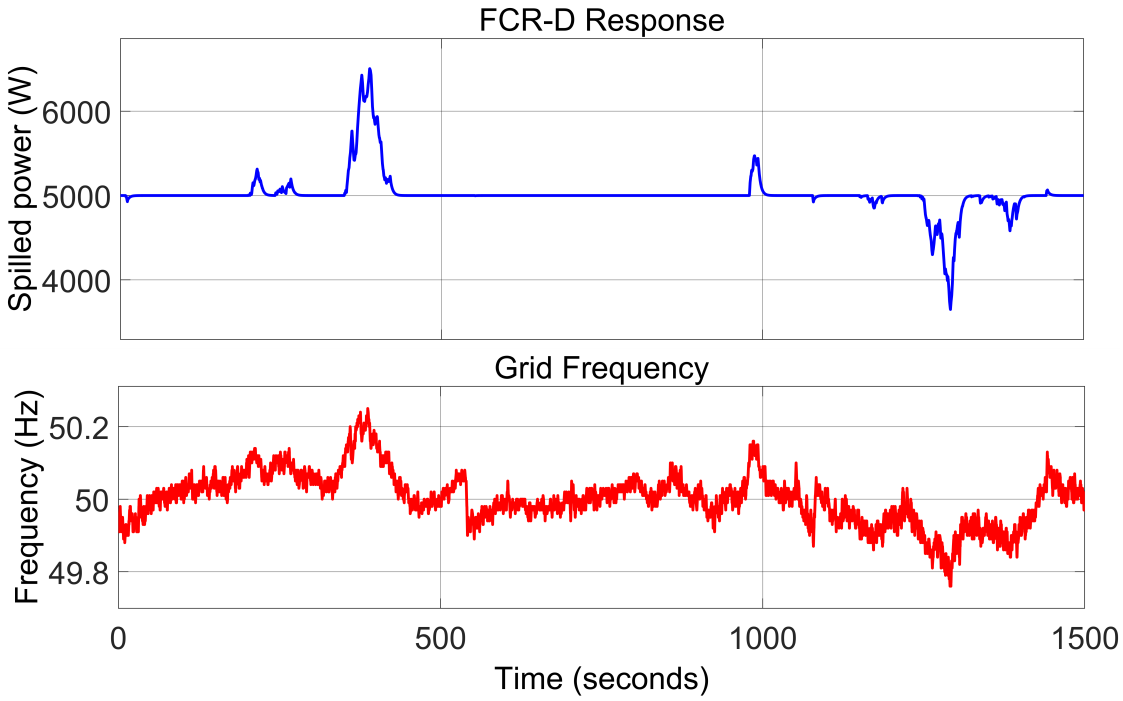

Evaluation of Ancillary Services from Wind Turbines

A study on frequency control and FCR-D Down response

Master's thesis in Sustainable Electric Power Engineering and Electromobility

Kristoffer Olsson, Nowroz Bin Nasim

DEPARTMENT OF ELECTRICAL ENGINEERING

CHALMERS UNIVERSITY OF TECHNOLOGY
Gothenburg, Sweden 2025
www.chalmers.se

Master's thesis 2025

Evaluation of Ancillary Services from Wind Turbines

A study on frequency control and FCR-D Down response

Kristoffer Olsson
Nowroz Bin Nasim

CHALMERS
UNIVERSITY OF TECHNOLOGY

Department of Electrical Engineering
Chalmers University of Technology
Gothenburg, Sweden 2025

Evaluation of Ancillary Services from Wind Turbines:
A study on frequency control and FCR-D Down response
Kristoffer Olsson, Nowroz Bin Nasim

Supervisor: Sara Fogelström, Department of Electrical Engineering
Examiner: Ola Carlson, Department of Electrical Engineering

Master's Thesis 2025
Department of Electrical Engineering
Chalmers University of Technology
SE-412 96 Gothenburg
Telephone +46 31 772 1000

Cover: Example of simulated FCR-D Down response from the Chalmers wind turbine model during a grid frequency event.

Typeset in LaTeX
Gothenburg, Sweden 2025

Evaluation of Ancillary Services from Wind Turbines:
A study on frequency control and FCR-D Down response

Kristoffer Olsson, Nowroz Bin Nasim
Department of Electrical Engineering
Chalmers University of Technology

Abstract

There is currently limited guidance on evaluating the performance of wind turbines in delivering ancillary services based on measured operational data. This thesis presents an evaluation method that uses grid frequency variations to estimate droop and ramp rate without relying on the predefined step signals used in Svenska kraftnät's prequalification process. The method is applied to a simulation of the Chalmers wind turbine and to measured data from a commercial wind farm, with a focus on FCR-D Down. Two days with different operating conditions were analyzed using the same evaluation procedure. The study examines power response, droop, ramp rate, and how well the response matched the accepted regulation bids. The results show that the commercial wind farm responded faster and with a stronger droop than the simulated turbine, which served as a reference model for Svk's minimum performance requirements. The proposed method can support further evaluation of frequency control from wind farms and assist wind farm operators in selecting turbines suitable for frequency regulation.

Keywords: wind turbine, frequency control, FCR-D Down, ancillary services, droop, ramp rate, spilled power.

Acknowledgements

We would like to thank our supervisor Sara Fogelström and our examiner Ola Carlson for their guidance and support throughout this thesis. Sara's help in coordinating communication with external contacts and making sure things moved forward smoothly was especially appreciated.

We are also grateful to SR Energy for giving us access to data from the Kronoberget wind farm. This made it possible for us to carry out the evaluation and comparisons in the study.

Finally, we want to thank everyone who supported us during this project.

Kristoffer Olsson & Nowroz Bin Nasim, Gothenburg, June 2025

List of Acronyms

Below is the list of acronyms that have been used throughout this thesis listed in alphabetical order:

AGC	Automatic Generation Control
aFRR	Automatic Frequency Restoration Reserve
BSP	Balancing Service Provider
ENTSO-E	European Network of Transmission System Operators for Electricity
FCR-D	Frequency Containment Reserve-Disturbances
FCR-N	Frequency Containment Reserve-Normal
FFR	Fast Frequency Reserve
FRR	Frequency Restoration Reserves
MPPT	Maximum Power Point Tracking
mFRR	Manual Frequency Restoration Reserve
NREL	National Renewable Energy Laboratory
PD	Proportional–derivative
RoCoF	Rate of Change of Frequency
Svk	Svenska kraftnät
TSO	Transmission System Operator
WTG	Wind Turbine Generator

Nomenclature

Below is the nomenclature of parameters that have been used throughout this thesis.

Parameters

ρ	Air density [kg/m^3]
A	Swept rotor area [m^2]
C_p	Power coefficient [–]
v_{wind}	Wind speed [m/s]
R_{rotor}	Rotor radius [m]
ω_{mech}	Mechanical rotational speed [rad/s]
J	Moment of inertia [kg·m^2]
b	Damping (or friction) factor [N·m·s]
η	Efficiency [–]
λ	Tip-speed ratio [–]
v_{tip}	Blade tip speed [m/s]
β	Blade pitch angle [°]
P_{mech}	Extracted mechanical power [W]
τ_{mech}	Mechanical torque [N·m]
τ_{elec}	Electrical torque [N·m]
ω_{elec}	Rotational speed of the generator [rad/s]
P_{elec}	Electrical power output [W]
N	Gearbox ratio [–]
R_{droop}	Droop constant [kW/Hz or %]
f_{nominal}	Nominal frequency [Hz]
P_{nominal}	Nominal power output [W]
f	Actual grid frequency [Hz]
Δf	Frequency deviation [Hz]
P	Active power output [W]
T	Air temperature [°C]
P_{sat}	Saturation vapor pressure [Pa]
P_v	Vapor pressure [Pa]
P_d	Dry air pressure [Pa]
R_d	Specific gas constant for dry air [J/kg·K]
R_v	Specific gas constant for water vapor [J/kg·K]
RH	Relative humidity [%]

P_{spill}	Spilled power [W]
$P_{\text{max,sim}}$	Maximum simulated spilled power [W]
P_{bid}	Accepted regulation bid [W]
P_{baseline}	Baseline spilled power [W]
$P_{\text{spill,norm}}$	Normalized spilled power [–]
$P_{\text{Svk,norm}}$	Normalized expected power response based on Svk requirements [–]

Contents

List of Figures

1 Introduction

The Swedish power grid operates at a standard frequency of 50 Hz, which must be maintained to ensure reliability and prevent blackouts. Since frequency depends on the balance between electricity supply and demand, any imbalance increases the risk of instability in the system [1]. Svenska kraftnät (Svk), the Swedish transmission system operator, is responsible for keeping this balance and acquires ancillary services to stabilize frequency during normal operations and disturbances. Historically, Sweden has relied on hydropower and large synchronous machines for frequency regulation [2], with hydropower being especially effective because it can rapidly adjust its output. However, the growing share of wind power, which is weather-dependent and variable, creates new opportunities and challenges for maintaining frequency stability.

By the end of 2024, wind turbines in Sweden were generating 40 TWh annually [3]. In the same year, wind power accounted for 35% of Sweden's electricity in December, surpassing hydro and nuclear for the first time [4]. This milestone highlights wind power's increasing role in the Swedish electricity system and its ability to replace traditional energy sources. Projections for 2027 indicate a rise to 19.3 GW of capacity and 55.1 TWh of annual generation [5]. As wind power makes up a larger share of electricity production, its variability means wind turbines need to play a more active role in frequency regulation. Allowing wind turbines to support frequency control is important for maintaining a stable and reliable power system as Sweden continues its transition to renewable energy.

This thesis builds on earlier work at Chalmers University of Technology, where control strategies such as synthetic inertia and de-loading were implemented and tested both in simulation and on Chalmers wind turbine [6,7]. These studies demonstrated that the turbine is capable of providing frequency support and also confirmed that the simulation model accurately reflects turbine behavior under rated operating conditions. Building on that work, this project focuses on evaluating frequency control performance using simulations of Chalmers wind turbine and measured data from a commercial wind farm to better understand their contribution to ancillary services in practice.

1.1 Aim

The aim of this thesis is to evaluate the performance of wind turbines in providing frequency control by comparing simulated and measured responses using measured operational data. The study focuses on Frequency Containment Reserve for Disturbances Down (FCR-D Down), using a simulation of Chalmers wind turbine with a defined controller and measured data from a commercial wind farm with unknown control strategies.

1.2 Problem statement

Even though wind turbines can technically support frequency control, it is not clear how well they perform under real operating conditions. Differences in control strategies and turbine designs make it difficult to compare their ability to deliver frequency control services. A structured evaluation method is needed to better understand

their performance and to support wind farm owners in selecting turbines that are suitable for frequency control.

1.3 Scope and limitations

This thesis focuses on evaluating frequency control from wind turbines using both simulation and measurement data. Chalmers wind turbine is evaluated through simulation for all three services within Frequency Containment Reserve: Normal (FCR-N), Disturbance Up (FCR-D Up), and Disturbance Down (FCR-D Down), including a combined control mode. The commercial wind farm, on the other hand, is only prequalified to provide FCR-D Down, which limits the comparison to that service.

The evaluation of Chalmers wind turbine is based on simulations at rated power only. This is due to an issue that affects the model's performance at medium wind speeds. Although the exact cause is unclear, it introduces uncertainty in the simulation results. To ensure reliable evaluation, only the rated operating range is used. Previous studies have shown that the model closely matches measured responses under these conditions, which supports its use for this analysis.

The commercial data is limited to one wind farm, representing a single turbine manufacturer. This allows for a comparison between Chalmers wind turbine and one commercial turbine type, but it does not provide a basis for comparing performance across different commercial manufacturers.

Economic aspects such as market participation, bidding strategies, and penalties for non-delivery are mentioned but not analyzed in detail. The focus of the thesis remains on the technical performance and frequency response characteristics.

1.4 Social and ethical aspects

Wind energy brings many benefits but also raises social and ethical questions. These include its effects on society, the environment, and how to balance its advantages with potential challenges. Addressing these issues is important for a fair and sustainable energy future.

1.4.1 Impact on Society

The expansion of wind energy has led to societal debate, with concerns raised about issues such as noise pollution, visual impact, land use, and potential effects on tourism [8]. Despite these challenges, replacing fossil-fuel generators with wind turbines delivers significant environmental advantages, including zero carbon emissions and promoting a sustainable energy transition. Integrating wind turbines into ancillary services further reduces dependence on non-renewable energy sources, which enhances the reliability of renewable energy systems, advances energy justice, and ensures fair energy access. This benefits society as a whole, including remote and disadvantaged areas [9].

1.4.2 Ecological impact

Wind turbines can affect birds, bats, and fish due to their placement. Birds, especially fowls and birds of prey, are at risk of collisions with rotor blades or towers

when turbines are near areas they use, like nesting or feeding spots [10]. To reduce these risks, creating buffers around nests can help protect bird populations. Bats are also affected because they are attracted to insects, which in turn are drawn to the heat generated by the turbines [10]. Collisions are more likely during certain seasons, and turning off turbines during high-risk periods can reduce the impact.

Fish are mainly affected during turbine construction, which can disrupt their habitats. These effects can be reduced by carefully planning construction times and by utilizing turbine foundations to create artificial reefs or protected areas that support marine life [11].

1.5 Thesis outline

Section 1 – Introduction: Outlines the purpose of the thesis, the motivation behind it, and the problem being addressed.

Section 2 – Theory: Explains the theoretical foundation of frequency control and wind turbine operation, along with an overview of the simulation model used in the study.

Section 3 – Data collection and processing: Describes the measurement data used for evaluation and the processing steps applied to both simulation and measurement data.

Section 4 – Methodology: Presents the structure of the evaluation method, how frequency events were selected, and how droop and ramp rate were estimated.

Section 5 – Results: Shows the evaluation outcomes for the Chalmers wind turbine model and the commercial wind farm, including plots of spilled power, droop, and ramp rate.

Section 6 – Discussion: Interprets the results in relation to control strategies, operating conditions, and limitations of the evaluation method. Suggestions for future work are also included.

Section 7 – Conclusion: Summarizes the main findings and reflects on the potential use of the method for evaluating wind turbines providing frequency control.

2 Theory

To support the evaluation of wind turbine performance in frequency control, this section presents the theoretical background for frequency regulation and the role of wind turbines in providing ancillary services. It begins with the structure of frequency regulation in the Nordic grid, followed by fundamental wind power theory and control strategies such as de-loading, synthetic inertia, and droop control. The estimation of available power is also discussed, as it is essential for accurate control and market participation. The section concludes with an overview of Chalmers wind turbine and its simulation model, which forms the basis for the evaluation.

2.1 Frequency control in power systems

Maintaining a stable frequency is one of the key challenges in the power system. In the Nordic region, the system frequency is standardized at 50 Hz. Deviations from this value can disturb the balance between power generation and consumption, leading to instability and potential equipment damage [1]. If these deviations become significant, they may cause equipment malfunctions, power outages, or other disturbances that impact the operation of the power grid [12].

In Sweden, Svenska kraftnät, the transmission system operator, is responsible for maintaining the frequency at the standardized value with the support of ancillary services provided by Balancing Service Providers (BSPs) [13, 14]. To provide these services, BSPs submit bids to the market, offering capacity for frequency regulation. These bids specify the amount of power they are willing to offer and at what price. Svenska kraftnät then selects bids based on price and volume, securing the required reserves through contracts. This ensures that a specific amount of power is available for ancillary services when needed. In return, BSPs are compensated for their contributions.

By continuously balancing active power generation and consumption in real-time, Svenska kraftnät works to prevent significant frequency deviations. To achieve this, power systems rely on different levels of frequency control, each designed to regulate frequency by adjusting generation and consumption in response to changing load conditions [15]. These control mechanisms help limit frequency deviations that could lead to cascading failures or blackouts [16].

2.1.1 Fundamentals of frequency stability

Frequency stability in the power system is managed through a hierarchy of control mechanisms. Figure 2.1 shows the structure of the frequency control hierarchy used in the power system.

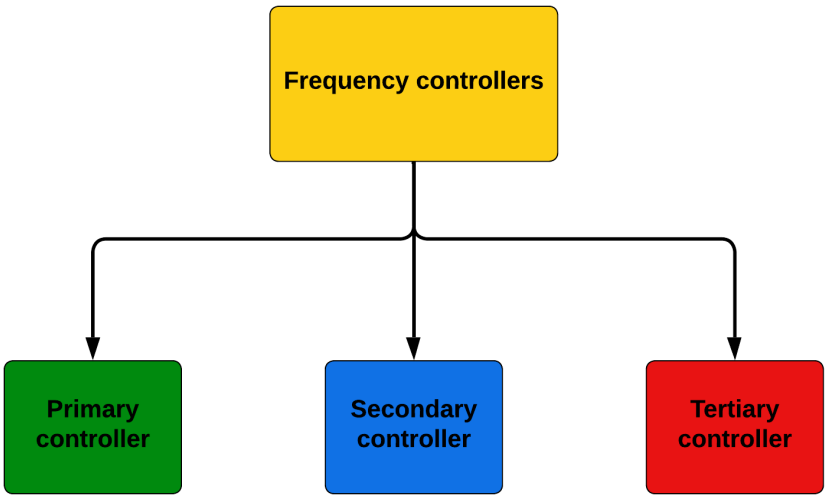

Figure 2.1: Hierarchy of frequency controllers in the power system.

As shown in Figure 2.1, the frequency controllers are divided into three levels: primary, secondary, and tertiary. Each controller has a specific function in regulating frequency [17]:

- **Primary controller:** The primary controller reacts quickly to counteract initial frequency deviations. It adjusts the active power output of generators within seconds to limit the deviation and keep the frequency within an acceptable range.
- **Secondary controller:** The secondary controller restores the frequency to its nominal value by correcting any remaining imbalance in the system. It operates over a longer timeframe than the primary controller and ensures that power generation matches consumption more accurately.
- **Tertiary controller:** The tertiary controller manages larger disturbances by reallocating power generation and adjusting reserves. It provides additional flexibility to maintain balance under changing system conditions.

2.1.2 Ancillary services for frequency regulation

Ancillary services used by Svk are employed to manage frequency deviations and maintain system balance. They provide the reserves required by the primary, secondary, and tertiary controllers to handle disturbances. Figure 2.2 shows the classification of these services.

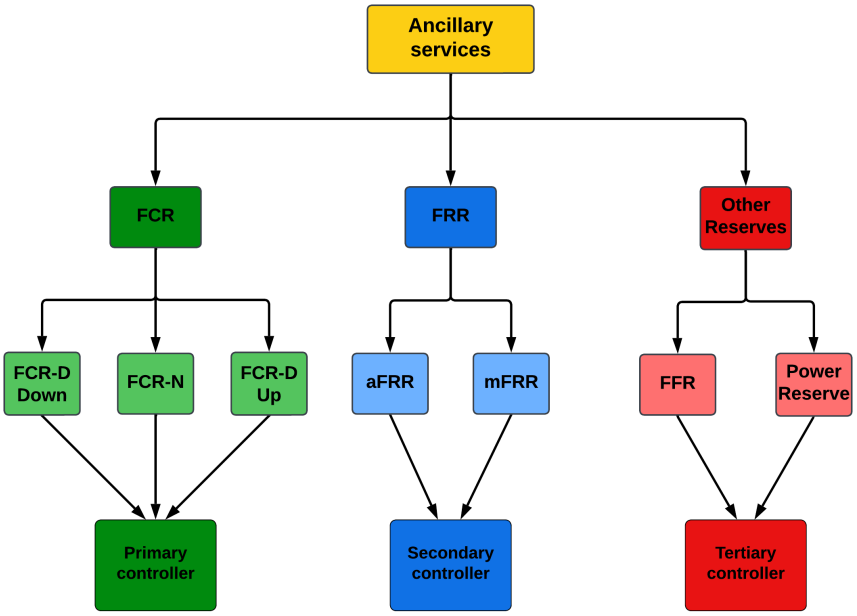

Figure 2.2: Overview of ancillary services in the Nordic power system.

As shown in Figure 2.2, ancillary services are divided into Frequency Containment Reserves (FCR), Frequency Restoration Reserves (FRR), and other reserves such as Fast Frequency Reserve (FFR) and power reserve [18]. These services support frequency regulation under different operating conditions. The activation times and specific roles of these services are defined by Svenska kraftnät and ENTSO-E and are explained in the following specifications [18, 19]:

Frequency Containment Reserve Normal (FCR-N) operates continuously to keep the frequency within the normal range of 49.90–50.10 Hz. It is linearly activated within this range, and it must activate 63% of its capacity within 60 seconds and 95% within 180 seconds. The minimum bid size is 0.1 MW.

Frequency Containment Reserve Disturbance Up (FCR-D Up) is activated when the frequency drops below 49.90 Hz. It is linearly activated within the range of 49.50–49.90 Hz, and it must reach 86% activation within 7.5 seconds and full activation within 30 seconds. The minimum bid size is 0.1 MW.

Frequency Containment Reserve Disturbance Down (FCR-D Down) is activated when the frequency exceeds 50.10 Hz. It is linearly activated within the range of 50.10–50.50 Hz, following the same activation profile as FCR-D Up, requiring 86% activation within 7.5 seconds and full activation within 30 seconds. The minimum bid size is 0.1 MW.

Automatic Frequency Restoration Reserve (aFRR) is automatically activated to restore system balance after FCR activation and to bring the frequency back toward 50.00 Hz. It must be fully activated within 5 minutes, with a minimum bid size of 1 MW.

Manual Frequency Restoration Reserve (mFRR) is manually activated to restore balance after larger disturbances. It must be fully activated within 15 minutes

and maintained for 1 hour, with a minimum bid size of 1 MW.

Fast Frequency Reserve (FFR) is a fast-acting reserve designed to address sudden frequency drops, particularly in low-inertia situations. It is triggered at 49.7 Hz or below and must reach full activation within:

- 0.7 seconds at 49.5 Hz
- 1.0 second at 49.6 Hz
- 1.3 seconds at 49.7 Hz

The duration of activation varies between 5 and 30 seconds. The minimum bid size is 0.1 MW.

Power Reserve is utilized to manage significant imbalances that cannot be corrected by other reserves. It is primarily activated during severe system disturbances or when other reserves have been depleted. Specific parameters such as activation times and minimum bid sizes are determined by Svenska kraftnät based on system needs.

Table 2.1 summarizes the ancillary services used for frequency regulation. Power Reserve is excluded, as it is only activated in exceptional cases when other reserves are insufficient.

Table 2.1: Activation characteristics of Nordic ancillary services.

Service	Activation Time	Endurance	Frequency Range	Min. Bid
FCR-N	63% in 60s 95% in 180s	1 hour	49.90 – 50.10 Hz	0.1 MW
FCR-D Up	86% in 7.5s 100% in 30s	20 min	49.50 - 49.90 Hz	0.1 MW
FCR-D Down	86% in 7.5s 100% in 30s	20 min	50.10 - 50.50 Hz	0.1 MW
aFRR	100% in 5 min	1 hour	N/A	1 MW
mFRR	100% in 15 min	1 hour	N/A	1 MW
FFR	100% in: 0.7s at 49.5 Hz 1.0s at 49.6 Hz 1.3s at 49.7 Hz	5 or 30 sec	N/A	1 MW

2.2 Fundamentals of wind turbine energy conversion

Wind turbines convert the energy in moving air into mechanical rotation, which drives a generator to produce electricity. As the wind flows through the rotor, the blades extract energy by slowing down the air and creating a rotational force on the hub [20]. The amount of mechanical power that can be extracted depends on several factors, including wind speed, rotor size, and aerodynamic efficiency. The fundamental power equation, shown in equation 2.1, expresses the extracted mechanical power as

$$P_{\text{mech}} = \frac{1}{2}\rho A C_p v_{\text{wind}}^3 \tag{2.1}$$

where ρ is the air density, A is the swept rotor area, v_{wind} is the wind speed, and C_p is the power coefficient. The value of C_p depends on the blade pitch angle β and the tip-speed ratio λ, which is defined in equation 2.2 as

$$\lambda = \frac{v_{\text{tip}}}{v_{\text{wind}}} = \frac{R_{rotor} \cdot \omega_{\text{mech}}}{v_{\text{wind}}} \tag{2.2}$$

where v_{tip} is the blade tip speed, R_{rotor} is the rotor radius, and ω_{mech} is the mechanical rotational speed of the turbine [20].

According to Betz's law, the theoretical upper limit for C_p is about 0.59, meaning that no wind turbine can extract more than 59% of the available wind energy, even under ideal conditions [20, 21]. In practice, various limitations such as aerodynamic losses, mechanical constraints, and system inefficiencies prevent turbines from reaching this limit, with typical values of C_p ranging between 0.35 and 0.45.

As the extracted mechanical power drives the rotation of the turbine, it is useful to express it in terms of torque. The mechanical torque transmitted through the rotor shaft depends on the extracted power and is given by

$$\tau_{\text{mech}} = \frac{P_{\text{mech}}}{\omega_{\text{mech}}} \tag{2.3}$$

Since P_{mech} is proportional to the power coefficient C_p, the torque is also influenced by C_p. To illustrate how C_p varies with λ and β, Figure 2.3 shows the power coefficient distribution for Chalmers wind turbine, highlighting the operating regions that maximize energy capture from the wind.

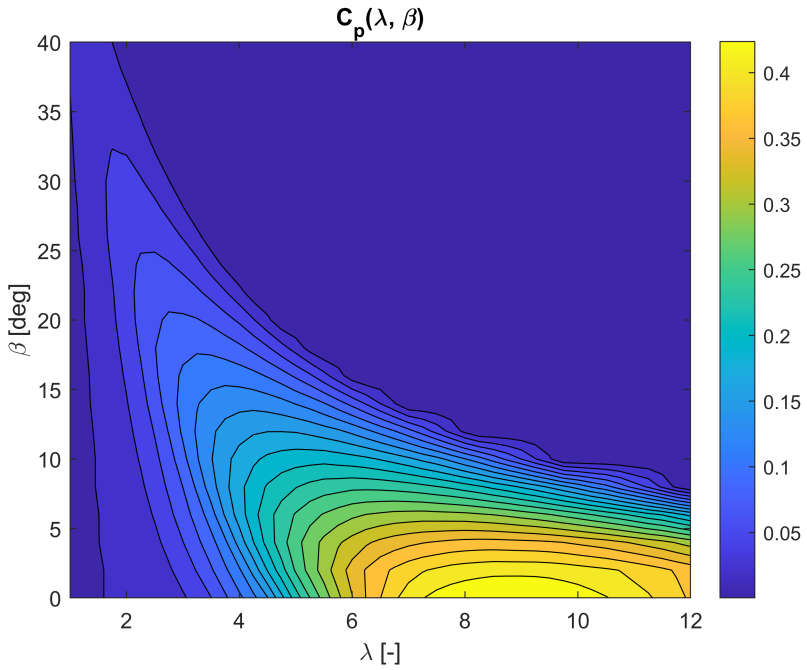

Figure 2.3: Contour plot of C_p for Chalmers wind turbine as a function of λ and β.

It can be seen that the highest values of C_p occur when λ is between approximately 8 and 10, with the pitch angle β at 0°. As β increases, C_p drops significantly, meaning

that to maximize power extraction, the pitch angle should remain low for higher λ. This indicates there is an optimal λ where C_p reaches its peak, leading to the most efficient turbine operation.

Equation 2.2 shows that the tip-speed ratio λ is determined by both the wind speed and the turbine's rotational speed ω_{mech}. To maintain the optimal λ, the rotational speed must continuously adjust. This is achieved by regulating the electrical torque, which counteracts the mechanical torque and controls the turbine's speed [22].

The generator converts mechanical power into electrical power with an efficiency η, giving the electrical power output as

$$P_{\text{elec}} = \eta \cdot P_{\text{mech}} \tag{2.4}$$

Using the relation $P = \tau \cdot \omega$, the electrical torque is expressed as

$$\tau_{\text{elec}} = \frac{\eta \cdot P_{\text{mech}}}{\omega_{\text{elec}}} \tag{2.5}$$

where ω_{elec} is the rotational speed of the generator.

Since the generator's torque opposes the motion of the turbine rotor, its acceleration is determined by the balance between mechanical and electrical torques. This relationship is governed by the equation of motion:

$$J\frac{d\omega}{dt} = \tau_{\text{mech}} - \tau_{\text{elec}} - b\,\omega \tag{2.6}$$

where J is the moment of inertia of the rotating system, and b is a damping (or friction) factor [22].

If a gearbox is used, the relation between the mechanical and electrical rotational speeds is

$$\omega_{\text{elec}} = N \cdot \omega_{\text{mech}} \tag{2.7}$$

where N is the gearbox ratio, relating the turbine and generator speeds.

2.3 Frequency support strategies in wind turbines

As the share of renewable energy in power systems increases, maintaining grid frequency stability becomes progressively more challenging [23]. Unlike conventional power plants, which naturally provide inertia through rotating masses, wind turbines rely on power electronic converters, meaning their inertia does not directly influence system frequency. As a result, alternative control strategies are required to help preserve grid stability. Given that wind power is expected to become a major contributor to Sweden's electricity grid, improving its ability to participate in frequency regulation is an important step [5].

To support grid frequency, wind turbines can employ different control strategies. These include de-loading/de-rating (also referred to as spilling power), where turbines operate below their rated power to maintain a reserve; synthetic inertia, which mimics the inertial response of conventional generators; and droop control, which regulates power output proportionally to frequency deviations. Droop control is often used together with de-loading to enhance frequency regulation [24, 25]. Each

of these methods supports frequency stability differently, with their effectiveness depending on factors such as wind availability, system conditions, and control implementation.

The following sections describe these frequency support strategies, focusing on their principles and role in grid frequency regulation.

2.3.1 De-loading power method

Wind turbines are typically designed to operate at maximum efficiency, capturing as much wind energy as possible. However, in power systems with a high share of renewables, the ability to adjust power output is necessary for grid stability [24]. While wind turbines cannot store energy in the same way that conventional power plants can, they can still participate in frequency regulation by operating below their maximum capacity. This technique, known as de-loading, creates a power reserve that can be utilized when needed [24].

One way to achieve de-loading is by adjusting the pitch angle of the turbine blades, which controls how much wind energy is converted into power output [26]. Under normal conditions, the blades are positioned to maximize energy capture. When wind speed exceeds the rated level, the pitch angle is increased to keep the turbine output constant and prevent it from exceeding its rated power. In de-loading mode, the pitch angle is instead increased already below rated wind speed, reducing aerodynamic efficiency and limiting power output to keep reserve capacity available for potential disturbances [26]. When the grid frequency drops, the control system responds by decreasing the pitch angle, allowing the turbine to generate additional power up to the maximum available and help stabilize the grid. Conversely, if the frequency rises above nominal, the pitch angle is further increased to reduce power output and avoid excessive generation.

A de-loaded turbine can provide FCR-N, FCR-D Up, and FCR-D Down, but a power reserve is primarily needed for up-regulation, as wind turbines cannot increase power beyond their available power. De-loading ensures they have additional capacity to respond quickly when frequency drops [26]. In contrast, down-regulation in FCR-D Down only requires reducing power, which can be done directly without the need for a reserve.

Figure 2.4 illustrates this method. The solid line represents normal operation, where the turbine maximizes wind power extraction, while the dotted line shows the de-loading curve. The difference between the curves, ΔP, represents the power reserve that can be utilized to increase generation when the frequency drops.

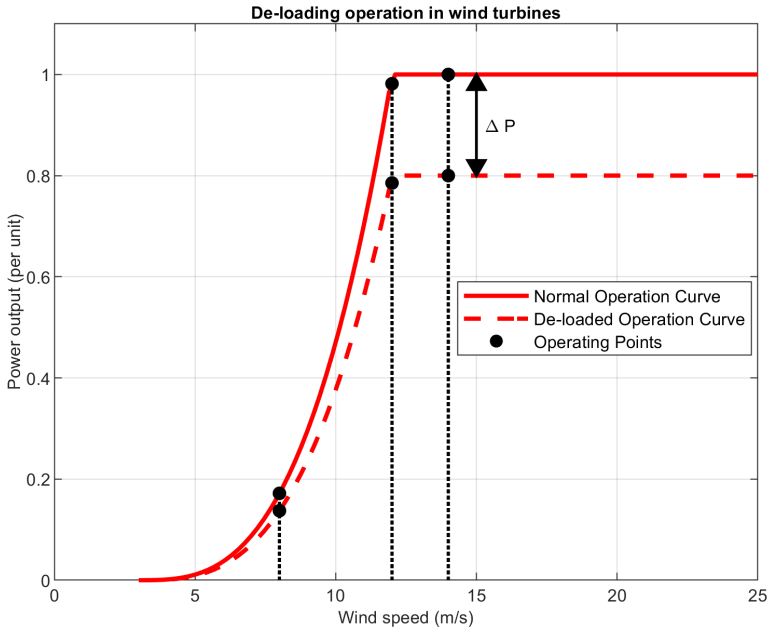

Figure 2.4: De-loading operation of a wind turbine, where ΔP indicates the reserved power capacity.

2.3.2 Synthetic inertia method

Conventional power plants provide inertia through the rotating mass of their generators, which helps resist sudden frequency fluctuations [27]. Wind turbines, on the other hand, are connected to the grid through power electronic converters, meaning their mechanical inertia does not directly influence the grid. To compensate for this, wind turbines can use synthetic inertia, which dynamically adjusts rotor speed in response to frequency variations [24, 27].

When the frequency drops, the control system reduces the generator torque, allowing the rotor to release stored kinetic energy as extra power [28]. Since the rotor has a large mass, it does not slow down immediately, so the excess energy is transferred to the grid during this time. When the frequency rises, the control system increases the generator torque, which slows the rotor down more quickly. This temporarily reduces power output and helps counteract the frequency rise.

By slowing down the rate of change of frequency (RoCoF), synthetic inertia contributes to grid stability. Unlike FCR, which adjusts power based on frequency deviations, synthetic inertia responds to the rate at which the frequency changes. It is not an ancillary service that can be bought or sold but rather a control strategy that can be implemented in wind turbines through power electronics. While synthetic inertia is not widely used today, it is being considered for future grid support as more converter-based generation is integrated [29].

Figure 2.5 illustrates its effect on frequency deviation, showing how different inertia levels impact the depth of frequency dips and recovery time. The frequency drop is modeled as an exponentially damped deviation from nominal frequency, triggered by a disturbance at $t = 1$ second. Lower inertia results in a higher RoCoF and a deeper frequency nadir, while higher inertia slows down frequency changes and

reduces the severity of the dip.

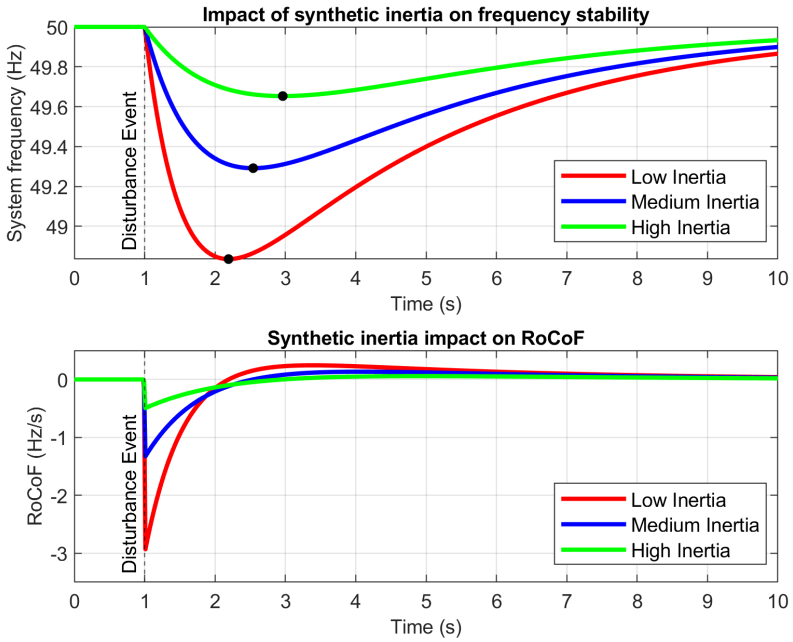

Figure 2.5: Effect of synthetic inertia on frequency stability and RoCoF. The nadir points, indicating the lowest frequency reached during a disturbance, are marked as black dots.

2.3.3 Droop control method

Droop control is a fundamental method used in power systems to regulate power output in response to frequency deviations. It adjusts the turbine's power output proportionally to changes in grid frequency, with the proportionality factor determined by the droop constant [25]. A lower droop constant gives a steeper slope, leading to more responsive power adjustments. Conversely, a higher droop constant results in a flatter slope, causing power output changes to be more gradual and providing weaker frequency regulation.

The relationship between power output and frequency deviation is given by:

$$P = P_{\text{nominal}} - \frac{1}{R_{droop}}(f - f_{\text{nominal}}) \tag{2.8}$$

where P is the active power output, P_{nominal} is the nominal power output, R_{droop} is the droop constant, f is the actual grid frequency, and f_{nominal} is the nominal frequency.

This approach is widely used in conventional power plants and is useful when multiple generators operate in parallel, such as in a wind farm [30]. By adjusting power output based on frequency changes, droop control distributes the regulation effort among all units, preventing any single turbine from handling too much of the adjustment. Since wind turbines do not provide natural inertia, droop control is often combined with other methods, such as de-loading, to support frequency regulation.

De-loading ensures that turbines maintain a power reserve, which droop control can utilize to adjust power output in response to frequency deviations when needed.

Figure 2.6 illustrates the droop control characteristics for FCR. The first subplot shows FCR-N, which is linearly activated between 49.9 Hz and 50.1 Hz and saturates outside this range, following a 10% droop characteristic. The second subplot shows FCR-D, which remains at zero between 49.9 Hz and 50.1 Hz but is linearly activated outside this interval, following a 5% droop characteristic. This separation is achieved by using a deadband and saturation in the frequency measurement. A deadband of $\pm$ 0.1 Hz ensures that only FCR-D is active outside this range, while saturation at 49.9 Hz and 50.1 Hz ensures that only FCR-N is delivered within it. The final subplot shows the combined response, where both techniques are used together to provide a frequency-dependent power adjustment across the entire range.

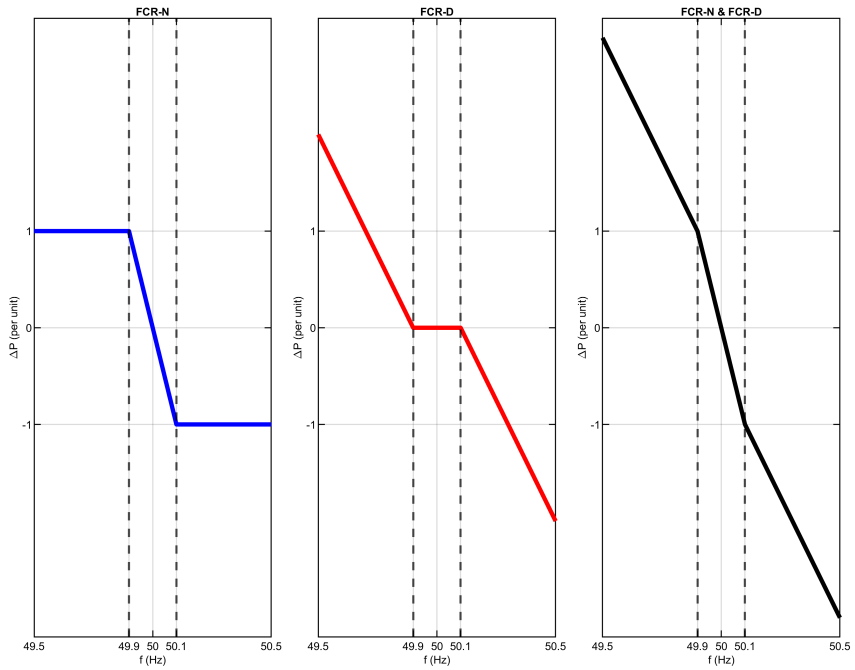

Figure 2.6: Droop control characteristics for FCR-N, FCR-D and their combined response.

2.4 Estimation of available power

Estimating available power is important for wind turbines providing frequency control. Since wind conditions vary, turbines need a way to determine how much power they can deliver at any time. Accurate estimation helps prevent situations where the turbine either fails to provide the expected response or does not fully utilize its potential.

2.4.1 Impact on frequency regulation

Available power affects how a wind turbine responds to frequency deviations. When frequency is low, the turbine increases power output, but this depends on how much wind energy is available. If power is overestimated, the turbine may not be able to deliver the required response, causing imbalances in the system [31]. When frequency

is high, the turbine reduces power output by curtailing generation. Inaccurate estimation can lead to unnecessary curtailment or failure to meet expected regulation performance.

Power estimation is especially important for de-loading operation, where the turbine runs below its maximum capacity to maintain a reserve for frequency support. Underestimating available power may cause the turbine to hold back capacity that could have been used for grid support, while overestimating can lead to a reserve that is larger than necessary, resulting in lower overall efficiency [32]. Accurate power estimation ensures that the turbine sets an appropriate reserve without limiting power output more than required.

2.4.2 Impact on market bidding

Wind farms participating in frequency control markets submit bids specifying the power they can provide in each time block, typically on an hourly basis. These bids represent an availability commitment rather than a continuous power output. When the transmission system operator activates the service, the wind farm must be able to deliver the offered capacity.

Figure 2.7 shows a day-ahead bidding schedule for Kronoberget wind farm on January 15, 2024. The bid curve follows a stepwise pattern, where each step represents the power capacity offered for a one-hour period. The bids shown here correspond to participation in FCR-D Down, where the wind farm commits to reducing its power output when the system frequency is between 50.1 and 50.5 Hz.

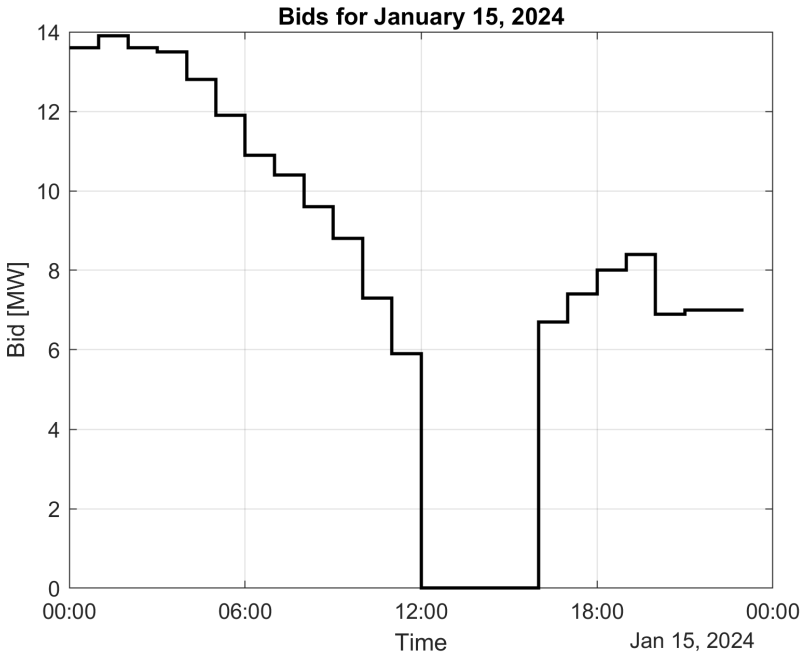

Figure 2.7: Day-ahead bidding schedule for Kronoberget wind farm on January 15, 2024, showing hourly capacity offers in MW for FCR-D Down participation.

If a wind farm fails to meet its commitment when activated, penalties or balancing costs may apply [33]. Overestimating available power can lead to under-delivery and

financial penalties, while underestimating reduces the reserve capacity offered, limiting potential revenue from ancillary services. To minimize these risks, wind farms use forecasting models to estimate power availability before bidding, as inaccurate forecasts can lead to either overcommitting or undercommitting reserves, both of which increase operational costs or result in lost revenue [32].

2.4.3 Estimation methods

The available power of a wind turbine can be estimated using different methods, ranging from simple lookup tables to more advanced filtering and forecasting techniques. These methods rely on turbine parameters, estimated wind conditions, or predictive models to determine how much power the turbine can generate at a given moment.

A challenge in power estimation is that nacelle wind speed measurements are often unreliable [34]. Anemometers are typically mounted on top of the nacelle behind the rotor, where the wind is disturbed by the rotating blades. This placement means they capture wind at a single, disturbed point behind the rotor and do not reflect how it varies across the full rotor area. These limitations introduce errors, especially in turbulent conditions or when wake effects are present. As a result, estimation methods need to account for how wind speed changes across the entire rotor to improve accuracy.

Several methods are commonly used to estimate available power:

Lookup tables based on the optimal tip-speed ratio: The relationship between the power coefficient, tip-speed ratio, and pitch angle is precomputed and stored in lookup tables. These tables are used to estimate the available power based on the wind speed and rotor speed. This method allows fast estimation with relatively low computational effort and has been used in several control strategies for wind turbines [35, 36]. Chalmers wind turbine uses a version of this method with a fixed pitch angle, where the optimal tip-speed ratio, predicted wind speed, and rotor radius are used to calculate an optimal rotor speed, which is then used to compute the tip-speed ratio and retrieve the power coefficient from a one-dimensional lookup table. The retrieved C_p is used together with the predicted wind speed in equation (2.1) to estimate the available mechanical power.

Mapping wind speed to the power curve: This approach calculates available power by applying historical wind speed data to the turbine's power curve, which defines expected output at different wind speeds. Because wind power is proportional to the cube of wind speed, even small errors can lead to significant deviations in the estimated power output [37].

Forecasting models: Historical wind data, weather conditions, and turbine performance are used to estimate available power over a given period. These models rely on statistical methods or machine learning techniques, such as neural networks, to analyze variations in power generation. Forecasting helps improve operational planning and is also used when estimating power availability for applications such as market bidding [38].

Kalman filters: A Kalman filter improves power estimation by combining model-based forecasts with real-time measurements. Estimated values are continuously

updated using a model-based prediction and corrected based on incoming observations. This approach accounts for short-term wind speed fluctuations by continuously refining the estimated power output [34, 39].

2.5 Chalmers wind turbine

This section provides an overview of Chalmers wind turbine and its simulation model, starting with the turbine's structure and control system, followed by a description of the model and its key components used to represent the turbine's behavior.

2.5.1 Structure of Chalmers wind turbine

A new research-oriented version of Chalmers wind turbine became operational at Chalmers University of Technology in 2021 [40]. Unlike commercial wind turbines, this updated version was specifically designed for experimentation and advanced analysis. It features a 45 kW variable-speed system with a direct-driven generator and a frequency controller, along with multiple sensors to support in-depth research on wind energy systems. Although the turbine is rated for 45 kW, it is currently operated at a maximum power level of 25 kW due to limitations in the control system.

In addition to its research purpose, the turbine was built with a focus on sustainable materials. A unique aspect of this wind turbine is its 30 meter wooden tower, which was implemented to examine the feasibility of using wood as a structural material. This approach aims to reduce the turbine's overall carbon footprint while maintaining reliability.

To support its experimental purpose, the turbine uses a digital control system developed at Chalmers. The measurement and control systems are based on CompactRIO hardware from National Instruments, with control algorithms implemented in LabVIEW [40].

2.5.2 Overview of the Simulink model

A simulation model of Chalmers wind turbine was developed in earlier work [6] to support ongoing research. The model represents the turbine's behavior and allows for performance analysis under different wind conditions, operating parameters, and frequency regulation strategies.

Figure 2.8 shows the overall updated model structure, divided into two main blocks: the available power estimation block and the wind turbine and control system block. Each block contains several internal components that represent turbine operations, such as power estimation and control functions.

The following sections describe these two blocks and their internal components. Additional details on the simulation model can be found in [6].

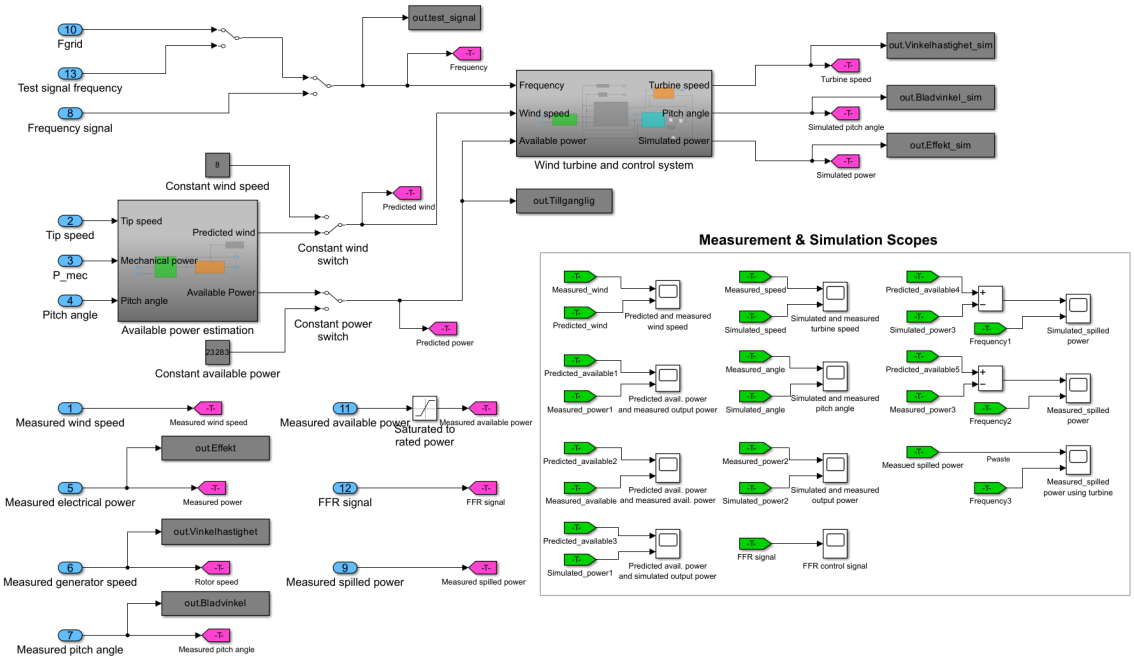

Figure 2.8: Overview of the Simulink model that represents the Chalmers wind turbine.

2.5.3 Available power estimation

The available power estimation block calculates the power the wind turbine can extract from the wind based on measured operational parameters. As shown in Figure 2.9, this process involves two main steps: estimating wind speed and predicting available power. These steps use three key inputs: mechanical power, tip speed, and pitch angle to determine the turbine's potential power output.

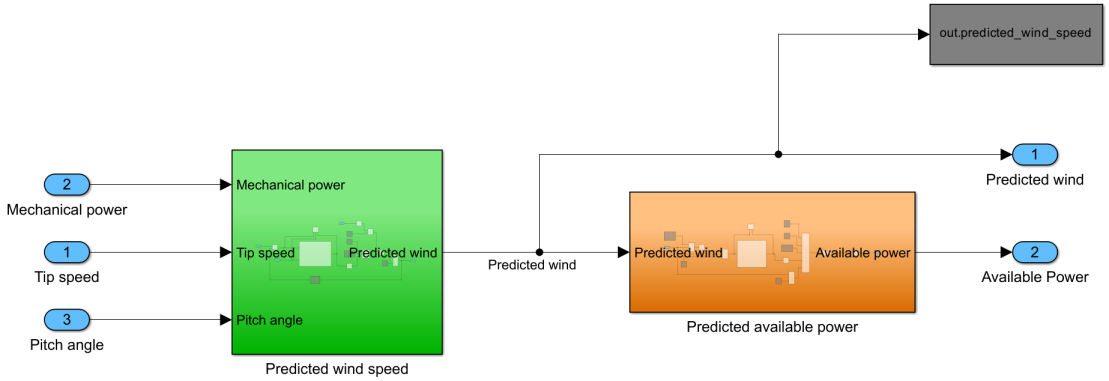

Figure 2.9: Available power estimation block in Simulink.

To better understand this process, the following explanations provide more detail on each step.

Predict wind speed: The wind speed is estimated using the measured mechanical power, tip speed, and pitch angle. This estimation is derived by rearranging equation

2.1, ensuring that the calculated wind speed reflects the actual power extracted by the turbine rather than relying on direct nacelle measurements.

Predict available power: Once the wind speed is estimated, it is used to predict the available power the turbine can extract under optimal operating conditions. The available mechanical power P_{mech} is calculated using equation 2.1, considering the turbine's optimal tip-speed ratio and power coefficient. A lookup table is used to determine C_p based on the optimal tip-speed ratio. The predicted power is then adjusted for system losses and efficiency before being used in the control system.

2.5.4 Wind turbine and control system

The wind turbine control system regulates the turbine's operation based on three inputs: grid frequency, wind speed, and available power. These inputs are processed through multiple control functions that manage power output, adjust the pitch angle, and determine generator torque. Figure 2.10 shows the structure of the control system and its main components.

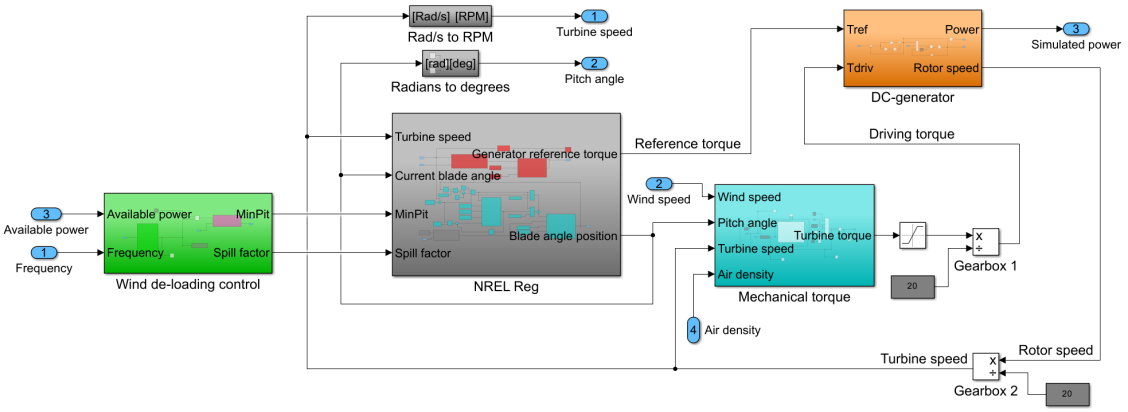

Figure 2.10: Wind turbine and control system block in Simulink.

The main components of the control system are described in more detail below.

Wind de-loading control: Adjusts the turbine's power output to support frequency stability by determining how much power should be spilled when a frequency deviation occurs. Based on this, the controller calculates a spill factor, which defines how much of the available power should be withheld to create a reserve used for ancillary services. This block also determines the minimum pitch angle required to achieve the power output defined by the spill factor.

NREL regulator: The main control block that manages the wind turbine's power extraction. It operates as a Maximum Power Point Tracking (MPPT) controller, using a lookup table to determine the electrical torque and pitch angle needed to maximize energy capture. The MPPT follows a torque-speed curve to adjust the turbine's response based on wind conditions, ensuring optimal operation. This controller is adapted from the wind turbine regulator developed by NREL for their

open-source reference turbine model [41].

Mechanical torque: Computes the mechanical torque acting on the turbine based on the estimated wind speed, turbine speed, and pitch angle. The calculation follows the power extraction principles in equation 2.1 and determines the mechanical torque using equation 2.3.

DC-generator: The generator converts mechanical power into electrical power by regulating its torque. It receives a reference torque from the NREL regulator, and a PI controller adjusts for deviations to keep the generator torque at this value. The rotational speed is calculated using equation 2.6, where the torque balance depends on the turbine torque τ_{mech} from the dynamic block. Since the model includes a gearbox, the generator speed is adjusted accordingly using equation 2.7. Finally, the electrical power output is determined based on equation 2.4.

2.5.5 Wind de-loading controller for frequency regulation

The wind de-loading control block in Simulink determines how much the wind turbine can contribute to ancillary services and is a focus of this paper, as it plays an important role in the evaluation process. The frequency controller currently implemented in the Simulink model is shown in Figure 2.11.

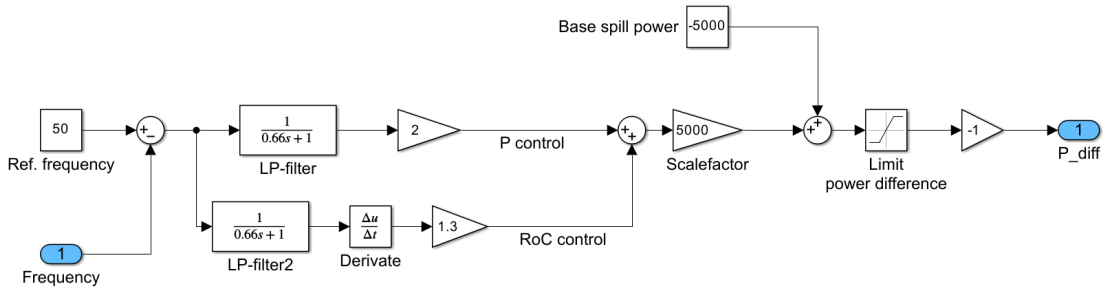

Figure 2.11: Frequency controller currently implemented in the Simulink model.

This controller operates by spilling a certain amount of power based on the frequency deviation. It measures how much the frequency deviates from the nominal 50 Hz, which generates an error. This error is then processed through a PD controller with two low-pass filters that smooth the corrections and shape the response to frequency deviations, influencing how quickly or slowly the controller reacts. The corrections are then summed and scaled by a factor to produce a value comparable to the base spill of 5 kW. The base spill power is a predefined reserve that ensures the turbine can respond to disturbances through both up and down regulation. The output is then limited to a maximum spill of 10 kW, which corresponds to 40% of the rated power of Chalmers wind turbine. This value is a design choice to limit how much power can be reduced during a frequency disturbance and make sure that it doesn't spill more than what is available.

2.6 Previous studies on frequency regulation performance

Wind turbines have been widely studied in terms of energy production and control strategies, but fewer studies have focused specifically on their performance in providing ancillary services in response to grid frequency variations. Much of the existing work relies on simulations with predefined input signals, such as step responses, rather than measured grid frequency data. Studies that compare simulation results with measured responses from wind turbines are also limited.

Among the available research, some studies have investigated how wind turbines respond under frequency control conditions. One study involving a 10 MW wind farm under real-time Automatic Generation Control (AGC) signals showed that good frequency regulation performance can be achieved when suitable reserve control strategies are implemented, especially for wind farms operating above rated power [42]. Another study examined how turbine control characteristics such as pitch angle behavior affect the delivery of ancillary services [43].

A third study compared wind farm control requirements and evaluation methods in several regions, such as Great Britain, Ireland and Denmark, and found notable differences in national grid codes [44]. It described the use of simulation-based testing, such as set-point tracking, delay analysis and transient response evaluation, as a way to evaluate turbine performance under grid code requirements. These methods are typically applied under defined input conditions and focus on control response rather than measured frequency variations [42–44].

Due to the limited number of studies that compare measured wind turbine responses with continuous variations in grid frequency, this thesis develops a method for evaluating frequency regulation performance using operational data. The aim is to capture how turbines respond to actual frequency deviations, rather than relying on predefined test signals.

3 Data collection and processing

Data were collected from three sources: Chalmers wind turbine, Kronoberget wind farm, and Finland's transmission system operator (Fingrid). These datasets include operational parameters such as wind conditions, turbine operation, and power output, recorded at one-second intervals, as well as grid frequency, sampled at 10 Hz. Chalmers wind turbine data were stored in multiple text files, each covering a 12-hour period, while Kronoberget and Fingrid data were stored as daily CSV files.

In addition to operational data, information on both the power bids placed by Kronoberget wind farm and the bids accepted by Svk for participation in ancillary services was collected, providing insight into the farm's daily market participation.

The following sections describe the collected data in more detail, including how the measurements were obtained.

3.1 Chalmers wind turbine data

Measurement data were collected from Chalmers wind turbine using its control and monitoring system, which operates through LabVIEW. The turbine is equipped with a detailed measurement system designed for experimental research, allowing for the collection of a wide range of operational parameters. The following parameters were used in this evaluation:

Table 3.1: Selected parameters from Chalmers wind turbine.

Parameter	**General description**
Wind speed	Measured wind speed
Pitch angle	Blade position control
Available power	Power the turbine can generate
Output power	Electrical power delivered
Spilled power	Unused available power
Frequency	Grid frequency

Meteorological data, including air temperature, pressure, and humidity, was collected from the mast next to Chalmers wind turbine.

3.2 Commercial wind turbine data

The commercial wind turbine data were collected from Kronoberget wind farm, which consists of 16 wind turbines with a rated power of 3.8 MW each, resulting in a total installed capacity of 60.8 MW [45]. The wind farm has an estimated annual energy production of approximately 200 GWh and is prequalified for FCR-D Down, meaning the turbines meet the requirements for providing downward frequency containment reserves during overfrequency events.

The specifications of the wind farm are summarized in Table 3.2.

Table 3.2: Kronoberget wind farm specifications.

Specification	Details
Number of turbines	16
Rated power per turbine	3.8 MW
Total installed capacity	60.8 MW
Annual energy production	Approx. 200 GWh
Ancillary service capability	Prequalified for FCR-D Down

The spatial layout of the wind turbines is shown in Figure 3.1 [46]. The turbines are spread out across a wide area, and their position relative to the wind direction can affect how much wind they are exposed to and whether they are influenced by wake effects. The layout helps provide context for how wind conditions vary across the site.

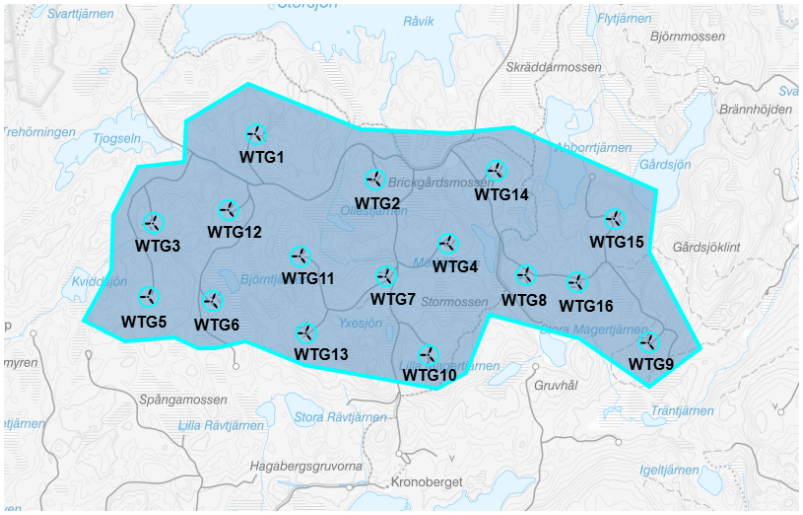

Figure 3.1: Layout of the 16 wind turbines at Kronoberget wind farm.

Similar to Chalmers wind turbine, Kronoberget wind farm records various operational parameters. However, for this study, the same parameters listed in Table 3.1 were used.

3.3 Grid frequency data

Grid frequency data were originally available from both Chalmers wind turbine and Kronoberget wind farm. However, since frequency is only measured when Chalmers wind turbine is in operation, data were only available during those periods. At the same time, archived frequency data from Kronoberget were missing for most of the analyzed periods. To ensure a consistent and complete dataset, frequency measurements were instead retrieved from Fingrid Open Data [47]. These measurements represent the Nordic synchronous system and are recorded at a 10 Hz rate.

3.4 Bid data

Bid data for ancillary services were collected from Kronoberget wind farm. For each day, one dataset shows the hourly power bids submitted for FCR-D Down,

while another indicates how much of this was accepted by Svk. These daily datasets provide insight into the wind farm's participation in the ancillary services market and make it possible to evaluate how the actual response compares to the accepted reserve. The data are given in megawatts with hourly resolution.

3.5 Data processing

Before the collected data could be analyzed, it was structured and processed. This involved preparing the datasets, handling inconsistencies and computing additional parameters. The overall workflow is shown in Figure 3.2.

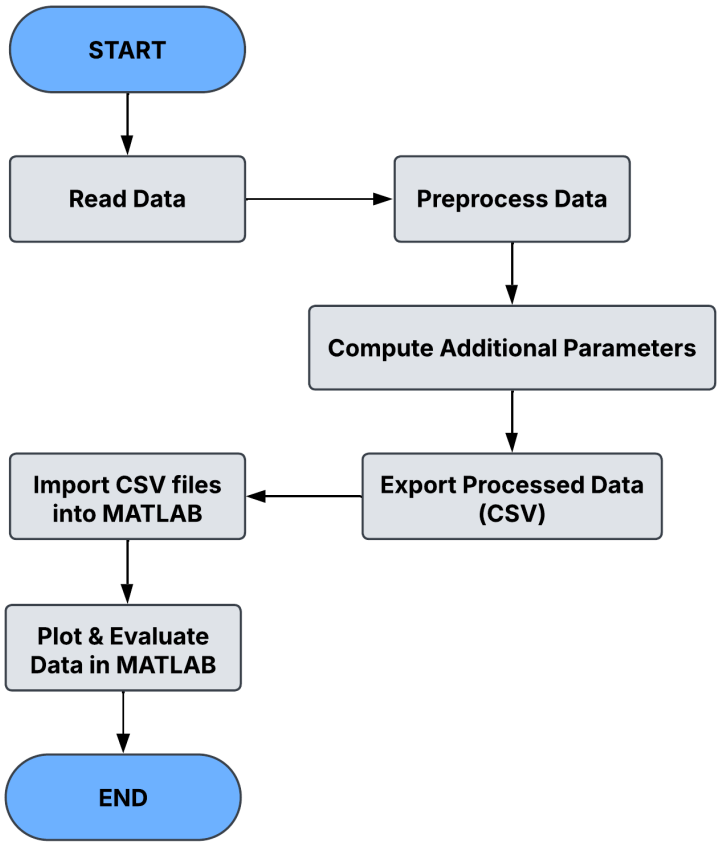

Figure 3.2: Overview of the data processing workflow.

The following sections describe each step of the data processing workflow.

Step 1 - Read Data: Measurement data from Chalmers wind turbine, Fingrid, and Kronoberget wind farm were imported into Python. Chalmers wind turbine data were stored in multiple text files, each covering a 12-hour period, which were merged into full-day datasets. Kronoberget wind farm and Fingrid data were provided as daily CSV files. Meteorological data from the mast next to Chalmers wind turbine were also stored in daily text files and imported in the same way. Data on daily bids from Kronoberget wind farm, including both placed and accepted bids, were also included. All datasets were structured into DataFrames for further processing.

Step 2 - Preprocess Data: The raw data were preprocessed to ensure consistency across datasets. This included assigning appropriate column names, handling miss-

ing values, and converting timestamps. Rows with missing values were removed to ensure consistency. The timestamps for Chalmers wind turbine were originally in epoch time and were converted to Unix timestamps in seconds, then adjusted for Swedish standard time. Frequency data from Fingrid were originally in UTC+2 and were shifted back one hour to align with the correct day in Swedish local time. Bid data were also formatted to align with the operational data.

Step 3 - Compute Additional Parameters: Additional parameters were computed. This included calculating the total available power and total output power for Kronoberget wind farm by summing the values from all 16 turbines. Spilled power was determined by subtracting output power from available power. The computed values were added as new columns in the datasets.

Step 4 - Export Processed Data: After preprocessing and computation, the processed datasets were exported as CSV files. The data was structured with time columns and cleaned measurements.

Step 5 - Import & Evaluation in MATLAB: The processed data was imported into MATLAB, where it was visualized through plots and used for further evaluation.

4 Methodology

This section describes how the study was carried out, including the steps taken to develop the model, implement control strategies, and evaluate the performance of wind turbines providing frequency control. The work is based on literature studies, further development of an existing Simulink model [6,7], and analysis of operational data. The methodology enables both simulation-based testing of Chalmers wind turbine and comparison with measured data from a commercial wind farm.

4.1 Literature review

The literature review focused on gathering the theoretical knowledge needed to develop and evaluate frequency control strategies for wind turbines. Studies on ancillary services, frequency stability and control methods such as droop control, synthetic inertia and de-loading were reviewed to support the design of the model. Guidelines from Svenska kraftnät and ENTSO-E were also studied to ensure that the implementation met technical requirements for FCR-N and FCR-D. In addition, earlier versions of the Chalmers wind turbine model and related work were used as a starting point for further development. Studies on wind turbine performance in frequency control were also reviewed, although the available literature in this area is limited.

4.2 Further development of the model

The existing frequency controller for the Chalmers wind turbine model was a general implementation and did not follow the specific requirements set by Svk and ENTSO-E. To address this, modifications were made to integrate FCR-N and FCR-D, enabling the Chalmers wind turbine model to deliver frequency regulation according to the minimum requirements. This allows it to serve as a reference for evaluating performance. To support this, a new control structure was developed, incorporating an activation block to determine which service should be applied. Figure 4.1 provides an overview of this updated controller.

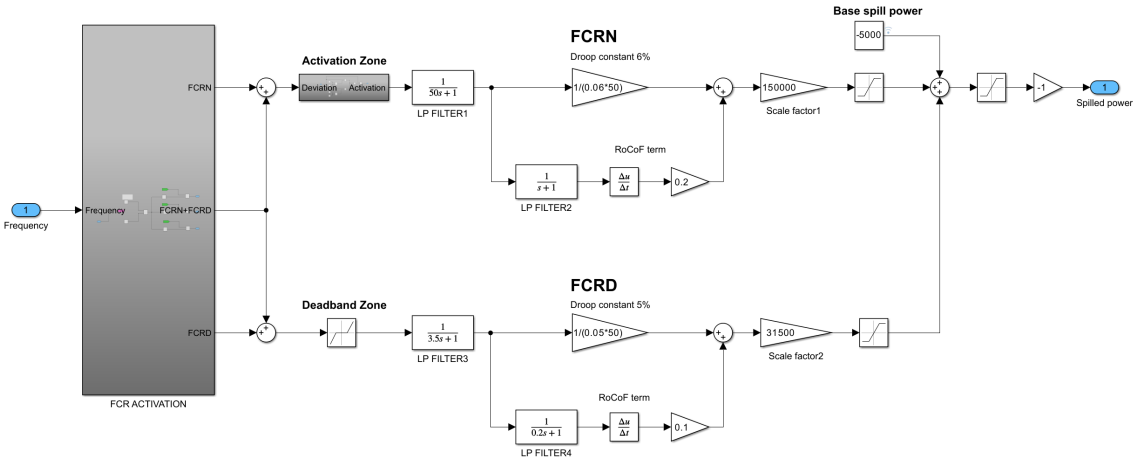

Figure 4.1: Overview of the new frequency controller.

The activation block, shown in Figure 4.2, determines which service should be used based on the selected mode. To do this, it first compares the measured frequency to

the nominal 50 Hz to calculate the frequency deviation. A selection signal, which can take values between 1 and 3, is then used to choose the active service.

- 1 activates FCR-N
- 2 activates FCR-D
- 3 enables both services (FCR-N + FCR-D)

The selection signal is compared to these values using logical conditions. If the selection matches a specific mode, the corresponding logical output is set to 1; otherwise, it remains 0. This output is then multiplied by the frequency deviation, ensuring that only the selected service receives the deviation as input. The resulting signal is then sent to the corresponding controller for processing.

The controller is described in more detail in the following sections, which cover FCR-N, FCR-D and the full combined version.

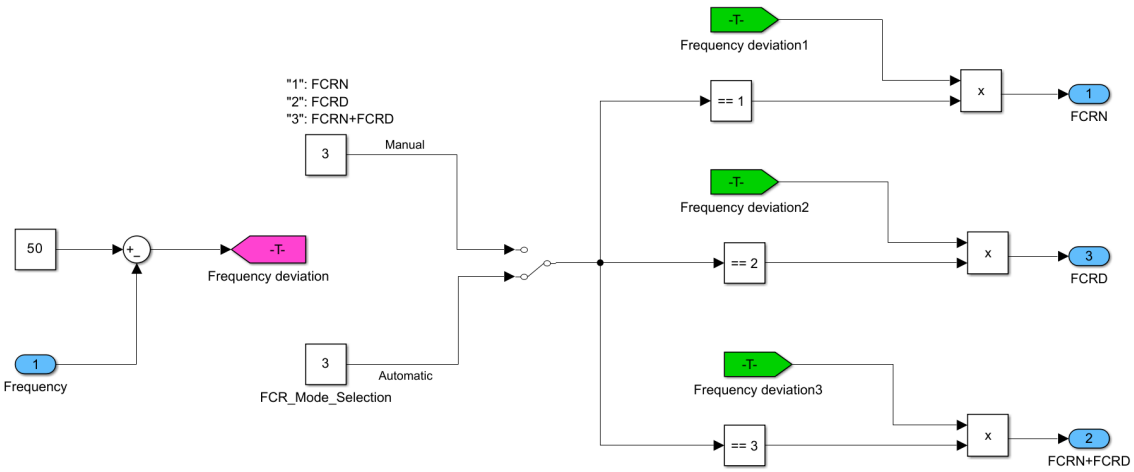

Figure 4.2: Activation block for selecting FCR-N, FCR-D or both.

4.2.1 Frequency controller for FCR-N

Figure 4.3 shows how the FCR-N frequency controller is implemented in the model. Like the previous frequency controller (Figure 2.11), it measures the frequency deviation from the nominal 50 Hz and processes the error. This version, however, is based on a droop control method with a fixed droop constant of 6%. The low-pass filters are also tuned to meet the minimum response requirements of ENTSO-E and Svk while also reducing high-frequency noise.

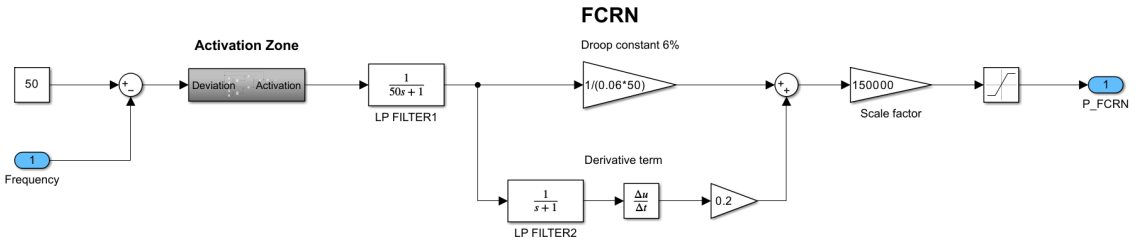

Figure 4.3: Frequency controller for FCR-N regulation.

FCR-N operates within the frequency range of 49.9 Hz to 50.1 Hz. To ensure this, an activation zone is used to determine when the controller should be active. As shown in Figure 4.4, this block checks whether the frequency deviation stays within the activation limits. A small tolerance is also included to avoid issues caused by floating point precision.

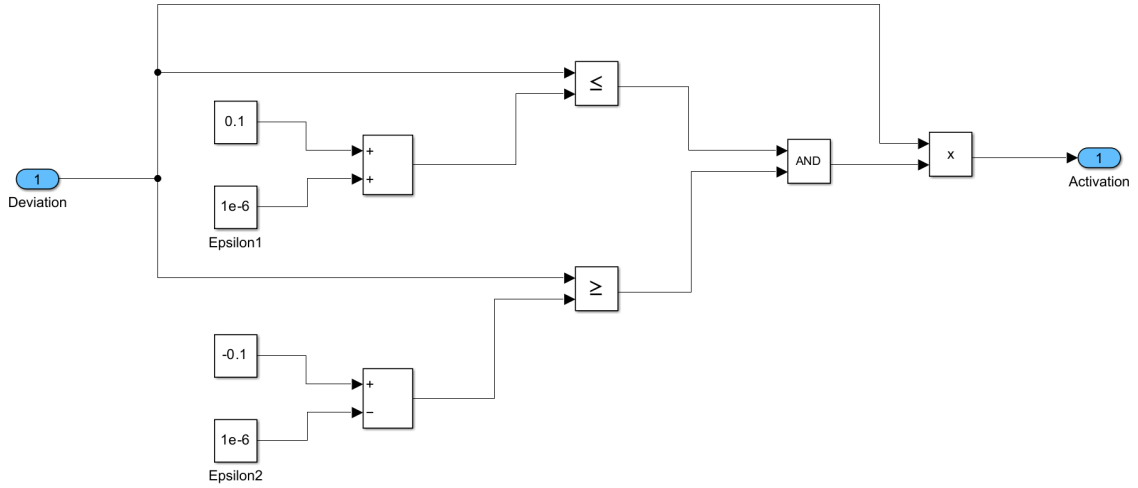

Figure 4.4: Activation zone of FCR-N.

Once the activation condition is met, the frequency deviation first passes through a low-pass filter, which helps set the overall response time. To prevent rapid fluctuations, another low-pass filter with a small time constant is placed before the derivative term. The corrections from both the droop and RoCoF terms are then combined and scaled according to the power reserve of 5000 W, which is the base spill power shown in Figure 4.1, providing up and down regulation capacity. A saturation block is then used to limit the spilled power between -5000 W and 5000 W, which forms the output of the FCR-N controller.

4.2.2 Frequency controller for FCR-D

Figure 4.5 shows how the FCR-D frequency controller is implemented in the model. While it follows the same general structure as FCR-N, it operates outside the 49.9 Hz to 50.1 Hz range and has some key differences. The droop control method is still used, but with a fixed droop constant of 5% instead of 6%, resulting in a stronger

response. A deadband prevents activation within 49.9 Hz to 50.1 Hz, ensuring regulation only occurs when the deviation exceeds 0.1 Hz.

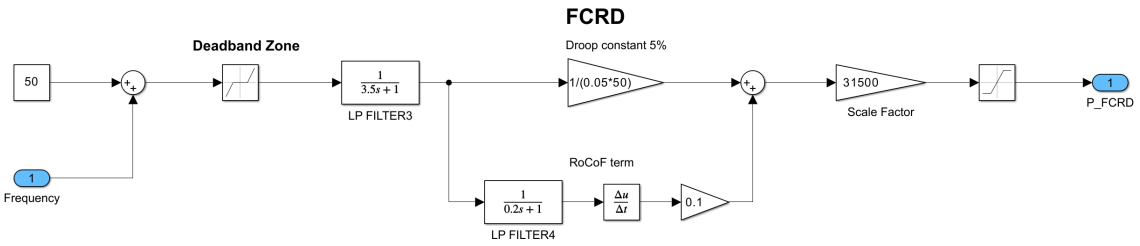

Figure 4.5: Frequency controller for FCR-D regulation.

FCR-D Up is activated when the frequency drops below 49.9 Hz and remains active down to 49.5 Hz. Similarly, FCR-D Down is activated when the frequency exceeds 50.1 Hz and stays active up to 50.5 Hz. Like FCR-N, the frequency deviation first passes through a low-pass filter, which helps set the controller's response time. Another low-pass filter is placed before the RoCoF term to smooth out rapid fluctuations.

The processed signal is then sent to the droop-based controller, where the RoCoF term adjusts for the rate of frequency change. As in the FCR-N controller, the adjustments from both terms are combined and scaled according to the available power reserve of 5000 W. A saturation block then limits the final power adjustment within -5000 W and 5000 W, which forms the output of the FCR-D controller.

4.2.3 Combined frequency controller for FCR-N and FCR-D

The final version of the controller is shown in Figure 4.6, where the FCR-N and FCR-D controllers are combined into a single frequency controller. The contributions from both controllers are summed with the power reserve of $-5000\,\mathrm{W}$ and then passed through a saturation block, which limits the power between 0 and $-10000\,\mathrm{W}$ before applying a sign change. This limit still corresponds to 40% of the rated power of Chalmers wind turbine, ensuring that the spilled power remains within the predefined operating range. The resulting signal then serves as the output of the frequency controller to the rest of the system, representing the desired spilled power based on the frequency deviation.

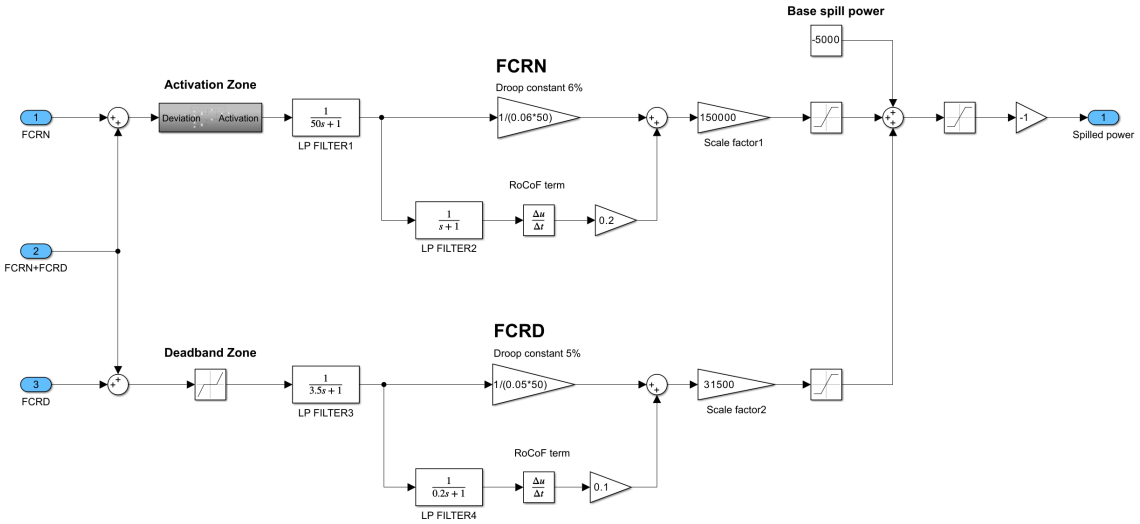

Figure 4.6: Combined frequency controller integrating FCR-N and FCR-D.

4.2.4 Implementation of dynamic air density and filtering

A dynamic air density block was implemented to replace the previous assumption of constant air density. This accounts for variations in air pressure, temperature and humidity which influence the prediction of wind speed, available power estimation and turbine torque calculations. Additionally, a low-pass filter was applied to the predicted wind speed to reduce short-term variations before it is used in the turbine model. A saturation block is applied after the filtering stage to keep the wind speed above zero and avoid division by zero. An overview of these components is shown in Figure 4.7.

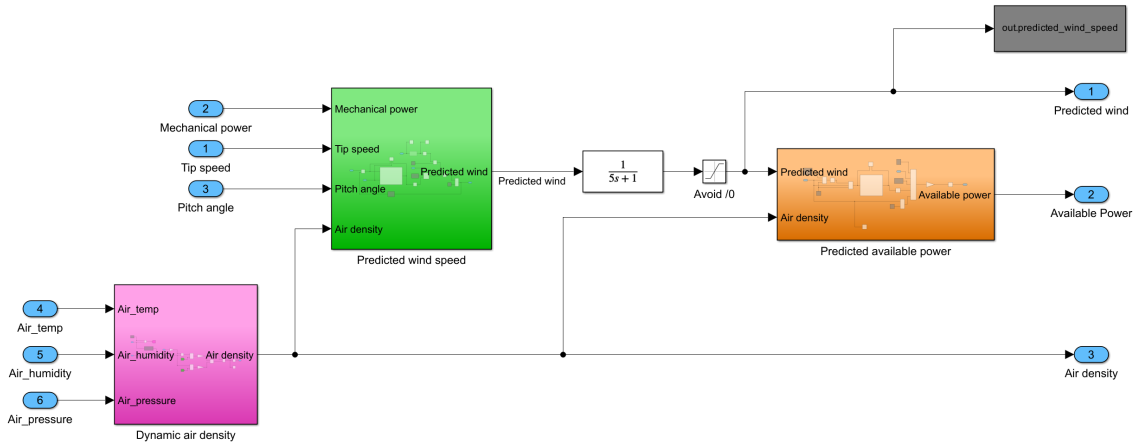

Figure 4.7: Overview of the air density integration in wind speed prediction and power estimation.

The air density is computed based on measured air temperature, humidity and pressure. This replaces the constant density assumption with a real-time calculation, as implemented in the dynamic air density block shown in Figure 4.8. The density is determined using the gas law:

$$\rho = \frac{P_d}{R_d T} + \frac{P_v}{R_v T} \tag{4.1}$$

where $P_d = P - P_v$ is the dry air pressure and P_v is the vapor pressure [48]. A constant air density value is also included, allowing the option to switch between dynamic and constant density calculations. A saturation block is applied to ensure that the air density remains within a valid range, preventing division by zero.

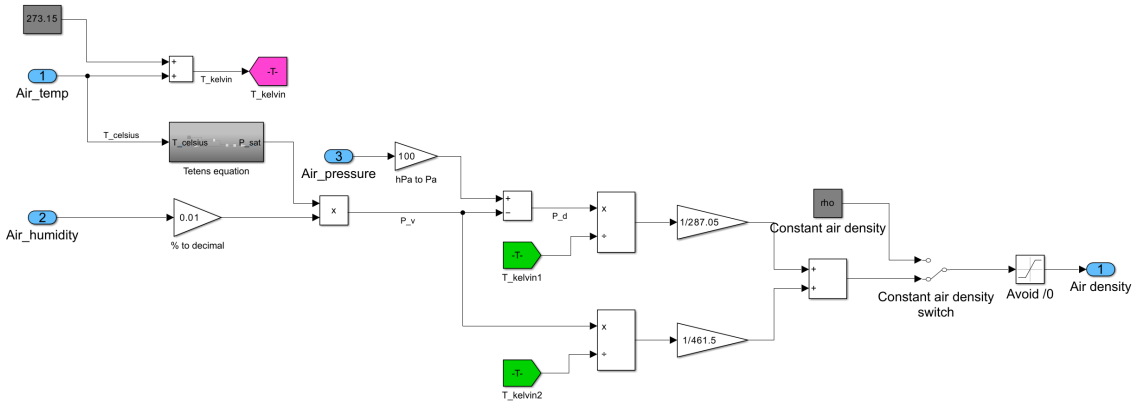

Figure 4.8: Dynamic air density block.

The vapor pressure is calculated using the Tetens equation, which is implemented in the block shown in Figure 4.9. The saturation vapor pressure is given by

$$P_{\text{sat}} = 610.6 \times \exp\left(\frac{17.269T}{T + 237.3}\right) \tag{4.2}$$

$$P_v = RH \cdot P_{\text{sat}} \tag{4.3}$$

where RH is the relative humidity expressed as a decimal and T is the air temperature in degrees Celsius [49]. In this form, P_{sat} is given in pascals.

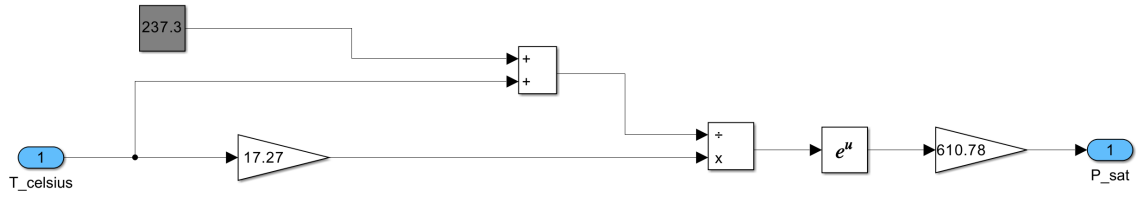

Figure 4.9: Tetens equation block.

The air density varies depending on environmental conditions. As shown in Figure 4.10, it can differ significantly from the constant reference value of 1.225 kg/m^3. In cold and dry conditions at -20°C, 1050 hPa, and 0% relative humidity, the air density is approximately 18% higher. In hot and humid conditions at 40°C, 950 hPa,

and 100% relative humidity, the density is around 16% lower. These represent extreme conditions, but they illustrate how air density changes depending on pressure, temperature, and humidity, which in turn affects wind speed prediction, available power estimation, and turbine torque calculations in the model.

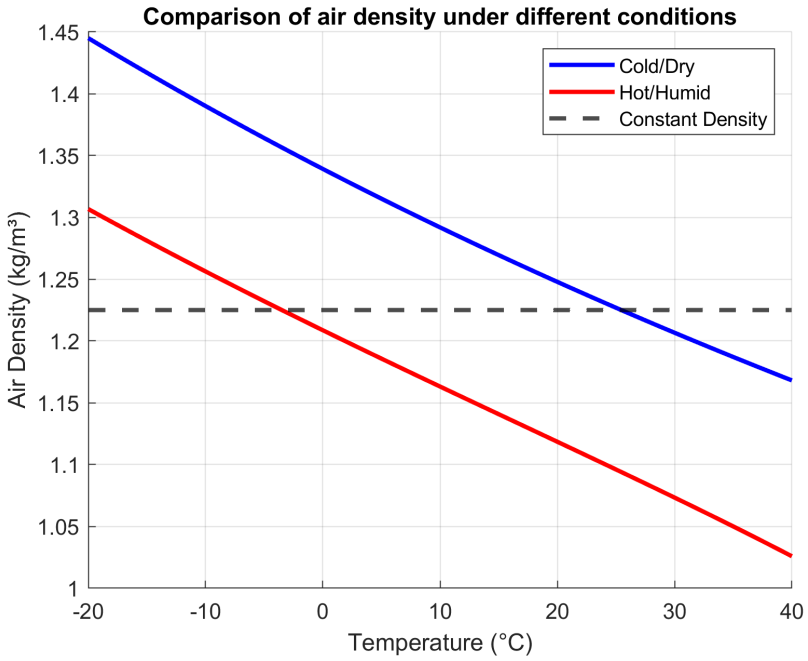

Figure 4.10: Dynamic air density variation under different conditions.

4.3 Evaluation method

This section describes how the wind turbines are analyzed for their response to frequency variations when providing ancillary services. The evaluation begins by testing the frequency controller of the Chalmers wind turbine model using both predefined step signals and a measured grid frequency signal. After that, the turbine response is simulated using two selected days with grid frequency and weather data. The same days are then used to evaluate the turbines at Kronoberget wind farm based on recorded operational data. Finally, the responses of both turbines are compared to examine differences in power regulation, reserve utilization, and activation times.

The evaluation method can be applied to FCR-N, FCR-D, or a combination of both. However, since the commercial wind turbines at Kronoberget are prequalified for FCR-D Down, the analysis focuses on that service.

The overall process used in this study is illustrated in the flowchart in Figure 4.11. Each step is explained in more detail in the following sections.

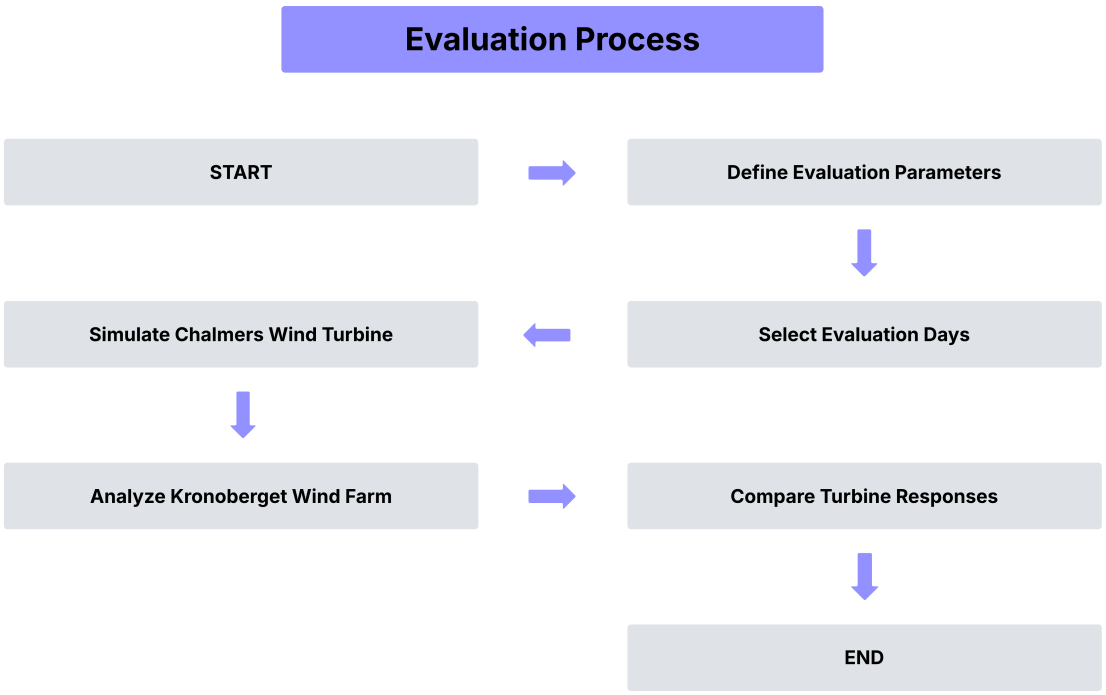

Figure 4.11: Evaluation process for ancillary service performance.

4.3.1 Evaluation parameters

The parameters in Table 4.1 are used to analyze how each turbine responds to frequency variations. These parameters were selected to evaluate power regulation, reserve availability, and how the turbines adjust their operation in response to grid conditions. The evaluation focuses on response time, delivered power, and how well the turbines meet the accepted FCR-D Down bids from Svenska kraftnät.

Table 4.1: Parameters used in the evaluation.

Parameter	Description
Power output	Electrical power delivered by the turbine.
Available power	Maximum power the turbine can generate under current wind conditions.
Spilled power	Difference between available and delivered power, indicating reserve power used for frequency support.
Pitch angle	Blade angle used to control aerodynamic power capture.
Wind speed	Measured wind speed at the turbine hub height.
Frequency	Grid frequency or simulated test signal used to trigger frequency response.
Bid (Kronoberget)	FCR-D Down regulating capacity offered by the wind farm to Svenska kraftnät.
Accepted bid (Svk)	FCR-D Down capacity approved by Svenska kraftnät for the specific time interval.

4.3.2 Selection of evaluation days

To perform the analysis, data from Chalmers wind turbine and Kronoberget wind farm were reviewed across 2024 to identify suitable evaluation periods. The aim was to select two days with different wind conditions: one with high wind speeds, where turbines operated near rated power, and one with more moderate wind speeds. This allows for evaluating turbine behavior both during full production and at lower power output.

The selection process was based on the following criteria:

- Chalmers wind turbine was in operation and actively connected to the grid
- Grid frequency deviations occurred that triggered FCR-D Down activation
- Wind conditions were suitable for evaluating turbine response at different power levels
- At Kronoberget wind farm, bid data showed that the wind farm was participating in ancillary services during the selected periods

The selected days are used both as input to the simulation of Chalmers wind turbine and for analyzing recorded data from Kronoberget wind farm, allowing for a direct comparison.

4.3.3 Droop and ramp rate estimation

To quantify how the wind turbines respond to frequency deviations, the evaluation includes estimation of droop and ramp rate from both simulated and measured data. The droop describes the proportional relationship between power output and frequency deviation, showing how much of the available reserve is activated per hertz. The ramp rate describes how quickly the power output changes over time and is used to evaluate the dynamic response relative to the FCR-D Down requirements.

Spilled power is analyzed in both absolute and normalized form. In the normalized case, spilled power is expressed as a fraction of the total available reserve. For the Chalmers wind turbine model, normalization is based on the difference between the maximum simulated spill capacity and the baseline spill:

$$P_{\text{spill,norm}} = \frac{P_{\text{spill}}}{P_{\text{max,sim}} - P_{\text{baseline}}} \tag{4.4}$$

where P_{spill} is the spilled power at a given time, $P_{\text{max,sim}}$ is the maximum simulated spilled power, and P_{baseline} is the output at the beginning of the frequency event.

For the commercial wind turbines at Kronoberget, normalization follows the same definition of baseline and is based on the accepted FCR-D Down bid from Svenska kraftnät:

$$P_{\text{spill,norm}} = \frac{P_{\text{spill}}}{P_{\text{bid}} - P_{\text{baseline}}} \tag{4.5}$$

where P_{bid} is the accepted bid. This defines the available regulation range that could be activated during overfrequency events.

The Chalmers wind turbine model can be operated to meet the minimum FCR-D Down requirements defined by Svenska kraftnät and ENTSO-E and is therefore used as a reference to compare the response of the commercial wind farm. Since Svenska kraftnät uses predefined step signals to verify compliance during the pre-qualification process, only such tests can confirm that a turbine meets the formal requirements [50]. However, the control system of the turbines at Kronoberget is not known in detail, other than that the wind farm is prequalified for FCR-D Down. By comparing its measured response to the verified performance of the Chalmers wind turbine model under the same frequency conditions, it is possible to evaluate how the commercial turbines follow the expected activation behavior. This provides a reasonable indication of their actual performance, despite not being tested with step signals.

The maximum simulated spilling of the Chalmers wind turbine model was initially set to 10,000 W, but dynamically adjusted in each evaluated interval so that the normalized available regulation range remained equal to or below that of Kronoberget. Since the model serves as a reference for the minimum FCR-D Down performance defined by Svenska kraftnät, this constraint reduces the risk of overestimating the expected response. A larger regulation range would require more time to reach full activation and could make the commercial turbine appear slower in comparison. Limiting the Chalmers model in this way provides a more consistent basis for comparing the measured response from Kronoberget to the expected performance.

An ideal Svk droop line is also included as a visual benchmark, representing the expected proportional response based on the requirements from Svenska kraftnät. It assumes a linear relationship between frequency deviation and power response across the available regulation range. The line is scaled to the same normalized range as the measured data using:

$$P_{\text{Svk,norm}} = \frac{P_{\text{bid}} \cdot \Delta f / 0.4}{P_{\text{bid}} - P_{\text{baseline}}} \tag{4.6}$$

where Δf is the deviation from 50.1 Hz, and P_{baseline} is the spilled power at the start or end of the frequency event, depending on direction. This scaling ensures that the Svk line reflects the expected response relative to the up-regulation capacity available in the selected interval. Since the grid frequency changes gradually and not as a step, the Svk line is not used to decide whether the turbines meet the requirements. Instead, it gives an indication of how closely the turbines follow the expected activation pattern during grid frequency disturbances, with the simulation model of the Chalmers wind turbine providing a reference for the expected minimum performance.

4.3.4 Comparison of evaluation outcomes

The comparison examines how each turbine regulates power and utilizes reserves in response to frequency variations. It considers how quickly the turbines respond, as well as how control signals such as pitch angle are used to manage power output.

The evaluation is structured around the following aspects:

- The full-day response from Kronoberget wind farm is analyzed to assess overall power variations and reserve activation. The analysis focuses on how the base

level of spilled power changes during the day, how quickly these adjustments occur, and how the actual power reserve compares to the bid for FCR-D Down.

- A one-hour period from both the Chalmers wind turbine model and Kronoberget wind farm is selected for direct comparison during the same frequency event. The interval is chosen based on when the grid frequency exceeds 50.1 Hz, ensuring that the turbines are evaluated during active FCR-D Down operation.

- A further zoomed-in analysis is used to evaluate short-term changes in power regulation and response time. This includes estimating droop and ramp rate based on selected data points and identifying possible delays between frequency changes and the turbine's power response.

- Pitch angle is also evaluated to understand how each turbine adjusts its operation in response to frequency variations, providing insight into the control behavior during FCR-D Down events. The analysis focuses on pitch ramp rates, as well as typical minimum and maximum angles during operation or shutdown, and the number of turbines providing reserve power during frequency events.

By applying the same frequency variations to the Chalmers wind turbine model and selecting matching periods from Kronoberget wind farm, the comparison enables consistent evaluation of response behavior and reserve contribution under FCR-D Down conditions.

5 Results

This chapter evaluates the performance of the Chalmers wind turbine model and Kronoberget wind farm in providing frequency control. It begins with tests of the newly developed frequency controller implemented in the Chalmers wind turbine model, including separate evaluations for FCR-N, FCR-D, and the combined controller mode. The evaluation then focuses on FCR-D Down using measured frequency events on two selected days. These days were chosen based on frequency conditions observed from Fingrid, with one day representing operation near rated power and the other reflecting more variable wind conditions. Since FCR-D Down is the only service for which the commercial wind farm is prequalified, the results are compared using this service, with the Chalmers wind turbine model serving as a reference for meeting Svenska kraftnät's minimum performance requirements.

5.1 Evaluation of the Chalmers wind turbine model

The first part of the evaluation focuses on the Chalmers wind turbine model, using step signals and measured grid frequency to evaluate the controller performance. The step signals are based on the activation ranges defined by Svenska kraftnät for prequalification testing and are used to verify that the turbine meets the required response times and reserve activation for frequency control. The turbine is assumed to operate at rated power, ensuring that frequency is the only varying input. A constant base spill power of 5000 W is used to evaluate the activation of FCR-N, FCR-D, and the combined controller. The second part evaluates FCR-D Down using measured frequency events from the two selected days.

5.1.1 FCR-N controller

The response of the FCR-N controller to the step signal is shown in Figure 5.1. The step signal includes a frequency increase from 50.0 to 50.1 Hz and a decrease from 50.0 to 49.9 Hz, representing the activation range for FCR-N as defined by Svenska kraftnät. These steps are used to evaluate both upward and downward regulation.

When the frequency exceeds 50 Hz, the turbine spills more power, and when it drops below 50 Hz, it spills less, which reflects the expected symmetrical behavior. At 110 seconds, corresponding to 60 seconds after the step, the turbine spills 8512 W, which is approximately 70% of the available reserve and meets Svk's requirement of delivering 63% within 60 seconds. At 230 seconds, or 180 seconds after the step, the spilled power reaches 9865 W, or around 97%, fulfilling the requirement of 95% within 180 seconds. Since FCR-N is symmetrical, the same activation profile applies to both upward and downward regulation, and the controller meets Svk's timing criteria in both directions.

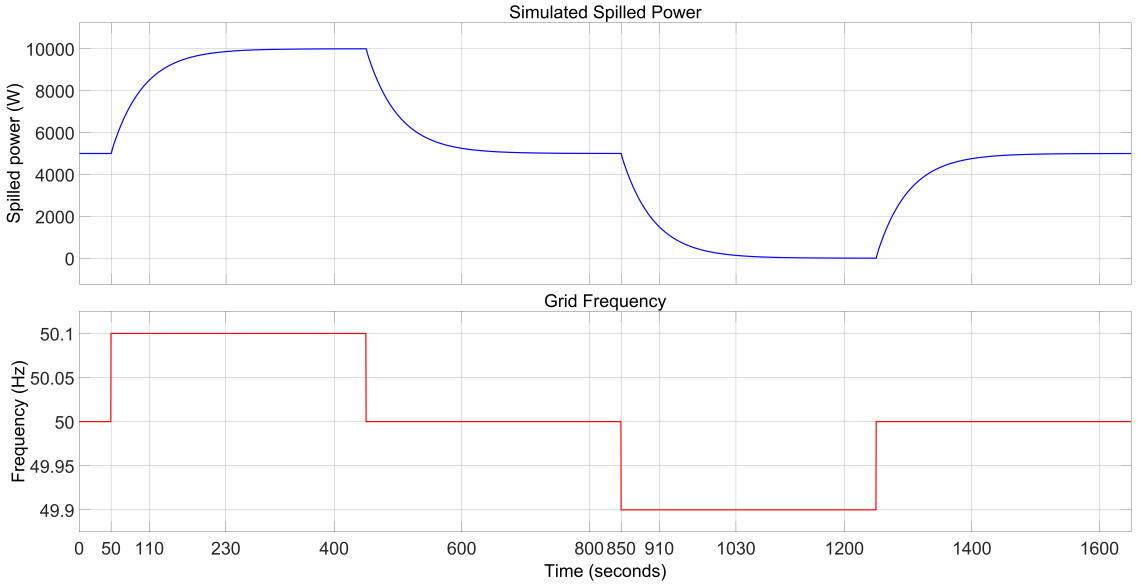

Figure 5.1: Spilled power response of the FCR-N controller to a step signal. The input frequency step is shown in red, and the resulting spilled power is shown in blue.

The FCR-N controller of the Chalmers wind turbine model was also tested using grid frequency data from January 27, 2025, provided by Fingrid. Figure 5.2 shows that the spilled power responds to frequency variations within the 49.9–50.1 Hz interval, with no activation outside this range. This demonstrates that the controller also behaves as expected when applied to measured grid frequency and follows the intended activation range defined by Svk's FCR-N requirement.

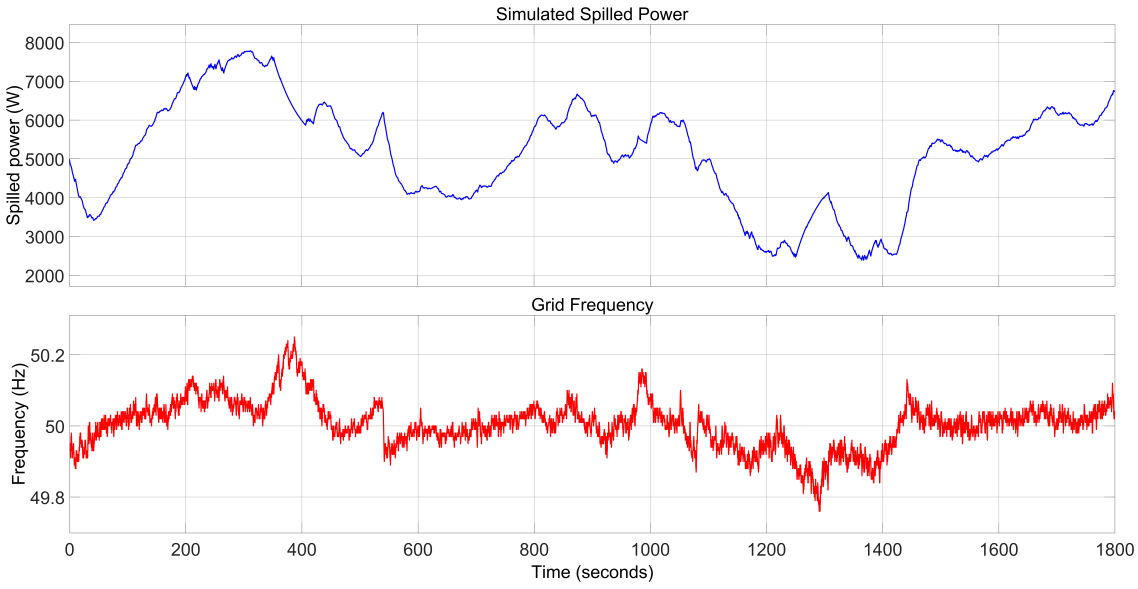

Figure 5.2: Response of the FCR-N controller to measured grid frequency on 27 January 2025. The grid frequency is shown in red, and the resulting spilled power is shown in blue.

5.1.2 FCR-D controller

Figure 5.3 shows the response of the FCR-D controller to the step signal. The signal includes a frequency increase from 50.1 to 50.5 Hz and a decrease from 49.9 to 49.5 Hz, covering the full activation range for FCR-D according to Svenska kraftnät. These steps are again used to evaluate the controller response for both upward and downward regulation.

When the frequency exceeds 50.1 Hz, the turbine spills more power, and when it drops below 49.9 Hz, it spills less. After 7.5 seconds, the spilled power reaches 9494 W, corresponding to 90% of the available reserve and meeting Svk's requirement of 86% activation within 7.5 seconds. Full activation is reached within 30 seconds, fulfilling the second timing requirement. As with FCR-N, the controller shows symmetrical behavior and meets Svk's activation criteria in both directions.

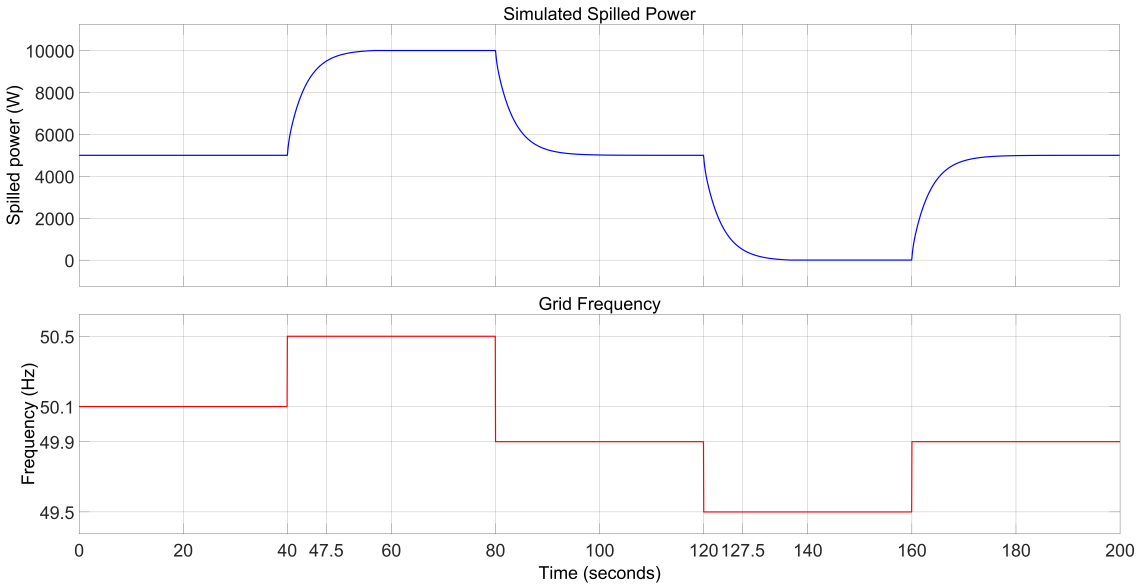

Figure 5.3: Response of the FCR-D controller to a test signal. The step signal is shown in red, and the spilled power response is shown in blue.

The same grid frequency data was also used to test the FCR-D controller. As expected, Figure 5.4 shows that the spilled power remains constant at the base level of 5000 W when the frequency stays within the 49.9–50.1 Hz interval. When the frequency exceeds 50.1 Hz or drops below 49.9 Hz, the controller activates and adjusts the spilled power accordingly.

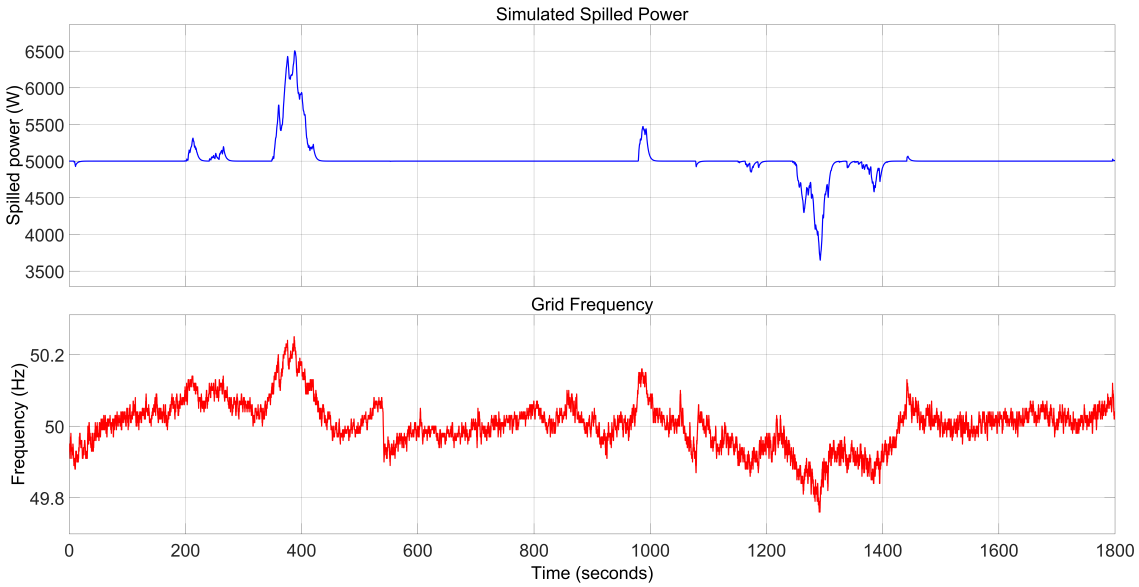

Figure 5.4: Response of the FCR-D controller to measured grid frequency on 27 January 2025. The grid frequency is shown in red, and the spilled power response is shown in blue.

5.1.3 Combined FCR controller

Figure 5.5 shows the response of the combined FCR controller, which integrates both FCR-N and FCR-D regions into a single control strategy. The step signal used here includes both the FCR-N steps between 49.9 and 50.1 Hz and the FCR-D steps outside this range, representing the full frequency activation span defined by Svenska kraftnät.

The figure illustrates how the response changes depending on which region is active and how the two parts interact. For steps that activate FCR-N, the response is slower compared to the faster reaction in the FCR-D region, which is consistent with previous results. A noticeable difference appears in the transition between the regions. Between 200 and 250 seconds, the frequency moves from the FCR-D to the FCR-N interval. During this time, the FCR-D response decreases quickly while the FCR-N response increases more gradually, which creates a visible shape in the curve due to the difference in response times. A similar shape is seen between 450 and 500 seconds. This behavior is expected and occurs during the recovery phase, where one region deactivates while the other becomes active.

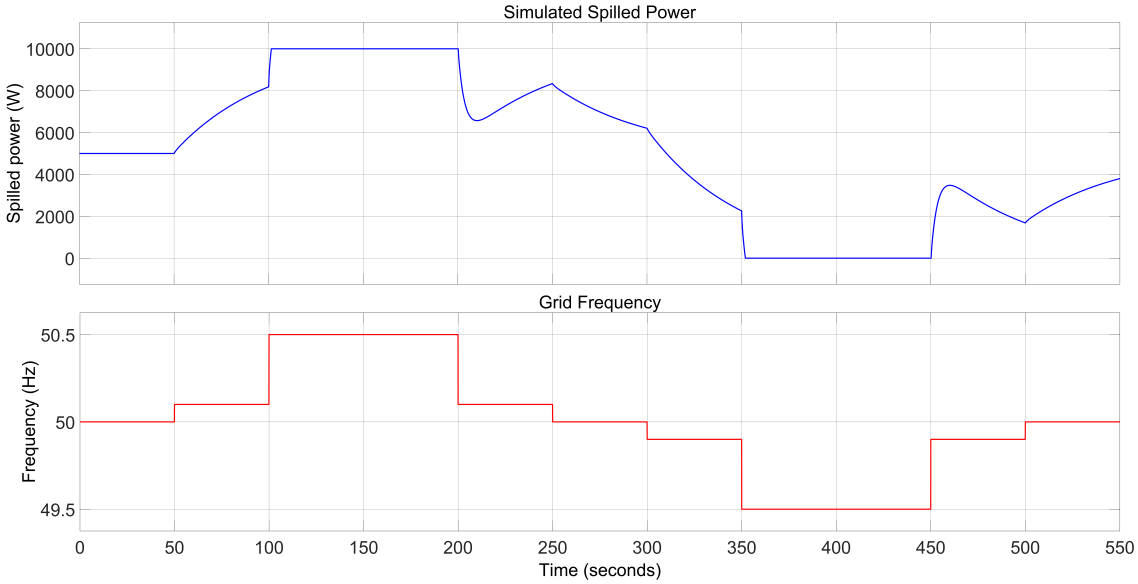

Figure 5.5: Response of the combined FCR-N and FCR-D controller to a test signal. The step signal is shown in red, and the spilled power response is shown in blue.

The combined FCR controller was also tested using the same grid frequency data as for the individual controllers. Figure 5.6 shows that the response follows the frequency variations, with each part of the controller active in its respective interval. The FCR-N controller operates between 49.9 and 50.1 Hz, while the FCR-D controller activates outside this range, with FCR-D Up between 49.5 and 49.9 Hz and FCR-D Down between 50.1 and 50.5 Hz. The response shows that both controllers operate correctly when combined into a single strategy.

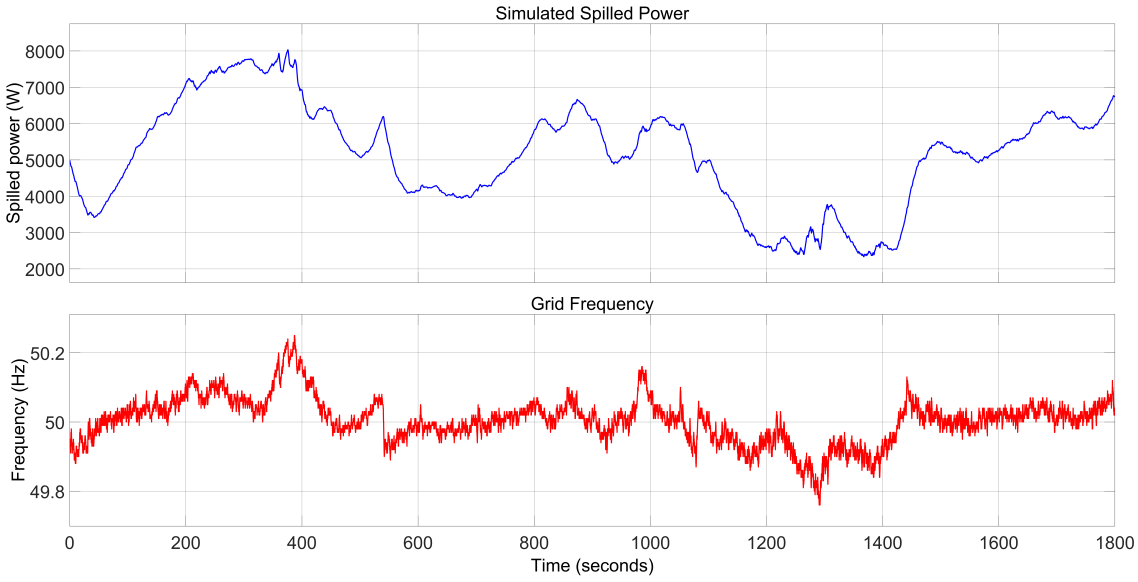

Figure 5.6: Response of the combined FCR-N and FCR-D controller to measured grid frequency on 27 January 2025. The grid frequency is shown in red, and the spilled power response is shown in blue.

5.1.4 Evaluation using selected days

Two days were selected for evaluating the frequency response of the Chalmers wind turbine model, based on measured frequency events where the grid frequency exceeded 50.1 Hz. To ensure stable operation near rated power, data input from 27 April 2023 was used in both cases to represent the wind conditions during the evaluated days, as the actual wind speeds on those days were in the medium range. This was necessary due to model limitations at medium/low wind speeds, which affect the turbine's ability to spill power correctly in response to frequency events. All other inputs, including the grid frequency, correspond to measurements from the actual evaluated days.

The evaluation for each day follows the same structure: an overview of wind speed and available power, turbine output and spilled power, a zoomed-in frequency event where the grid frequency exceeds 50.1 Hz, and two selected time intervals used to estimate delay, droop, and ramp rate. Since the turbine operates for limited periods, each simulation was performed for one hour.

Air density during the one-hour simulation was measured using weather data from the turbine site. The average value was approximately $1.2526\,\mathrm{kg/m^3}$, which is about 2.3% higher than the standard value of $1.225\,\mathrm{kg/m^3}$ that was used in the previous version of the model. While the change in air density only had a minor impact on the estimated turbine response, it slightly improved the accuracy of the simulation. To reduce the impact of fast fluctuations that caused spikes in the response due to noise, the wind signal was also filtered. The variation in air density over the interval is illustrated in Figure A.1 in Appendix A.1.

5.1.4.1 Case 1: 3 February 2024

Figure 5.7 shows the predicted and measured wind speed along with the corresponding available power for the Chalmers wind turbine model during the one-hour period on 3 February 2024. This hour was selected to evaluate the turbine's response to measured frequency events, as the grid frequency exceeded 50.1 Hz several times during the interval. The wind conditions during this period were relatively high, allowing the turbine to operate close to rated power. The predicted wind speed follows the measured values well, and the available power remains stable apart from a few small variations.

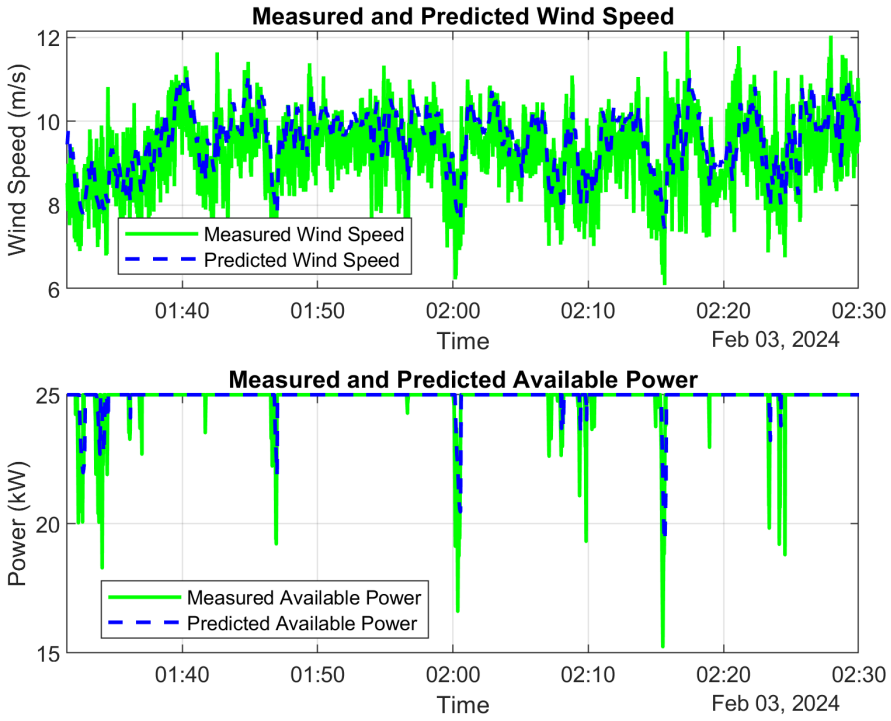

Figure 5.7: Predicted wind speed and available power for the Chalmers wind turbine model during a one-hour period on 27 April 2023, representing wind conditions and available power for the evaluation period on 3 February 2024.

Figure 5.8 shows the response of the Chalmers wind turbine model during the selected hour, which includes instances where the grid frequency exceeded 50.1 Hz, activating FCR-D Down operation. When the frequency crosses this threshold, the turbine responds by increasing spilled power through a reduction in output power, as expected. Outside of the activation range, the turbine maintains spilled power at its base level, as expected from the controller design. The observed downward spikes in spilled and output power are caused by reductions in wind speed, which lead to lower available power and thereby reduce the spill factor, while the upward spikes are related to unknown issues in the control system of the model.

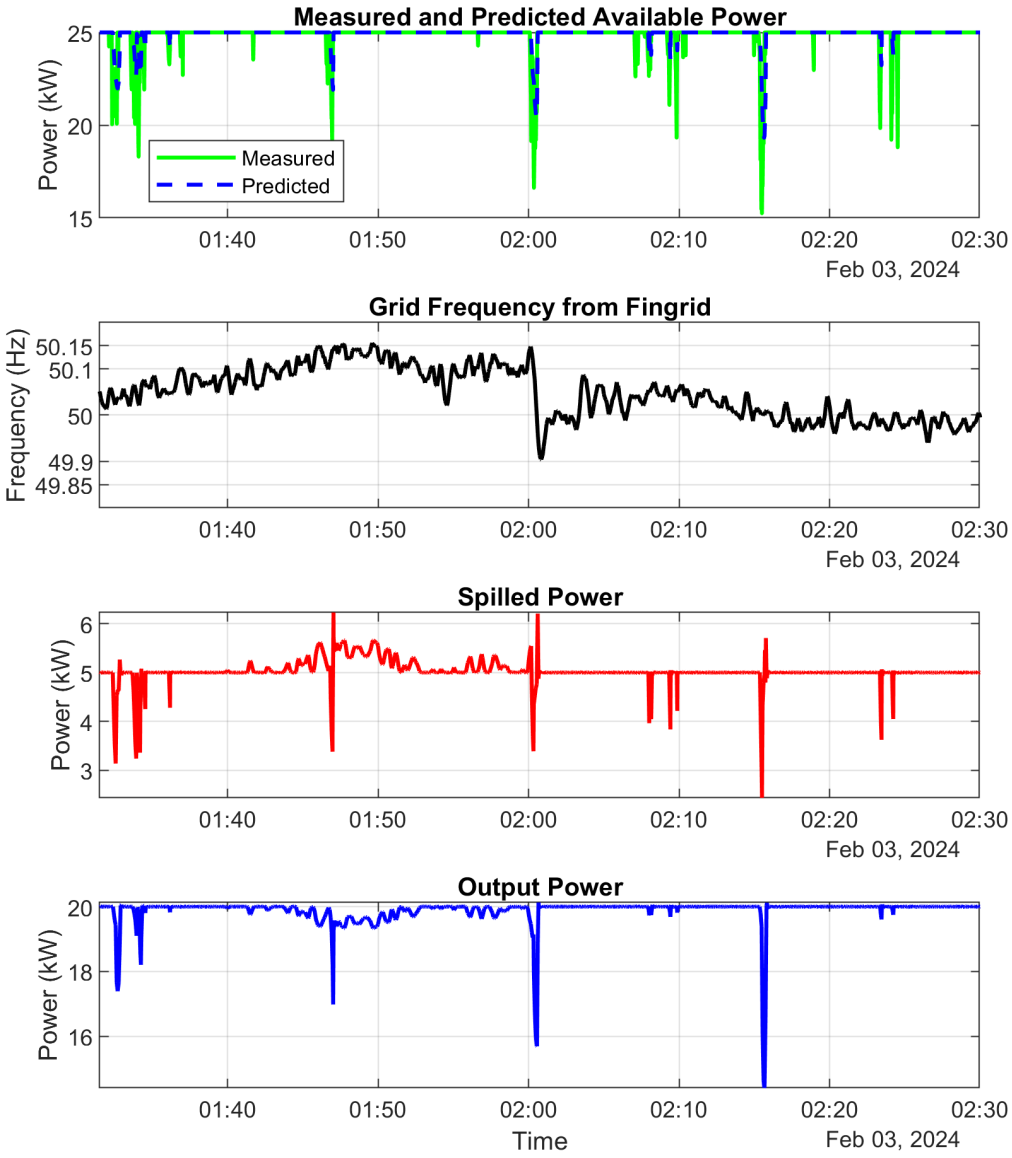

Figure 5.8: One-hour overview of the Chalmers wind turbine model response on 3 February 2024 during an FCR-D Down event.

A zoomed-in view of the grid frequency exceeding 50.1 Hz is shown in Figure 5.9, together with the corresponding spilled power and reference spilled power. The red curve represents the reference response assuming constant rated power. The simulated spilled power generally aligns with the reference, except during spikes caused by fluctuations in available power and the turbine's control system. During FCR-D Down activation, the frequency controller responds to the frequency deviations as intended and maintains the base spill level when outside the activation range.

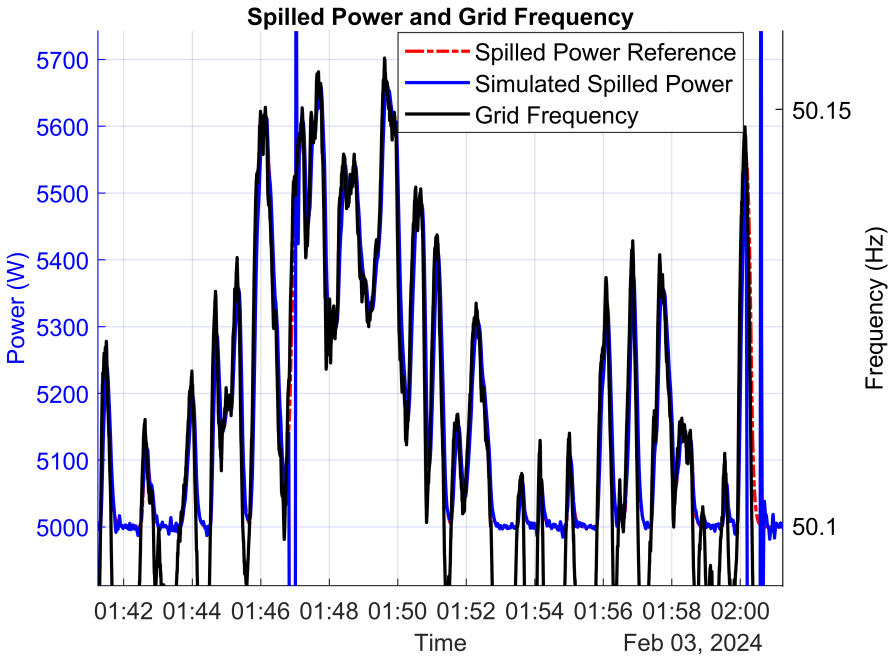

Figure 5.9: Zoomed-in view of spilled power and grid frequency for the Chalmers wind turbine model when frequency exceeded 50.1 Hz, activating FCR-D Down response.

A further zoomed-in view of two sample periods when the frequency exceeded 50.1 Hz is shown in Figure 5.10 and Figure 5.11 below. These plots provide a more detailed view of how the spilled power responds to frequency variations and the timing of the activation. The response begins within approximately 100 ms after the frequency crosses the 50.1 Hz threshold, followed by a gradual increase shaped by the controller's filter settings. Since the model of Chalmers wind turbine was designed to serve as a reference for meeting the minimum requirements from Svenska kraftnät, the droop and time response are estimated here for later comparison with the performance of the commercial wind turbines at Kronoberget at the same sample points. Two time intervals were selected for each sample, each lasting 15 seconds, and are highlighted in the figures. These intervals are used to estimate the magnitude and timing of the response.

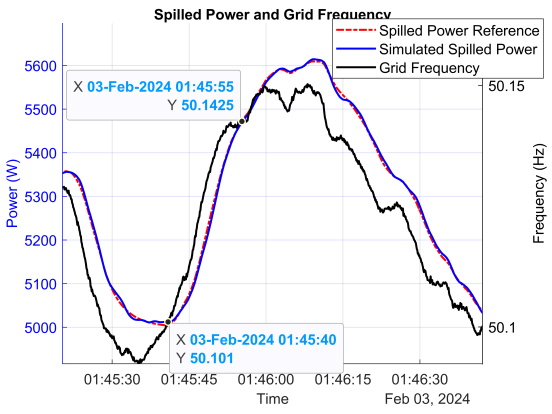

Figure 5.10: Sample 1: Zoomed-in spilled power response between 01:45:40 and 01:45:55.

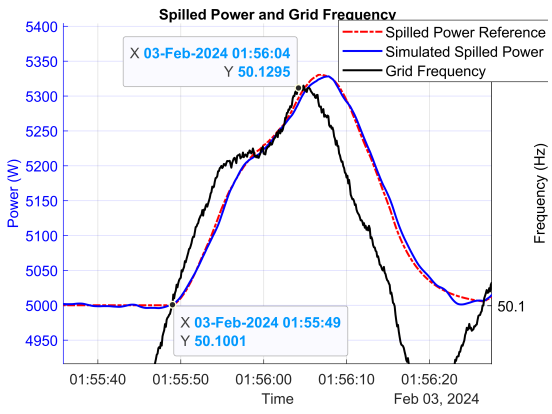

Figure 5.11: Sample 2: Zoomed-in spilled power response between 01:55:49 and 01:56:04.

The estimated droop response for the two sample periods is shown in Figure 5.12 and Figure 5.13. The response is based on normalized spilled power, expressed as a fraction of the available reserve, following the method described in the evaluation section. Each plot shows all data points within the selected 15-second interval in blue, a red dotted line representing the linear best fit used to estimate the droop, and a black dashed line indicating the expected Svk droop response. This Svk line assumes a linear step in frequency from 50.1 Hz to the maximum frequency within the interval and serves only as a benchmark. Since Svenska kraftnät uses step responses for compliance testing, while the analysis here is based on measured grid frequency, the Svk line does not represent a requirement but helps interpret how strongly the turbine responded in relative terms.

The slope of the fitted line indicates the rate at which the available reserve is activated in response to frequency deviation. For Sample 1, the estimated droop is 0.50 Hz/p.u., and for Sample 2 it is 0.41 Hz/p.u. These values suggest that full activation of the available reserve would occur over a frequency deviation of 0.50 Hz and 0.41 Hz, respectively, measured above 50.1 Hz. The lower values observed here reflect that only part of the reserve was activated within the analyzed interval, as the turbine response ramps up gradually due to the frequency profile and controller filtering. The difference between the two values shows how the activation varied between the two events. Similar behavior can be observed during the ramp-down events, shown in Appendix A.3.1.

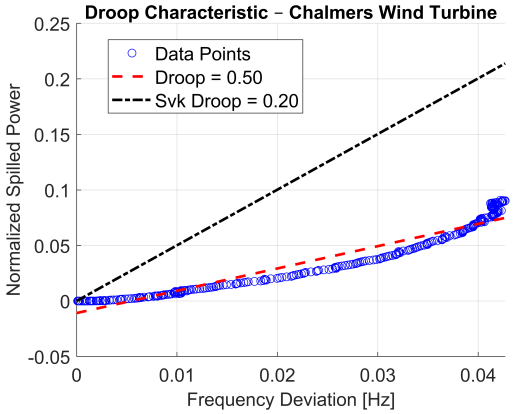

Figure 5.12: Sample 1: Estimated droop response for the Chalmers wind turbine model between 01:45:40 and 01:45:55.

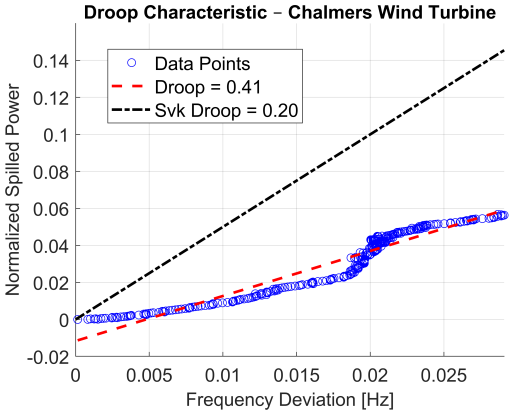

Figure 5.13: Sample 2: Estimated droop response for the Chalmers wind turbine model between 01:55:49 and 01:56:04.

The estimated ramp rate for the two sample periods is shown in Figure 5.14 and Figure 5.15. As with the droop estimation, the spilled power is normalized by the available reserve. In this case, the x-axis represents time rather than frequency deviation. Each plot shows all data points within the selected 15-second interval in blue, and a red dotted line indicating the linear best-fit slope used to estimate the ramp rate. For Sample 1, the estimated ramp rate is 0.0071 s^{-1}, and for Sample 2 it is 0.0040 s^{-1}, meaning that the turbine increased its spilled power by 0.71% and 0.40% of the available reserve per second, respectively. The difference between the two samples reflects variation in the turbine's dynamic response, shaped by the frequency input and how it is processed by the controller's filtering. The corresponding ramp-

down responses for these events are shown in Appendix A.3.1.

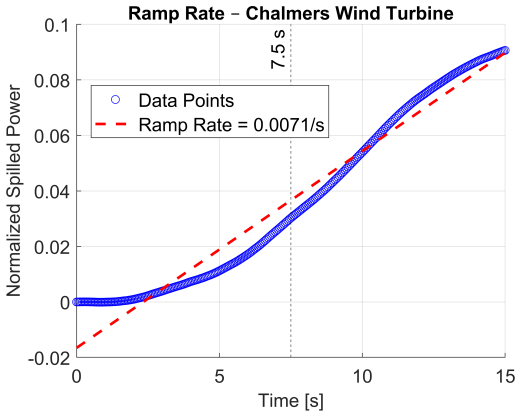

Figure 5.14: Sample 1: Estimated ramp rate for the Chalmers wind turbine model between 01:45:40 and 01:45:55.

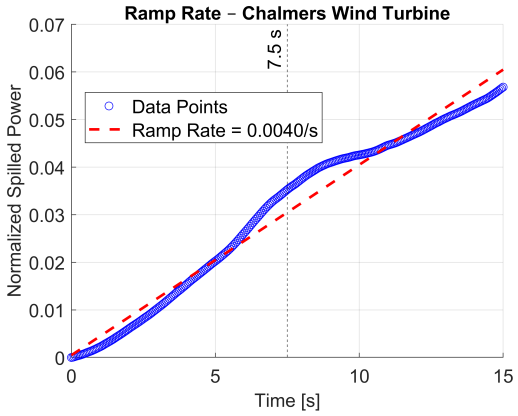

Figure 5.15: Sample 2: Estimated ramp rate for the Chalmers wind turbine model between 01:55:49 and 01:56:04.

5.1.4.2 Case 2: 4 February 2024

The same data input from 27 April 2023 is used to represent wind conditions and available power for the evaluation period on 4 February 2024. Figure 5.16 shows once again the predicted and measured wind speeds together with the corresponding available power for a specific hour on 4 February 2024. This hour was selected because the grid frequency exceeded 50.1 Hz at several instances and can be used to evaluate the FCR-D Down response under a different frequency profile than in the previous case.

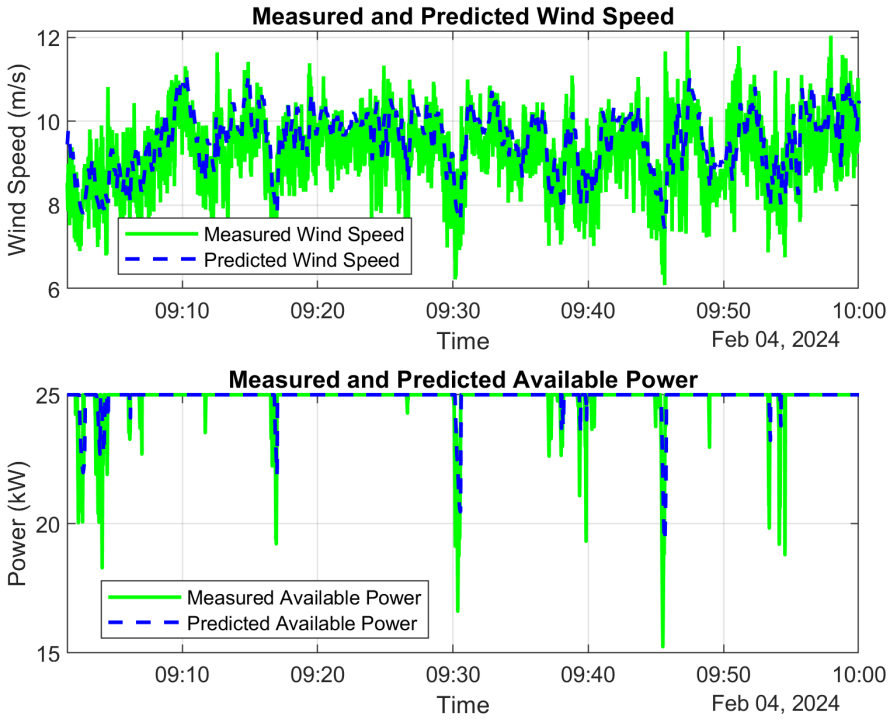

Figure 5.16: Predicted wind speed and available power for the Chalmers wind turbine model during a one-hour period on 27 April 2023, representing wind conditions and available power for the evaluation period on 4 February 2024.

Figure 5.17 shows the response of the Chalmers wind turbine model during the selected hour on 4 February 2024. The grid frequency exceeded 50.1 Hz at several instances, triggering FCR-D Down operation with higher peaks and more frequent changes compared to 3 February. When the frequency crosses the activation threshold, the turbine responds by increasing spilled power and reducing output power, following the controller logic as before. Outside the activation range, spilled power remains at its base level, consistent with the expected behavior. Similar to 3 February, spikes caused by fluctuations in available power can be seen, along with opposite spikes likely related to issues in the control system of the model.

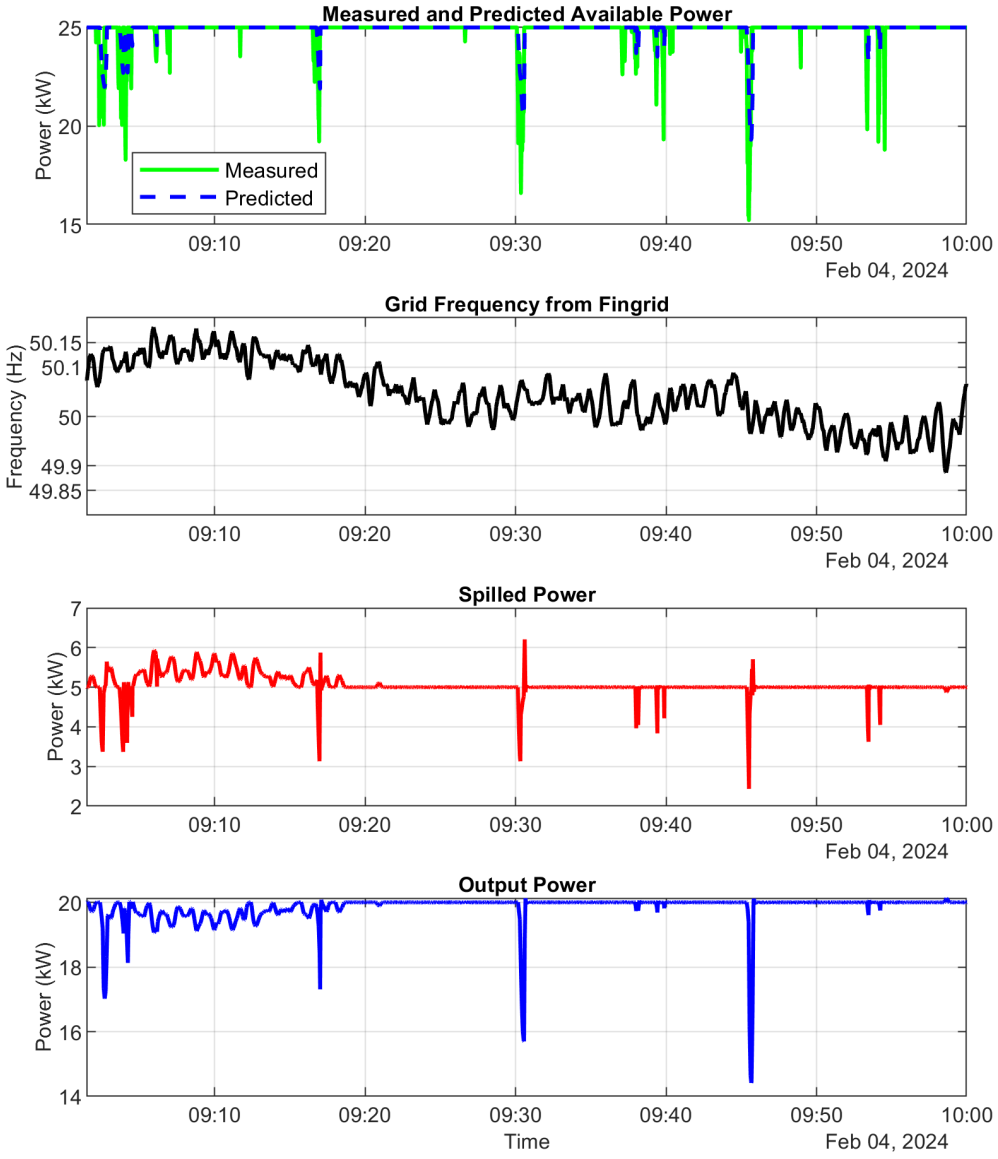

Figure 5.17: One-hour overview of the Chalmers wind turbine model on 4 February 2024 during an FCR-D Down event.

Figure 5.18 provides a zoomed-in view of the previous figure, focusing on the period when the grid frequency exceeded 50.1 Hz and activated the FCR-D Down response.

The spilled power is shown together with the reference response, assuming constant rated power. The turbine response generally follows the frequency variations, with a delay similar to that observed on 3 February, which is influenced by both the controller design and the characteristics of the frequency profile.

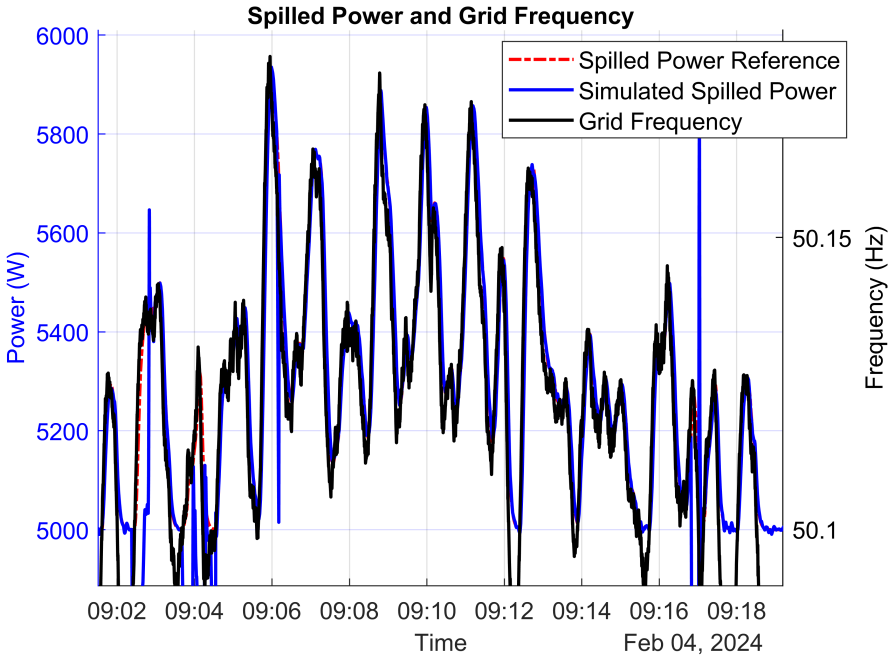

Figure 5.18: Zoomed-in view of spilled power and grid frequency for the Chalmers wind turbine model when frequency exceeded 50.1 Hz on 4 February 2024, activating FCR-D Down response.

A further zoomed-in view of two frequency events on 4 February 2024 is shown in Figure 5.19 and Figure 5.20. These plots provide a detailed view of the spilled power response following frequency deviations above 50.1 Hz. As on 3 February, the response begins shortly after the threshold is crossed and follows a gradual increase shaped by the controller's design. One interval of 11 seconds and one of 10 seconds were selected for estimating droop and ramp rate, using the same method as before for comparison with Kronoberget.

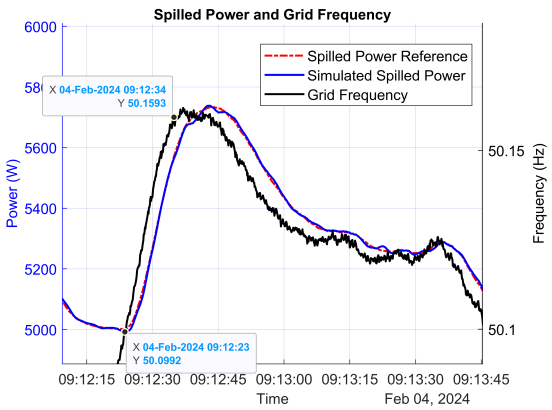

Figure 5.19: Sample 1: Zoomed-in spilled power response between 09:12:23 and 09:12:34.

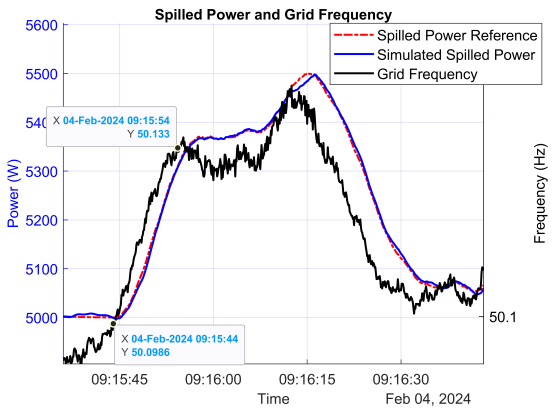

Figure 5.20: Sample 2: Zoomed-in spilled power response between 09:15:44 and 09:15:54.

The estimated droop response for the two sample periods on 4 February 2024 is shown in Figure 5.21 and Figure 5.22. The response is once again based on normalized spilled power, expressed as a fraction of the available reserve, using the same method as in the 3 February analysis. The estimated droop is 0.18 Hz/p.u. for Sample 1 and 0.14 Hz/p.u. for Sample 2, with all data points shown in blue and the fitted droop line in red. As in the 3 February analysis, a black dashed line representing the indicative Svk droop response is included for reference. The corresponding ramp-down responses can be found in Appendix A.3.1.

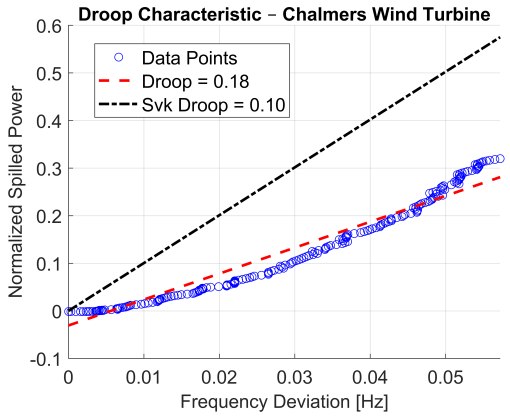

Figure 5.21: Sample 1: Estimated droop response for the Chalmers wind turbine model between 09:12:23 and 09:12:34.

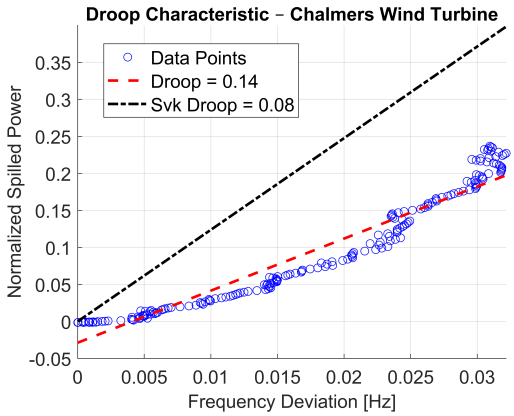

Figure 5.22: Sample 2: Estimated droop response for the Chalmers wind turbine model between 09:15:44 and 09:15:54.

The estimated ramp rate for the two sample periods on 4 February 2024 is shown in Figure 5.23 and Figure 5.24. For Sample 1, the estimated ramp rate is 0.0326 s^{-1}, and for Sample 2 it is 0.0265 s^{-1}, meaning that the turbine increased its spilled power by 3.26% and 2.65% of the available reserve per second, respectively. As on 3 February, the difference between the two samples reflects variation in the turbine's dynamic response, shaped by the characteristics of the grid frequency and the controller's filtering. Ramp-down results from the same events are presented in Appendix A.3.1.

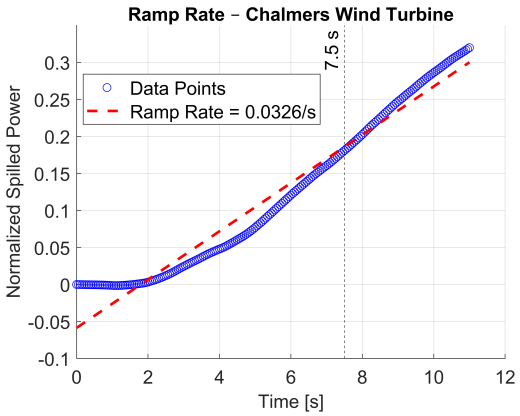

Figure 5.23: Sample 1: Estimated ramp rate for the Chalmers wind turbine model between 09:12:23 and 09:12:34.

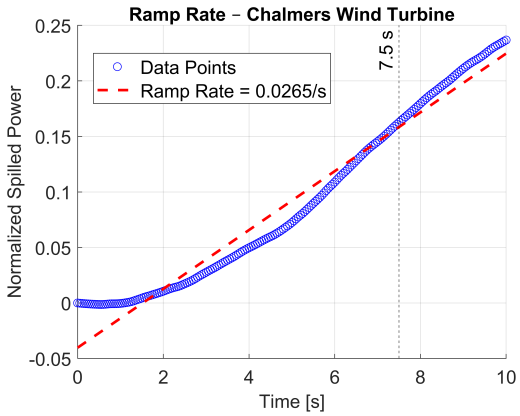

Figure 5.24: Sample 2: Estimated ramp rate for the Chalmers wind turbine model between 09:15:44 and 09:15:54.

5.2 Evaluation of Kronoberget wind farm

Kronoberget wind farm was evaluated for the same two days as the Chalmers wind turbine model to allow a fair comparison of their operation and to assess how well the commercial units deliver ancillary services, using Chalmers as a reference for meeting Svenska kraftnät's requirements. On both days, WTG15 was not in operation, reducing the total available capacity to approximately 57 MW.

5.2.1 Case 1: 3 February 2024

The evaluation of 3 February consists of a full-day analysis and a one-hour analysis to compare with the Chalmers wind turbine model. This day was chosen due to the high wind speed, to evaluate how the wind farm operates close to rated power.

5.2.1.1 Full day - analysis

Figure 5.25 shows the wind speed and available power for Kronoberget wind farm on 3 February 2024. The wind speed is measured at WTG5, which, due to its placement and the wind direction on this day, is exposed to the incoming wind and is therefore less affected by wake effects. This makes it suitable for representing the general wind conditions at the site. The available power represents the total from all turbines. Overall, it was a day with high wind availability, and the farm operated close to rated power for most of the day. The drop in available power between 10:00 and 11:40 is due to one turbine being shut down.

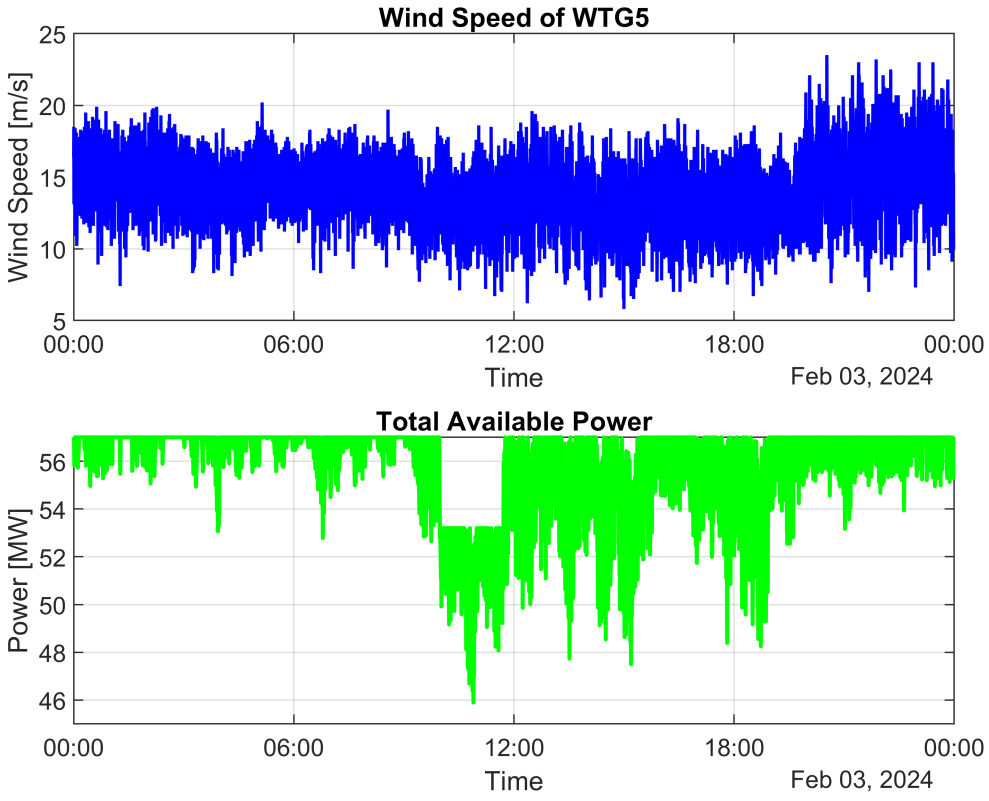

Figure 5.25: Wind speed and available power for turbine 5 at Kronoberget wind farm during the full day on 3 February 2024. The turbine is used to represent the wind conditions at the site.

An overview of Kronoberget wind farm on this day is shown in Figure 5.26. The figure includes the evaluation parameters used to analyze how the wind farm provides frequency support and how this compares to the submitted and accepted bids for FCR-D Down. It can be seen that the wind farm maintains a base spilled power of around 3 MW, even though it is only prequalified for FCR-D Down, which does not require a power reserve. A possible explanation, based on the figure, is that the output power is regulated using the spilled power due to grid limitations. When the available power fluctuates, the spilled power adjusts to keep the output power relatively constant by reducing the amount of curtailed power. Another observation is that the base spilled power changes sometimes during the day. For example, between 09:00 and 10:00 the spilled power increases from around 3 MW to 7 MW while all turbines remain active, which supports the interpretation that the output is being limited due to grid constraints.

The figure also shows that when the frequency exceeds 50.1 Hz, the spilled power increases, which is the expected behavior for FCR-D Down. The bid plot shows how much output power the wind farm offers to reduce during a disturbance, and the accepted bid shows how much of the offer was accepted for that specific hour. By plotting the accepted bid minus the spilled power, it becomes possible to see how closely the farm follows the committed capacity. For this day, the difference remained high, suggesting that Svenska kraftnät did not need to activate much of the capacity due to small frequency deviations.

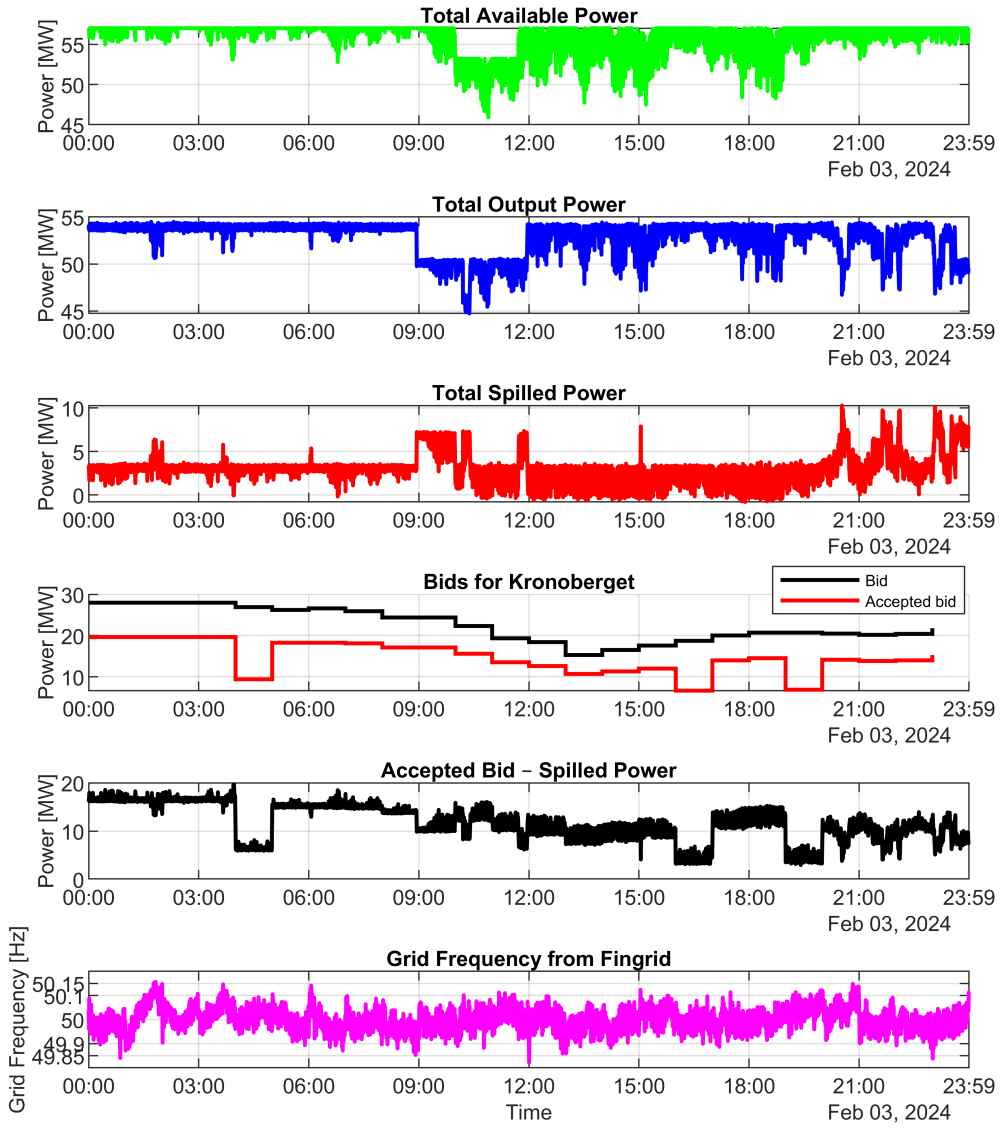

Figure 5.26: Full-day overview of Kronoberget wind farm on 3 February 2024.

Figure 5.27 shows an overview of the control system for WTG7 to support frequency regulation. Details for the other turbines are provided in Appendix A.4. For this day, the pitch angle mostly follows the wind speed to keep the turbine near rated power for safety reasons. However, it also increases when the frequency exceeds 50.1 Hz. This is harder to observe directly, but it appears more clearly in the spilled power plot. The turbines operate on different schedules, and 15 out of 16 were active in providing ancillary services during various events throughout the day.

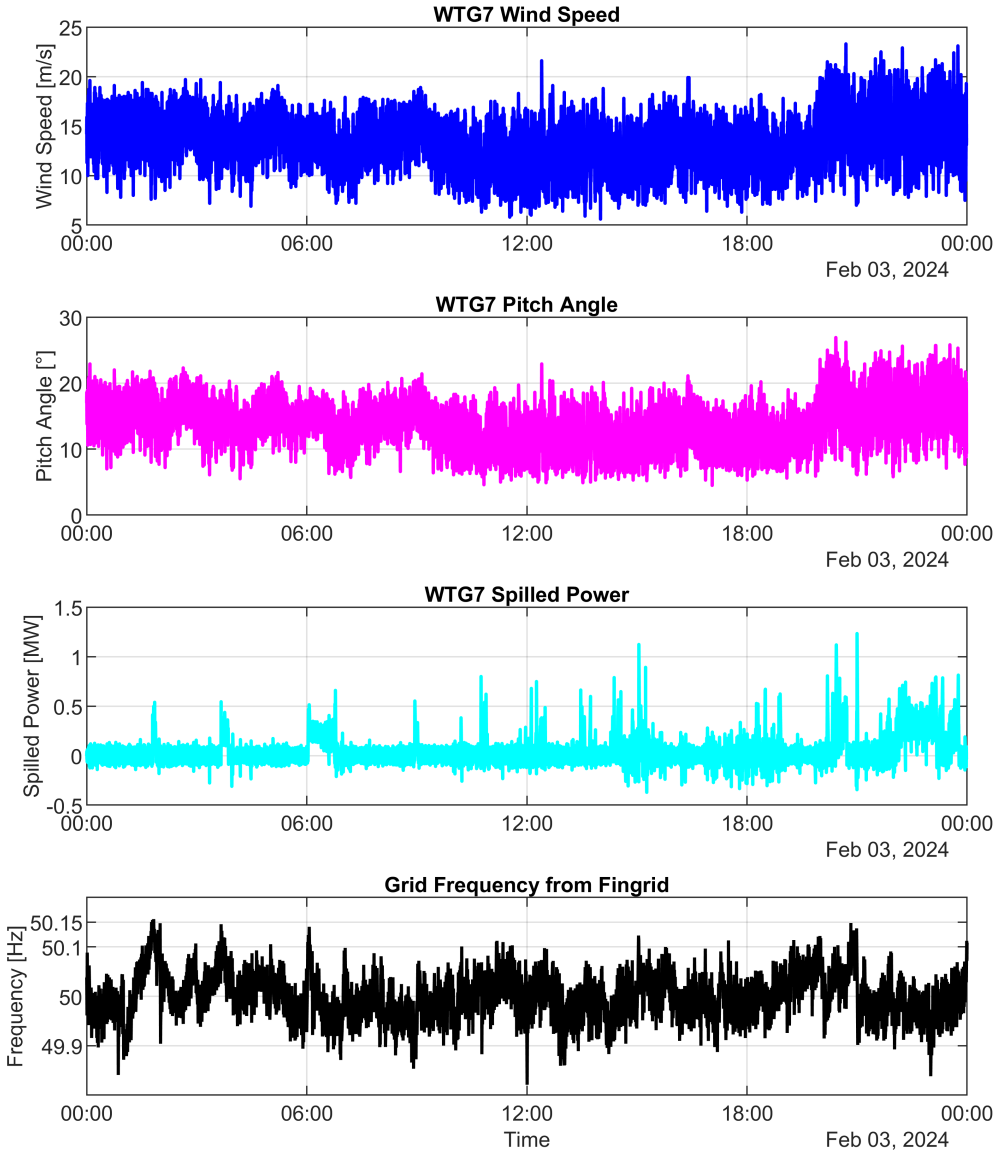

Figure 5.27: Full-day overview of turbine 7 at Kronoberget wind farm on 3 February 2024.

5.2.1.2 Hour - analysis

A one-hour analysis of Kronoberget wind farm was done to compare with the Chalmers wind turbine model for the same hour. An overview of this period is shown in Figure 5.28. The spilled power increases when the frequency exceeds 50.1 Hz, similar to what was observed for the Chalmers wind turbine model, which is expected for FCR-D Down. Otherwise, it remains at the base level of around 3 MW when FCR-D Down is not activated. The figure also shows that the bid is high due to the high available power, while Svenska kraftnät does not need to activate much of the capacity because of the small frequency disturbances.

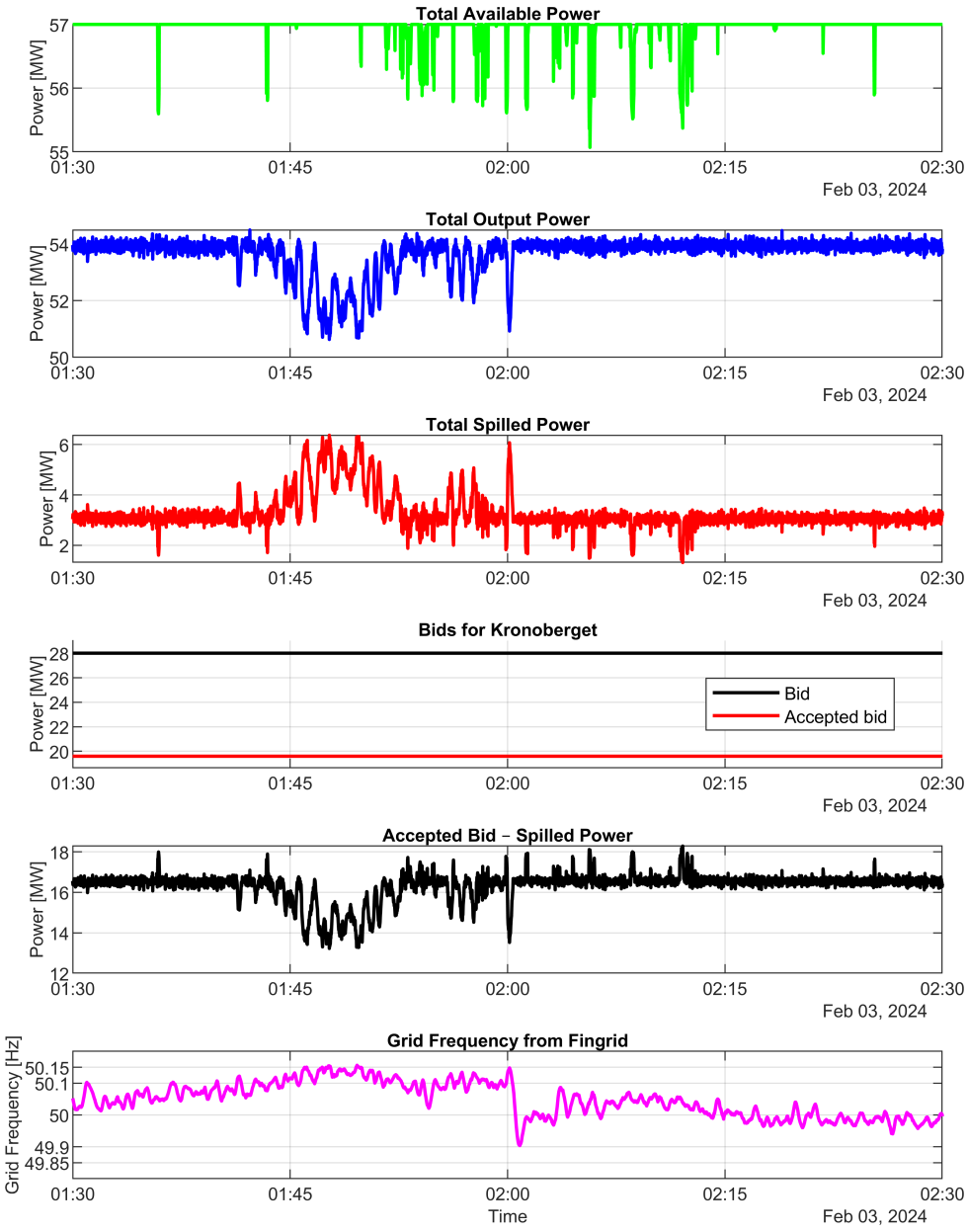

Figure 5.28: One-hour overview of spilled power for Kronoberget wind farm on 3 February 2024.

Figure 5.29 shows the zoomed-in view of the frequency event where FCR-D Down was activated. The spilled power from the wind farm increases when the frequency exceeds 50.1 Hz and appears to follow the variations with almost no delay. When the frequency is below the activation threshold, the spilled power remains at the base level of around 3 MW.

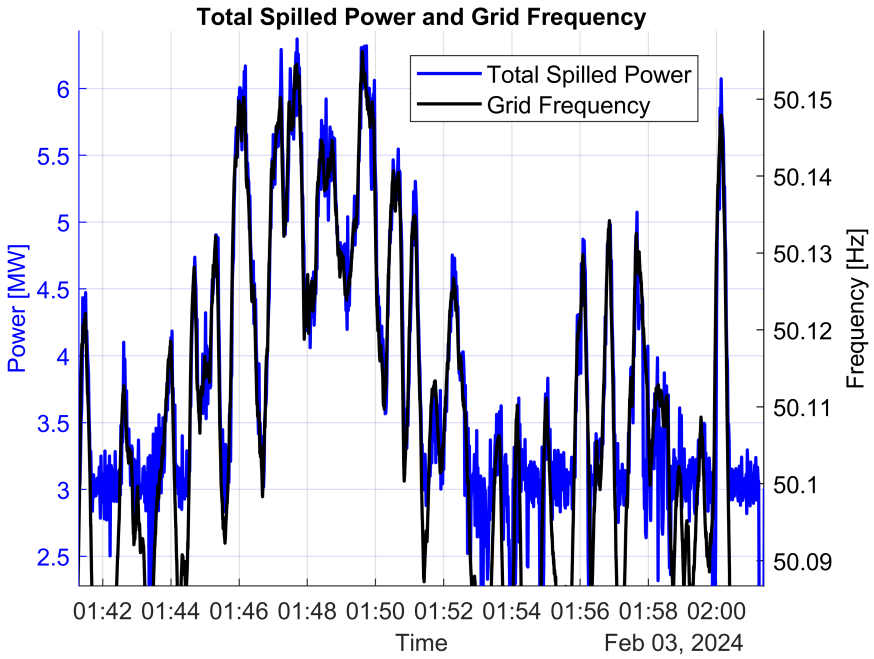

Figure 5.29: Zoomed-in view of spilled power and grid frequency for Kronoberget wind farm when frequency exceeded 50.1 Hz, activating FCR-D Down response.

A further zoomed-in view of two selected events from the frequency response is shown in Figure 5.30 and Figure 5.31. These plots cover the same time intervals and use the same data labels as analyzed for the Chalmers wind turbine model, and are used to estimate the ramp rate and droop. It can be seen that the spilled power here shows a more aggressive response and follows the frequency closely with almost no delay. Similar to the Chalmers wind turbine model, the response when the frequency exceeds 50.1 Hz occurs within a few hundred milliseconds, although this is slightly harder to observe here due to the sampling rate. The spilled power appears more spiky because it is sampled at 1 Hz, while the frequency is sampled at 10 Hz, but the overall shape still follows the expected behavior.

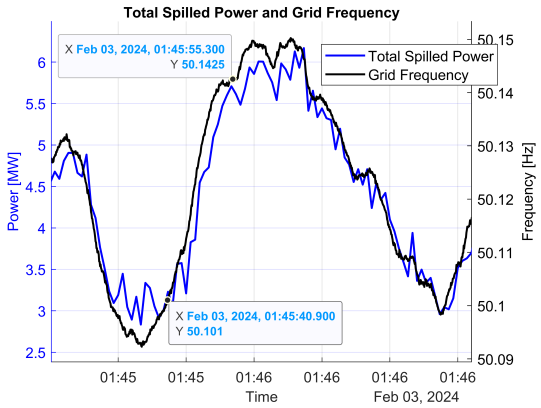

Figure 5.30: Sample 1: Zoomed-in spilled power response between 01:45:40 and 01:45:55.

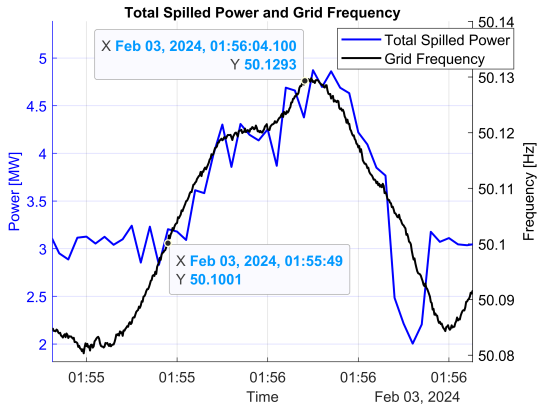

Figure 5.31: Sample 2: Zoomed-in spilled power response between 01:55:49 and 01:56:04.

The droop response of Kronoberget wind farm for the two samples is shown in

Figure 5.32 and Figure 5.33. The blue dots represent the selected data points within each interval, and the red dotted line indicates the linear best-fit used to estimate the droop. The response is normalized to the available regulation range, which for Kronoberget is assumed to correspond to the accepted bid from Svenska kraftnät. In both cases, the estimated droop is approximately 0.28 Hz/p.u., meaning that full activation of the available reserve would occur over a 0.28 Hz frequency deviation above 50.1 Hz. Since the frequency deviations during these intervals were small, only part of the reserve was activated. Each plot also includes the Svk droop line for comparison. In these samples, Kronoberget's response lies closer to that line than in the Chalmers case, indicating a steeper power increase relative to the frequency deviation compared to the Chalmers wind turbine model. The ramp-down responses for the same events are presented in Appendix A.3.2, where Kronoberget's response appears even stronger during the recovery phase.

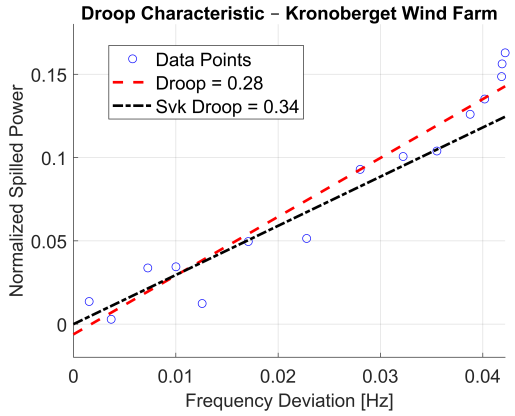

Figure 5.32: Sample 1: Estimated droop response for Kronoberget wind farm between 01:45:40 and 01:45:55.

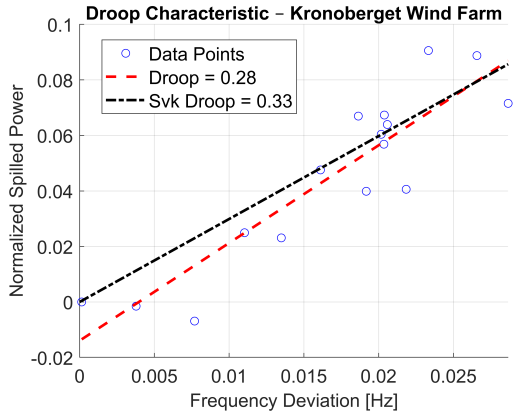

Figure 5.33: Sample 2: Estimated droop response for Kronoberget wind farm between 01:55:49 and 01:56:04.

The estimated ramp rate of Kronoberget wind farm for the two samples is shown in Figure 5.34 and Figure 5.35. As before, the spilled power is normalized to the accepted bid from Svenska kraftnät. For Sample 1, the ramp rate is 0.0119 s^{-1}, and for Sample 2 it is 0.0056 s^{-1}, meaning that the spilled power increased by approximately 1.19% and 0.56% of the accepted bid per second, respectively, during these two intervals. The corresponding ramp-down rates, reflecting how the output decreased after each event, are presented in Appendix A.3.2.

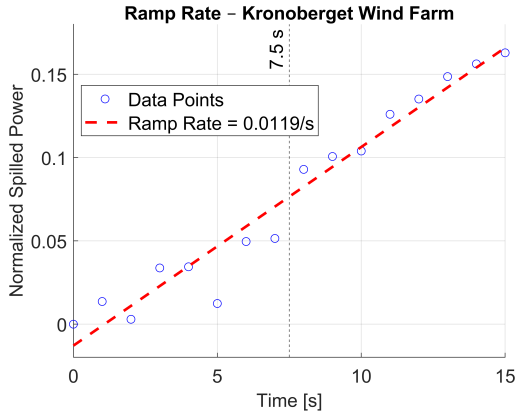

Figure 5.34: Sample 1: Estimated ramp rate for Kronoberget wind farm between 01:45:40 and 01:45:55.

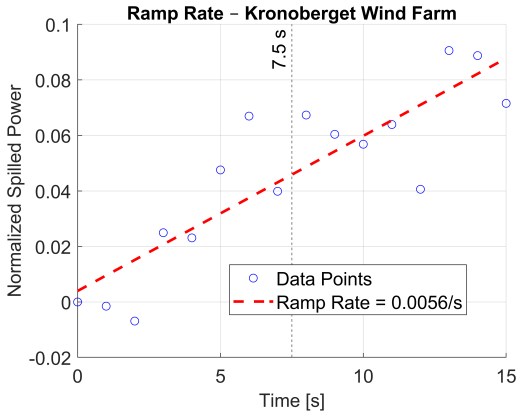

Figure 5.35: Sample 2: Estimated ramp rate for Kronoberget wind farm between 01:55:49 and 01:56:04.

A zoomed-in view of the one-hour control system analysis for WTG7 is shown in Figure 5.36. It is easier to see that the spilled power follows the frequency when FCR-D Down is activated, while changes in pitch angle are more difficult to observe due to the high wind speed on this day. At the beginning of the period, the frequency is within the FCR-D Down activation range, but the turbine is not spilling any power. This suggests that a central control system in the wind farm decides which turbines are selected to spill during a disturbance. For this event, 13 out of 16 turbines were actively spilling power.

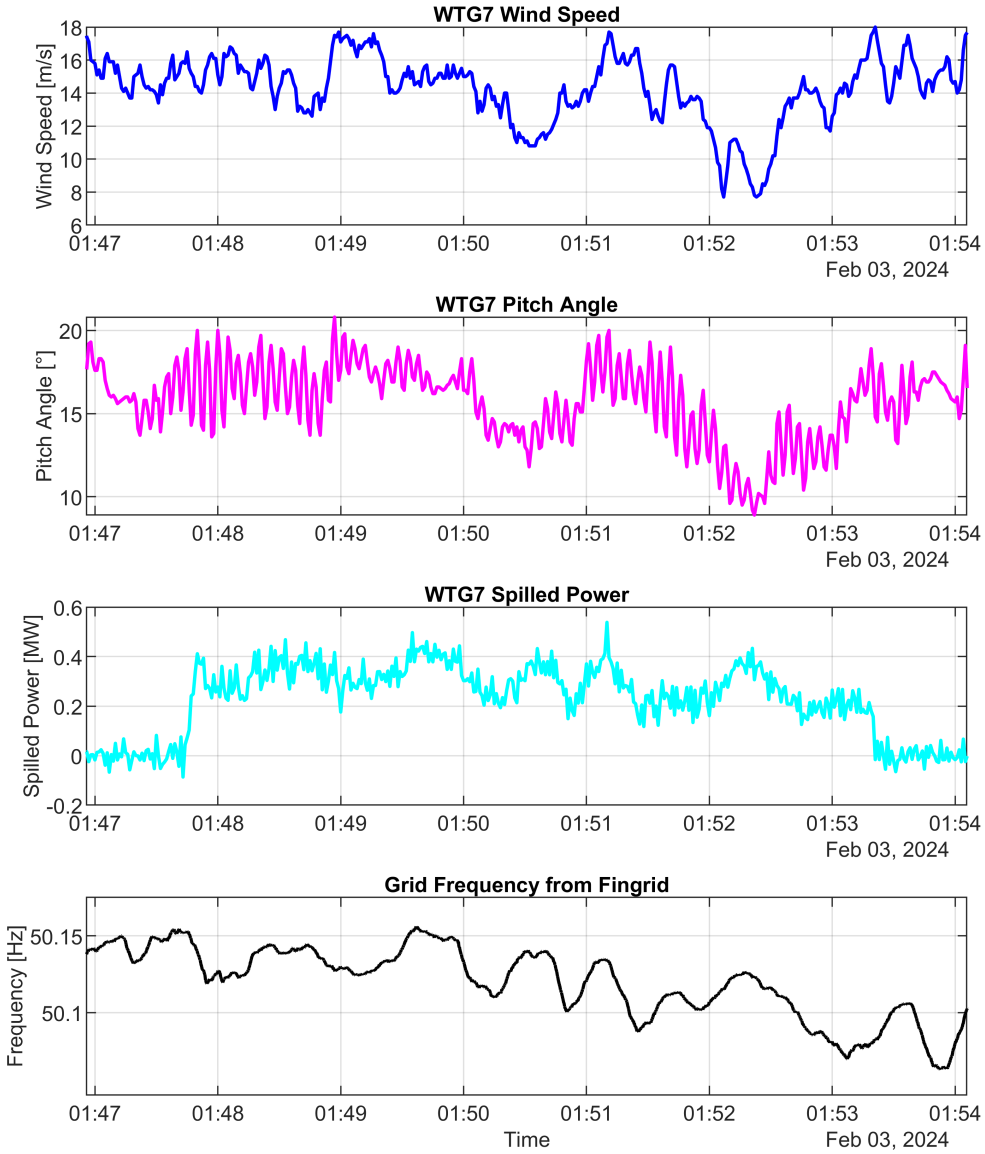

Figure 5.36: One-hour overview of turbine 7 at Kronoberget wind farm on 3 February 2024.

5.2.2 Case 2: 4 February 2024

The evaluation of 4 February follows the same structure as in the previous case, with a full-day analysis and a one-hour period selected for closer comparison. This day was chosen due to its variable power availability, making it suitable for evaluating how the wind farm responds under conditions where it does not operate near rated power.

5.2.2.1 Full day - analysis

Figure 5.37 shows the wind speed and available power at the Kronoberget wind farm on 4 February 2024. Wind speed was measured at WTG5 once again, which, due to its position and the wind direction on this day, was directly exposed to the

incoming wind and therefore less affected by wake effects. This made it suitable for representing the wind conditions at the site. The wind conditions varied throughout the day, with rated power reached in the early hours, followed by more variable conditions later on. This confirms that the day is suitable for evaluating the farm's response under non-rated power conditions.

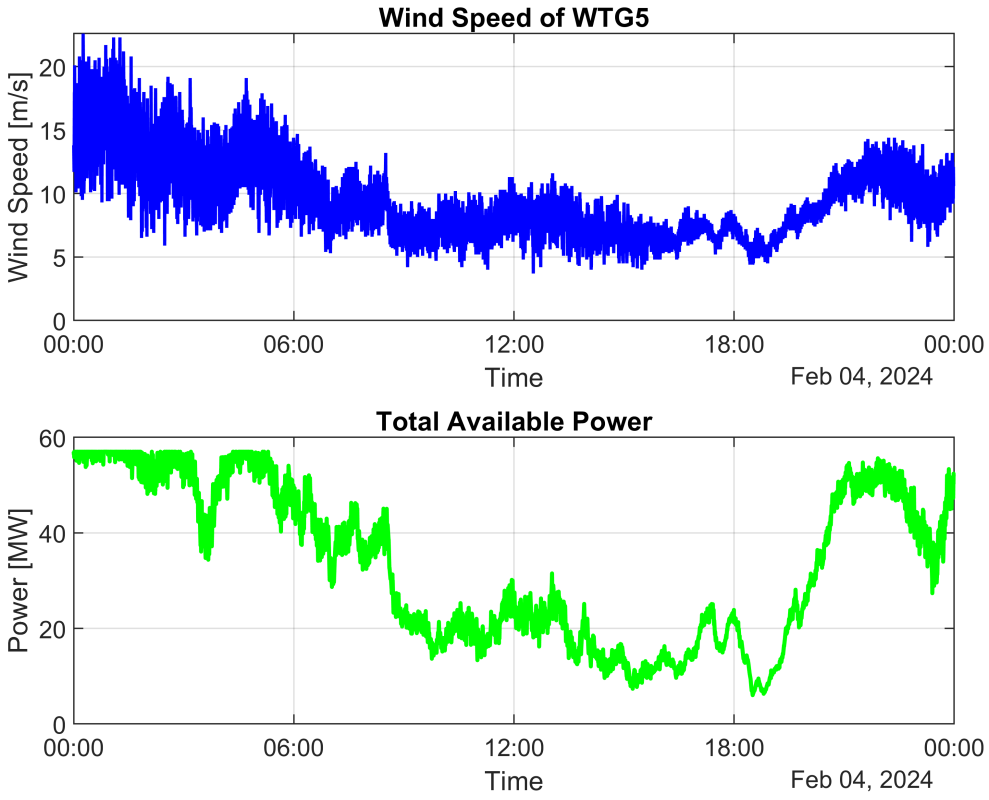

Figure 5.37: Wind speed and available power for turbine 5 at Kronoberget wind farm during the full day on 4 February 2024. The turbine is used to represent the wind conditions at the site.

Figure 5.38 shows a full-day overview of Kronoberget wind farm on 4 February 2024. The figure includes the evaluation parameters used to analyze how the farm provides frequency support and how this relates to the submitted and accepted bids for FCR-D Down. The available power varies more throughout the day, with rated values reached in the early morning and lower levels observed during the rest of the day. Similar to 3 February, the output power remains more stable than the available power, with a base spill power appearing to smooth fluctuations in the wind, due to grid limitations, but only when a bid is active.

As before, the bid and accepted bid plots show how much capacity was offered and accepted for FCR-D Down each hour. In the early hours, the bids are relatively high due to greater wind availability, while later in the day they are reduced and at sometimes set to zero. Most of the day, the accepted bid is higher than the spilled power, indicating that only part of the committed capacity was used. However, during some periods with low bids, the difference becomes negative, meaning that more power was spilled than what was accepted.

The grid frequency is also shown in the figure, with several instances where it exceeds 50.1 Hz. During these periods, the spilled power increases and output power decreases, which is the expected behavior for FCR-D Down. This response is only observed when a bid has been submitted. When no bid is active, the farm does not adjust its output in response to frequency deviations.

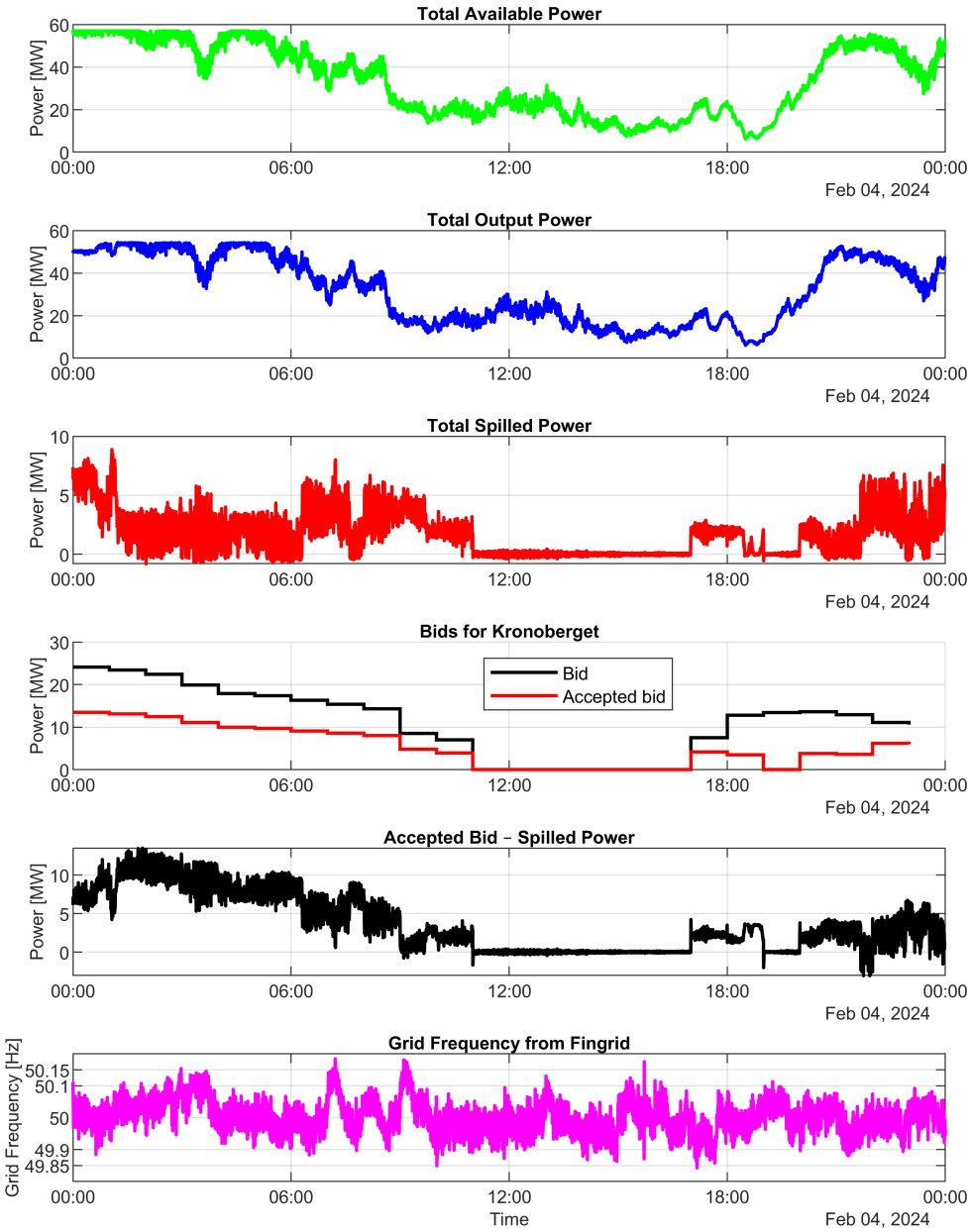

Figure 5.38: Full-day overview of Kronoberget wind farm on 4 February 2024.

Figure 5.39 presents the control behavior of WTG3 throughout 4 February 2024. Additional turbine plots are provided in Appendix A.5. Early in the day, the pitch angle tracks the wind speed to maintain rated power and limit mechanical stress.

Later, as wind levels decrease, the pitch angle remains near its minimum of 3.8 degrees to maximize energy capture. Similar to 3 February, the turbine responds to frequency deviations by increasing the pitch angle when the frequency exceeds 50.1 Hz, reducing power output to support frequency regulation. This can be seen in the spilled power plot, where changes in pitch angle are followed by increased spilled power. All turbines were active at different times during the day and participated in frequency regulation during various events.

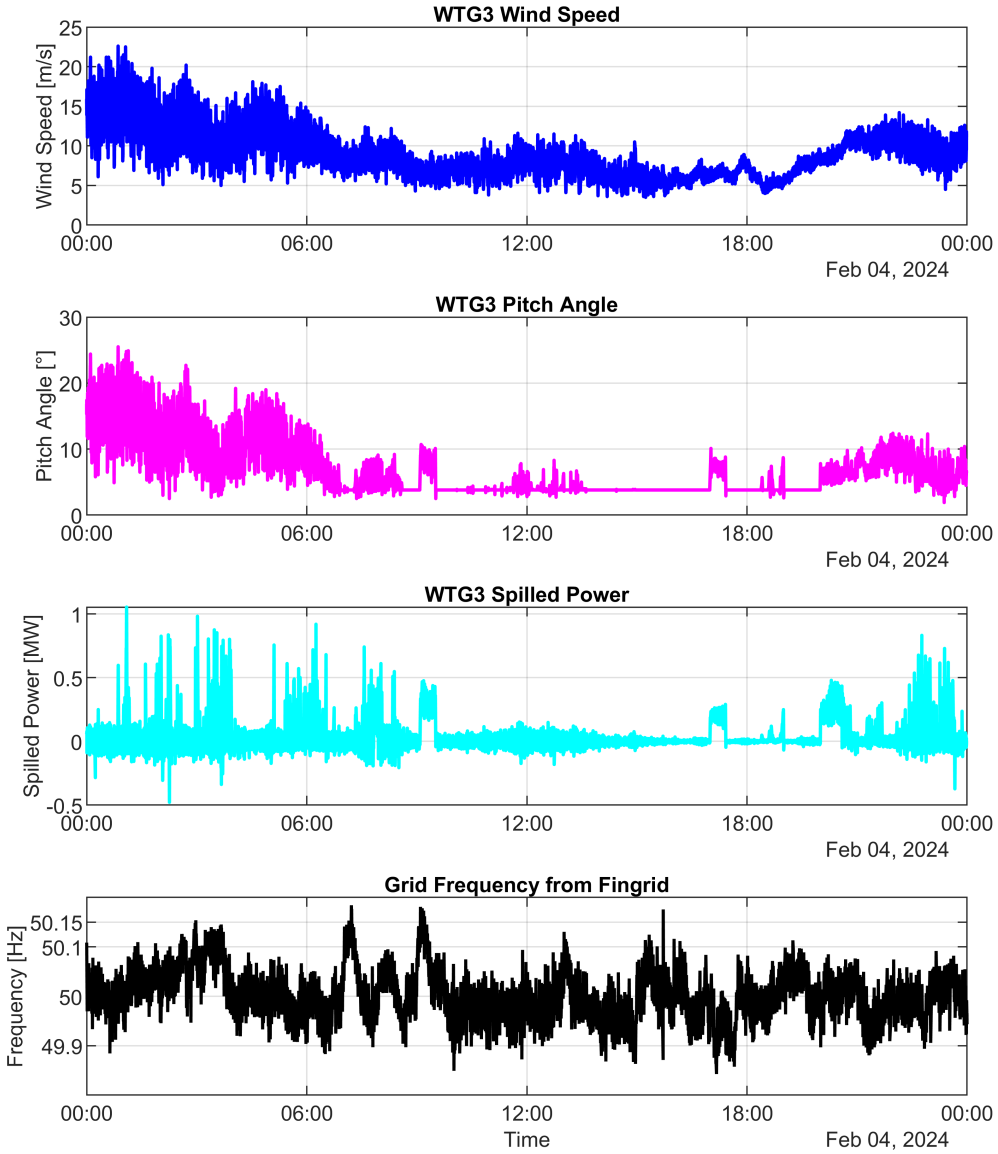

Figure 5.39: Full-day overview of turbine 3 at Kronoberget wind farm on 4 February 2024.

5.2.2.2 Hour - analysis

A one hour analysis of Kronoberget wind farm on 4 February 2024 was done to compare with the Chalmers wind turbine model for the same period. An overview

of this interval is shown in Figure 5.40. The wind farm responds when the frequency exceeds 50.1 Hz, as expected for FCR-D Down, but the response is not as easy to observe in this case. This is because the wind farm regulates its output power to always export as much as the grid limitations allow, which results in smoothing the output when the available power changes, similar to what was observed on 3 February. As a result, some spilling occurs even when the frequency is below 50.1 Hz, which can be seen in the figure. The base spill power during this hour is close to 4 MW, which is used to smooth the output power. Since the accepted bid is 4.8 MW, the reserve margin is small. When a frequency event occurs or the available power suddenly increases, the spilled power exceeds the accepted bid for short periods. This leads to negative values in the reserved capacity plot, showing that the wind farm contributed more than the committed reserve at certain times.

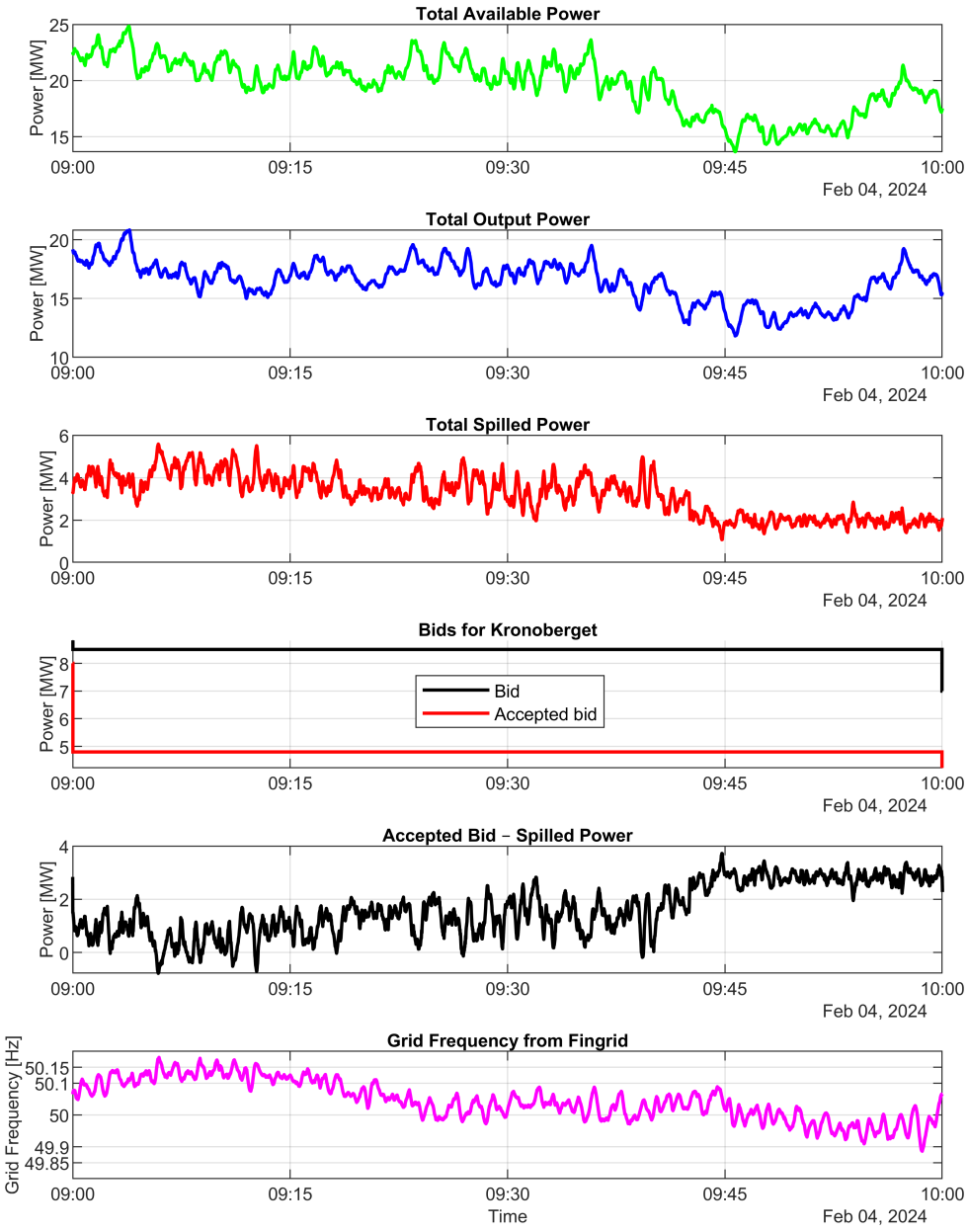

Figure 5.40: One-hour overview of spilled power for Kronoberget wind farm on 4 February 2024.

Figure 5.41 shows the zoomed-in response of the wind farm during the frequency event where FCR-D Down was activated. Compared to 3 February, the available power varied more during this period, which affects how the wind farm responds. As shown in the figure, the spilled power still follows the frequency when it exceeds 50.1 Hz, but the response is not as close as on the previous day. There is more delay and several sharper peaks in the spilled power, which is related to the wind farm also using spill to regulate its output when the available power changes.

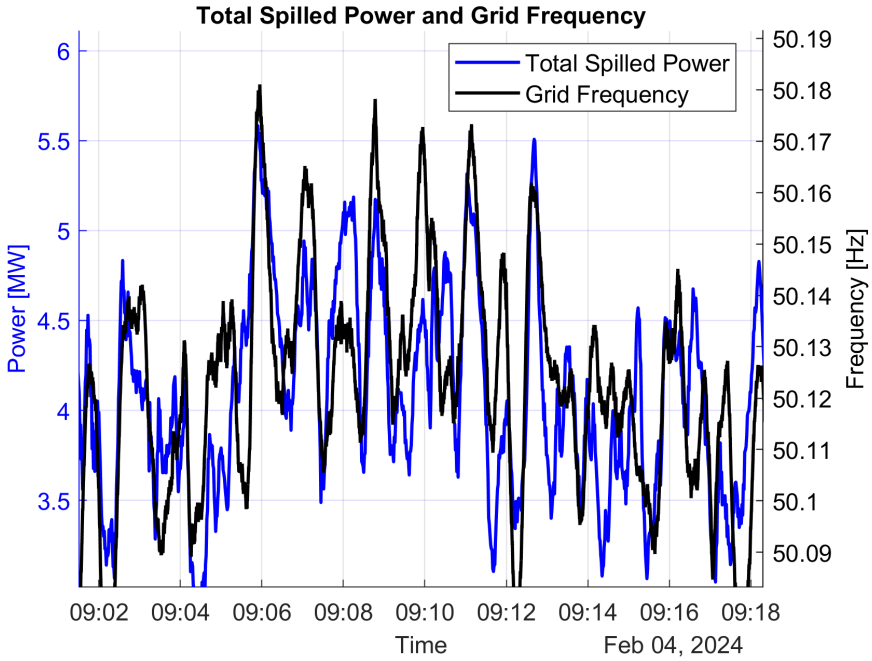

Figure 5.41: Zoomed-in view of spilled power and grid frequency for Kronoberget wind farm when frequency exceeded 50.1 Hz, activating FCR-D Down response.

A more detailed view of two selected events from the frequency response is shown in Figure 5.42 and Figure 5.43 below. These intervals are the same as those studied for the Chalmers wind turbine model and are again used here to estimate the ramp rate and droop for the Kronoberget wind farm, following the same approach as on 3 February. In both cases, the spilled power begins to increase after the frequency exceeds 50.1 Hz, but this is harder to observe here due to the variability in available power. Although the overall response follows the frequency, fluctuations in available power interfere with the expected activation pattern. This is particularly noticeable in Sample 2 around 09:16, where the spilled power increases even though the frequency is decreasing. A base spill power of 3.5 MW was used to set the scale, but the actual baseline may vary slightly due to the changing available power.

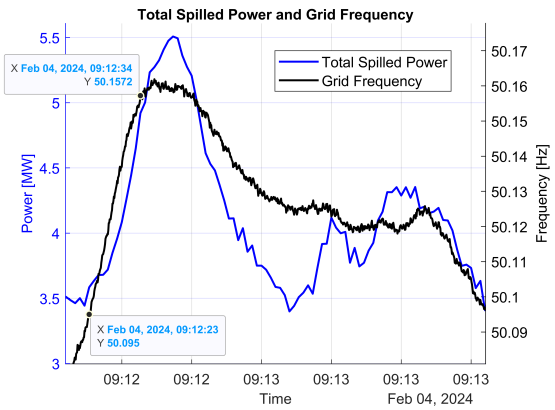

Figure 5.42: Sample 1: Zoomed-in spilled power response between 09:12:23 and 09:12:34.

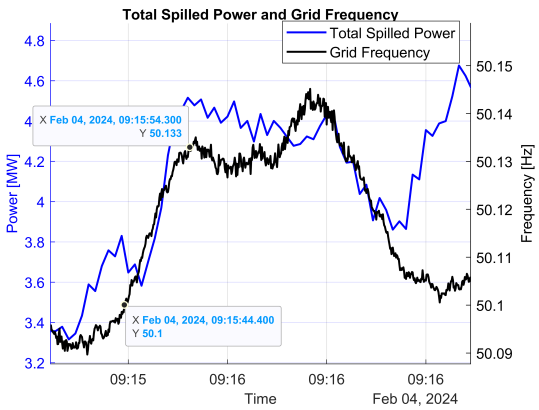

Figure 5.43: Sample 2: Zoomed-in spilled power response between 09:15:44 and 09:15:54.

The droop response of the Kronoberget wind farm for the two samples on 4 February is shown in Figure 5.44 and Figure 5.45. The data points from each interval are plotted together with the estimated droop line. In the first sample, the frequency deviation is larger, which leads to a greater portion of the bid being activated and gives an estimated droop of 0.06 Hz/p.u. This is also reflected in the spilled power, which briefly exceeds the accepted bid, indicating that most of the available power was used to support frequency stability. In the second sample, the frequency deviation is smaller, but the response is stronger due to a faster ramp in frequency. This results in a lower estimated droop of 0.04 Hz/p.u., suggesting a more sensitive reaction to the smaller deviation. As shown earlier in Figure 5.43, there is a short disturbance in available power at the start of Sample 2. For a brief moment, the frequency increases while the spilled power decreases, causing some data points to show negative values. This behavior slightly affects the droop estimate.

As with the 3 February cases, the estimated droop values in both samples are lower than the activation rate defined by Svenska kraftnät, indicating a stronger response from the wind farm compared to the Chalmers wind turbine model. The corresponding ramp-down responses, presented in Appendix A.3.2, show a similarly strong response during the recovery phase.

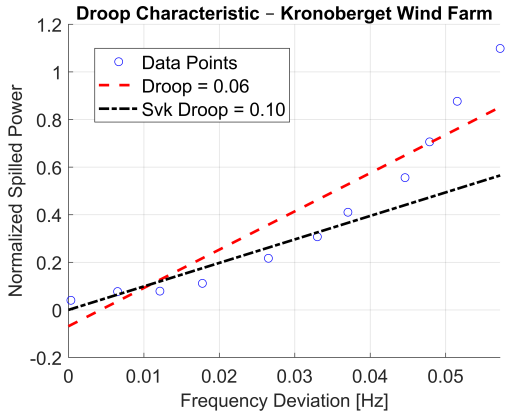

Figure 5.44: Sample 1: Estimated droop response for Kronoberget wind farm between 09:12:23 and 09:12:34.

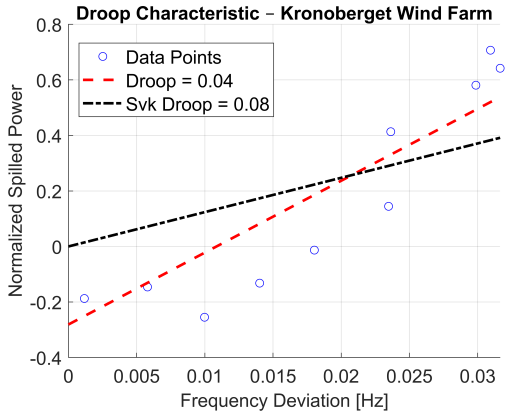

Figure 5.45: Sample 2: Estimated droop response for Kronoberget wind farm between 09:15:44 and 09:15:54.

The estimated ramp rate of Kronoberget wind farm for the two samples is shown in Figure 5.46 and Figure 5.47. Here, the ramp rate is 0.0958 s^{-1} for Sample 1 and 0.0968 s^{-1} for Sample 2. This means that the spilled power increased by approximately 9.58% and 9.68% of the accepted bid per second during the respective intervals. As mentioned earlier, some data points in Sample 2 show negative spilled power due to variations in available power, which affects the slope of the estimated ramp. The corresponding ramp-down responses are presented in Appendix A.3.2.

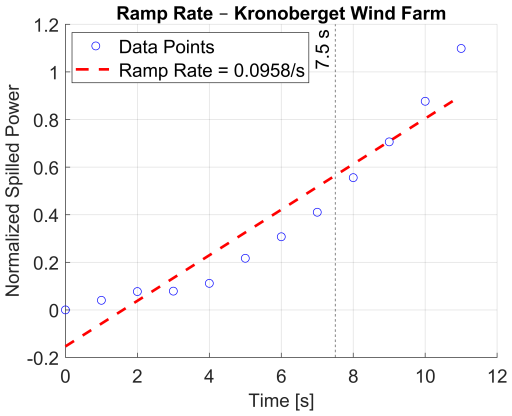

Figure 5.46: Sample 1: Estimated ramp rate for Kronoberget wind farm between 09:12:23 and 09:12:34.

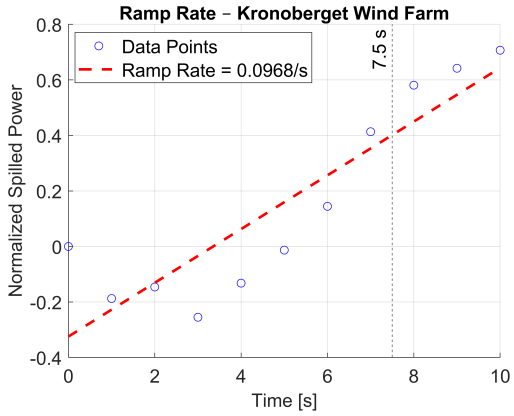

Figure 5.47: Sample 2: Estimated ramp rate for Kronoberget wind farm between 09:15:44 and 09:15:54.

A zoomed-in view of the control system for WTG3 is shown in Figure 5.48. During the event, this turbine contributed to frequency regulation by increasing its pitch angle and spilling more power when the frequency exceeded 50.1 Hz. Some spilling was also present when the frequency was within the normal range to keep a power reserve, as explained before. When no spilling occurred, the pitch angle remained at the minimum value of 3.8 degrees. In total, 10 out of 16 turbines were actively spilling during this event, again showing that not all turbines are used at the same time, similar to the behavior observed on 3 February.

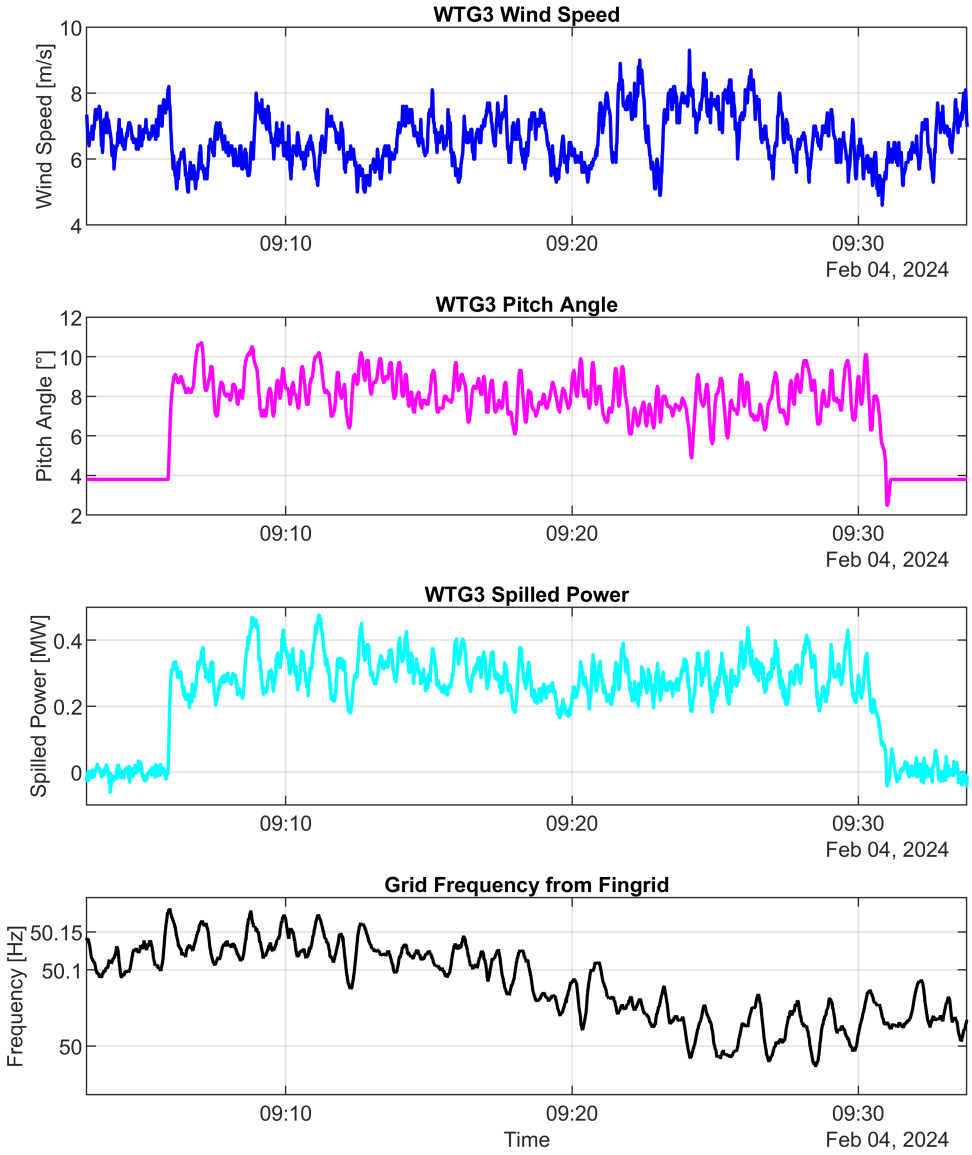

Figure 5.48: One-hour overview of turbine 3 at Kronoberget wind farm on 4 February 2024.

5.3 Comparison of wind turbine performance

This section compares the performance of the Chalmers wind turbine model and Kronoberget wind farm in providing FCR-D Down during the frequency events on 3 February and 4 February 2024. The comparison highlights differences in response behavior, dynamic performance, and control system characteristics. It also evaluates whether they provide equally good ancillary service and how Kronoberget wind farm compares to the minimum requirements from Svenska kraftnät, using the Chalmers wind turbine model as a reference. The analysis is based on the outcomes from the previous sections, and additional ramp-down comparisons for the same events are included in Appendix A.3.3.

5.3.1 Case 1: 3 February 2024

Figure 5.49 shows the available and output power for the Chalmers wind turbine model and the Kronoberget wind farm on 3 February 2024. It can be seen that the Kronoberget wind farm regulates its output power using the spilled power, resulting in a relatively constant output. This regulation is driven by the goal of always exporting as much power as the grid limitations allow, which in turn smooths the output when the available power fluctuates. When the available power decreases due to lower wind speeds, the base spill reserve is used to compensate. In contrast, the output power of the Chalmers wind turbine model closely follows the available power, since the simulation links them directly. This suggests that the spilled power at Kronoberget is used both for frequency regulation and for maximizing power export within grid limitations.

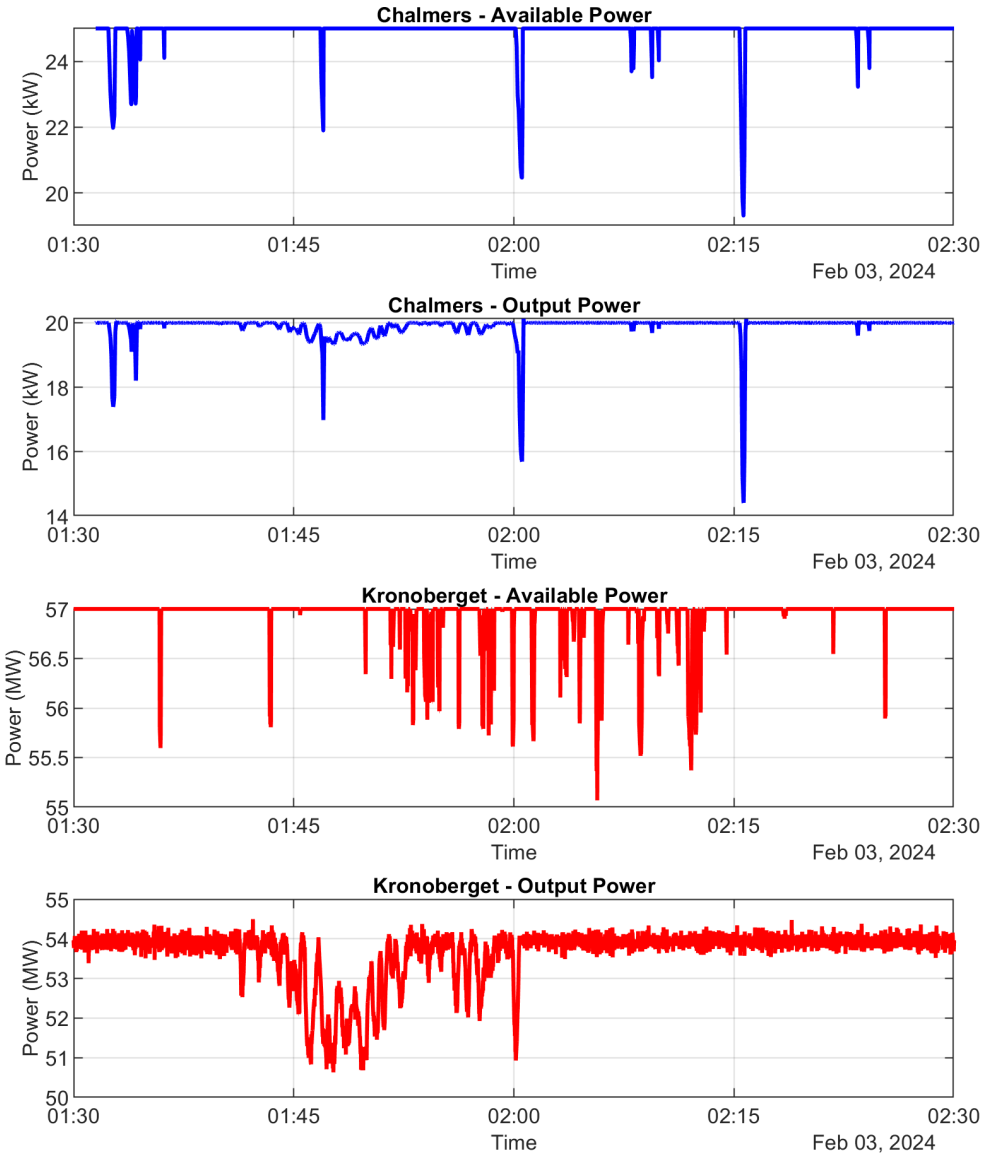

Figure 5.49: Comparison of available power and output power for the Chalmers wind turbine model and Kronoberget wind farm on 3 February 2024.

A comparison of the previously studied frequency events on 3 February for the Chalmers wind turbine model and Kronoberget wind farm is shown in Figure 5.50 and Figure 5.51. It can be seen that both follow the frequency deviations, with Kronoberget showing a slightly more aggressive response, especially during the recovery phase. This faster and more dynamic response indicates that Kronoberget reacts more quickly than the Chalmers wind turbine model. In Figure 5.51, the spilled power at Kronoberget briefly drops to around 2 MW during the recovery phase. This is related to output power regulation, where the spilled power is adjusted to compensate for changes in available power.

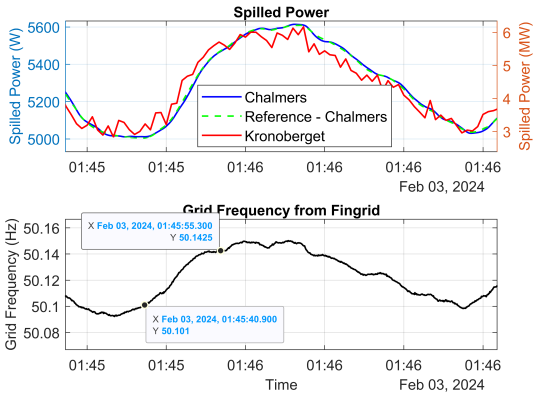

Figure 5.50: Sample 1: Comparison of spilled power and grid frequency between the Chalmers wind turbine model and Kronoberget wind farm from 01:45:40 to 01:45:55.

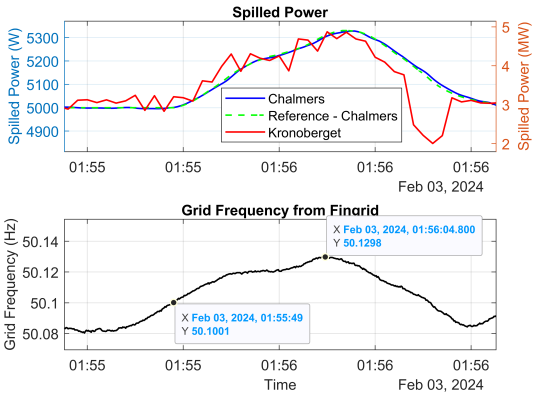

Figure 5.51: Sample 2: Comparison of spilled power and grid frequency between the Chalmers wind turbine model and Kronoberget wind farm from 01:55:49 to 01:56:04.

The estimated droop comparison is shown in Figure 5.52 and Figure 5.53 for the two samples. In both cases, Kronoberget has a lower droop value, which means it is more sensitive to frequency deviations and provides a stronger response compared to the Chalmers wind turbine model. This can also be seen in the slope of the fitted droop curves, where Kronoberget shows a noticeably steeper response. For Sample 1, Kronoberget has a droop of 0.28 Hz/p.u. while Chalmers has 0.50 Hz/p.u., meaning Kronoberget responds approximately 1.8 times more aggressively relative to its own available reserve. In Sample 2, the droops are 0.28 Hz/p.u. and 0.41 Hz/p.u. for Kronoberget and Chalmers respectively, corresponding to a response that is about 1.5 times stronger for Kronoberget.

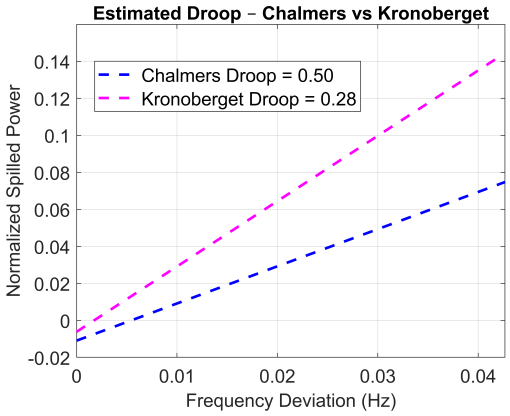

Figure 5.52: Sample 1: Comparison of estimated droop response between the Chalmers wind turbine model and Kronoberget wind farm from 01:45:40 to 01:45:55.

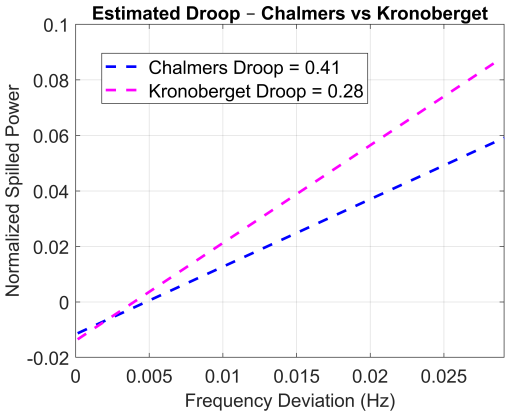

Figure 5.53: Sample 2: Comparison of estimated droop response between the Chalmers wind turbine model and Kronoberget wind farm from 01:55:49 to 01:56:04.

The estimated ramp rate comparison is shown in Figure 5.54 and Figure 5.55 for the two samples. For Sample 1, the Chalmers wind turbine model has a ramp rate of 0.0071 s^{-1} while Kronoberget has 0.0119 s^{-1}, meaning Kronoberget adjusts its power output approximately 1.7 times faster relative to its own available reserve. In Sample 2, the ramp rates are 0.0040 s^{-1} for Chalmers and 0.0056 s^{-1} for Kronoberget, corresponding to a response that is about 1.4 times faster.

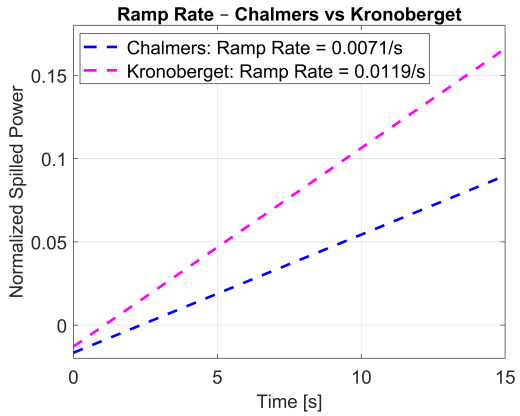

Figure 5.54: Sample 1: Comparison of estimated ramp rate between the Chalmers wind turbine model and Kronoberget wind farm from 01:45:40 to 01:45:55.

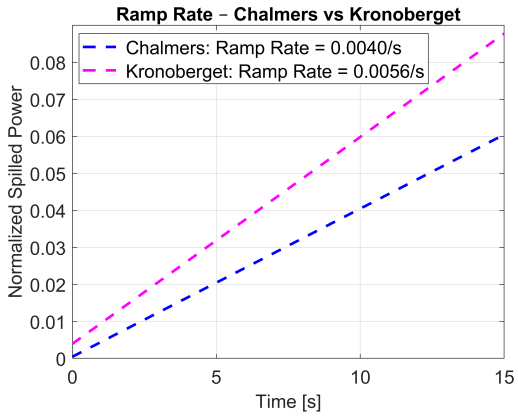

Figure 5.55: Sample 2: Comparison of estimated ramp rate between the Chalmers wind turbine model and Kronoberget wind farm from 01:55:49 to 01:56:04.

Table 5.1 and Table 5.2 summarize the estimated droop and ramp rate values for each sample, including both absolute and normalized results. The last column shows the relative difference, where Chalmers is compared to Kronoberget (C/K). In both events, the results indicate that Kronoberget provides a faster and stronger response relative to its available reserve, despite differences in the frequency profile. Since the Chalmers wind turbine model was designed to meet the minimum FCR-D Down requirements from Svenska kraftnät and both systems were evaluated using the

same frequency input, its response serves as a reference for the expected activation behavior. For each sample, the regulation range of the Chalmers model was also adjusted to remain smaller than that of Kronoberget, ensuring a fair comparison while avoiding bias caused by larger reserve capacity making the response appear stronger and faster. The ramp-down responses for the same events, presented in Appendix A.3.3, show a similar trend, with Kronoberget responding more strongly and quickly during the recovery phase. Together, these results suggest that the commercial wind farm is capable of meeting the required activation times under comparable conditions.

Table 5.1: Comparison of estimated droop and ramp rate between the Chalmers wind turbine model and Kronoberget wind farm for the frequency event between 01:45:40 and 01:45:55.

Parameter	**Chalmers**	**Kronoberget**	**Relative (C/K)**
Droop	10.02 kW/Hz	58.59 MW/Hz	–
Normalized Droop	0.50	0.28	1.8× stronger
Ramp Rate	35.36 W/s	0.20 MW/s	–
Normalized Ramp Rate	0.0071	0.0119	1.7× faster

Table 5.2: Comparison of estimated droop and ramp rate between the Chalmers wind turbine model and Kronoberget wind farm for the frequency event between 01:55:49 and 01:56:04.

Parameter	**Chalmers**	**Kronoberget**	**Relative (C/K)**
Droop	12.16 kW/Hz	57.71 MW/Hz	–
Normalized Droop	0.41	0.28	1.5× stronger
Ramp Rate	20.00 W/s	0.09 MW/s	–
Normalized Ramp Rate	0.0040	0.0056	1.4× faster

5.3.2 Case 2: 4 February 2024

Figure 5.56 shows the available and output power for the Chalmers wind turbine model and Kronoberget wind farm on 4 February 2024. As on 3 February, Kronoberget regulates its output power using spilled power, although this is harder to observe here due to more variable wind conditions. In some cases, changes in available power do not result in similar changes in output power, which suggests that the spill reserve is also used to maximize power export within grid limitations during fluctuating wind conditions. In contrast, the output power of the Chalmers wind turbine model continues to follow the available power closely, as expected from the simulation model.

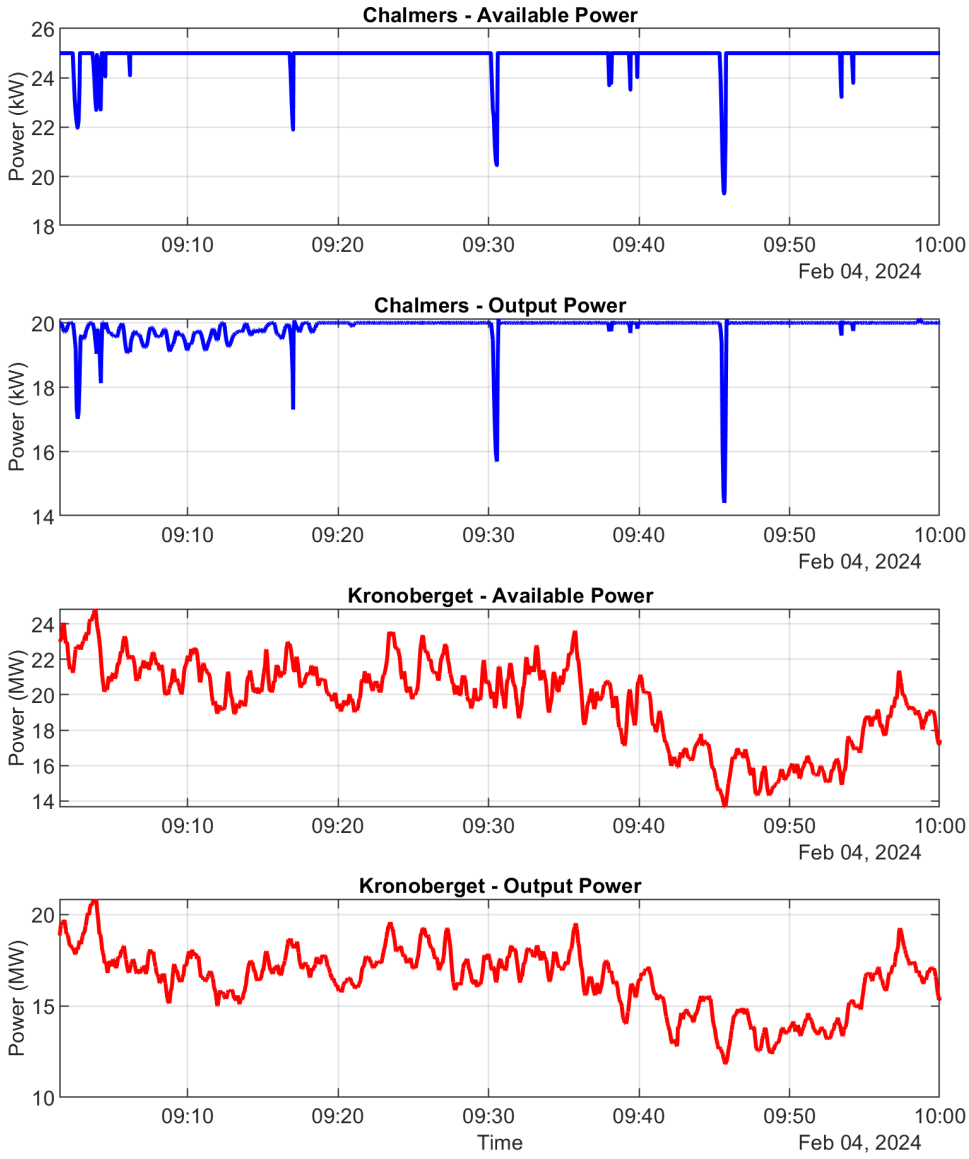

Figure 5.56: Comparison of available power and output power for the Chalmers wind turbine model and Kronoberget wind farm on 4 February 2024.

The frequency response of the Chalmers wind turbine model and Kronoberget wind farm on 4 February is compared in Figure 5.57 and Figure 5.58. Here, the response varies depending on how much the available power changes during each sample. In Sample 1, the available power remains relatively stable, and both units respond similarly when FCR-D Down is activated. The initial response time is nearly the same, but Kronoberget shows a faster recovery when the frequency decreases. In Sample 2, the available power varies more, and a clear difference in the response can be seen. While the spilled power still follows the frequency when FCR-D Down is activated, the shape of the response differs due to the influence of output power regulation. As mentioned earlier, when the available power changes significantly, the spilled power is also used to smooth the output, which affects the ability to follow the frequency signal. This behavior is more common on this day due to the more variable wind conditions.

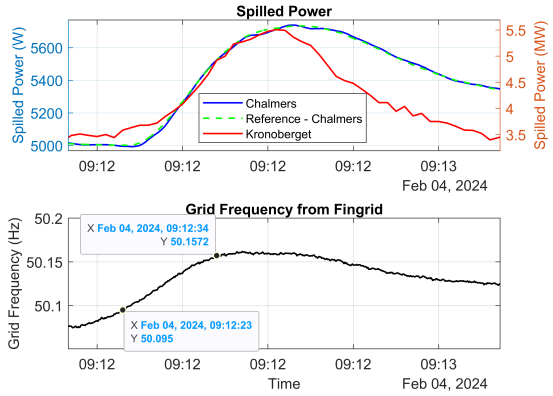

Figure 5.57: Sample 1: Comparison of spilled power and grid frequency between the Chalmers wind turbine model and Kronoberget wind farm from 09:12:23 to 09:12:34.

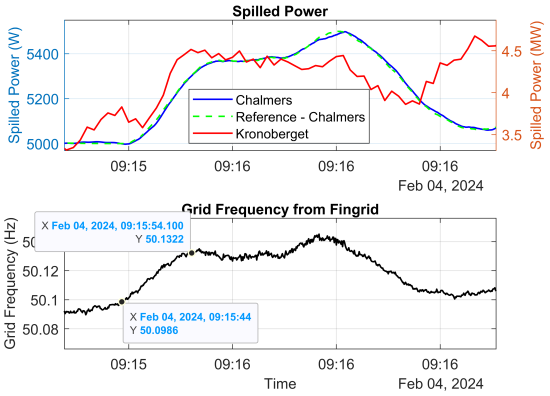

Figure 5.58: Sample 2: Comparison of spilled power and grid frequency between the Chalmers wind turbine model and Kronoberget wind farm from 09:15:44 to 09:15:54.

The estimated droop comparison is shown in Figure 5.59 and Figure 5.60 for the two samples on 4 February. Similar to 3 February, Kronoberget shows a higher sensitivity to frequency deviations compared to the Chalmers wind turbine model in both cases. In Sample 1, Kronoberget has a droop value of 0.06 Hz/p.u. while Chalmers has 0.18 Hz/p.u., corresponding to a response that is about 3 times stronger for Kronoberget. A similar pattern is seen in Sample 2, where the droop values are 0.04 Hz/p.u. and 0.14 Hz/p.u. respectively, giving a response that is roughly 3.5 times stronger. The difference in response strength is influenced by the available reserve at Kronoberget during these events. Since the spilled power was already close to 3.8 MW when the frequency deviation occurred, the remaining up-regulation capacity was limited to approximately 1 MW. The Chalmers model was again evaluated using a regulation range smaller than that of Kronoberget.

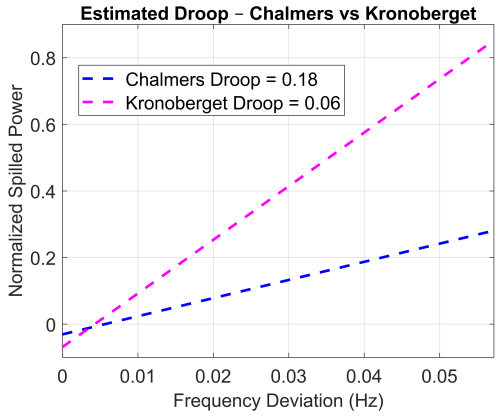

Figure 5.59: Sample 1: Comparison of estimated droop response between the Chalmers wind turbine model and Kronoberget wind farm from 09:12:23 to 09:12:34.

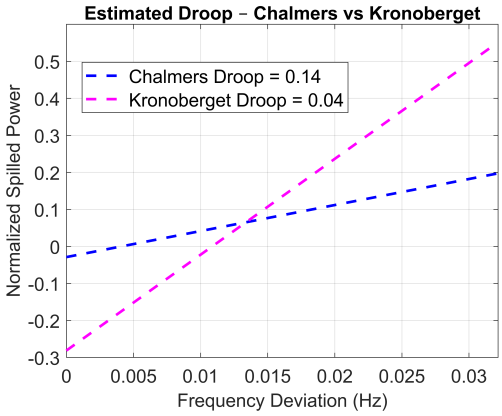

Figure 5.60: Sample 2: Comparison of estimated droop response between the Chalmers wind turbine model and Kronoberget wind farm from 09:15:44 to 09:15:54.

The estimated ramp rate comparison is shown in Figure 5.61 and Figure 5.62 for the two samples on 4 February. In Sample 1, Chalmers shows a ramp rate of 0.0326 s^{-1}, while Kronoberget reaches 0.0958 s^{-1}, indicating a response that is approximately 2.9 times faster relative to its available reserve. In Sample 2, the ramp rate for Kronoberget increases slightly to 0.0968 s^{-1}, while Chalmers shows 0.0265 s^{-1}, corresponding to a response about 3.7 times faster.

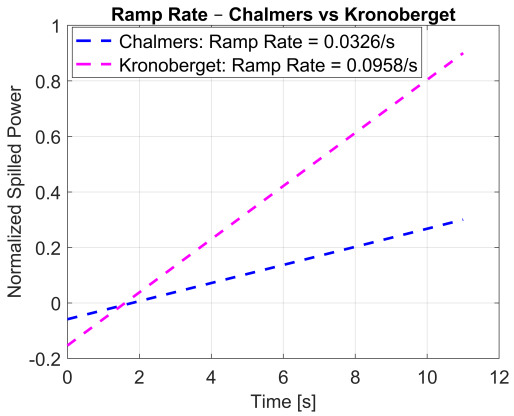

Figure 5.61: Sample 1: Comparison of estimated ramp rate between the Chalmers wind turbine model and Kronoberget wind farm from 09:12:23 to 09:12:34.

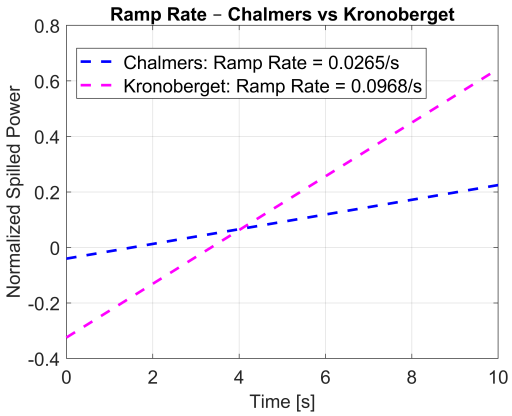

Figure 5.62: Sample 2: Comparison of estimated ramp rate between the Chalmers wind turbine model and Kronoberget wind farm from 09:15:44 to 09:15:54.

Table 5.3 and Table 5.4 summarize the estimated droop and ramp rate values for the two frequency events on 4 February, including both absolute and normalized results. Kronoberget was faster and stronger in both samples, showing higher sensitivity and quicker response relative to its available reserve. These results are consistent with those from 3 February, even though the turbines operated under different wind conditions and accepted bids. Ramp-down responses showed similar patterns and are provided in Appendix A.3.3.

Table 5.3: Comparison of estimated droop and ramp rate between the Chalmers wind turbine model and Kronoberget wind farm for the frequency event between 09:12:23 and 09:12:34.

Parameter	**Chalmers**	**Kronoberget**	**Relative (K/C)**
Droop	9.01 kW/Hz	19.56 MW/Hz	–
Normalized Droop	0.18	0.06	3.0× stronger
Ramp Rate	53.94 W/s	0.116 MW/s	–
Normalized Ramp Rate	0.0326	0.0958	2.9× faster

Table 5.4: Comparison of estimated droop and ramp rate between the Chalmers wind turbine model and Kronoberget wind farm for the frequency event between 09:15:44 and 09:15:54.

Parameter	**Chalmers**	**Kronoberget**	**Relative (K/C)**
Droop	8.89 kW/Hz	25.13 MW/Hz	–
Normalized Droop	0.14	0.04	3.5× stronger
Ramp Rate	33.51 W/s	0.094 MW/s	–
Normalized Ramp Rate	0.0265	0.0968	3.7× faster

6 Discussion

This chapter discusses the observations made during the evaluation and how they relate to the control strategies, model assumptions, and available data. The comparison between the Chalmers wind turbine model and Kronoberget wind farm focuses on how each system responds to grid frequency events and whether their behavior aligns with Svenska kraftnät's requirements for FCR-D Down. The discussion is structured around turbine behavior, estimated droop and ramp rate, and the influence of operating conditions. Finally, suggestions are presented for how the evaluation approach could be developed further in future work.

6.1 Evaluation approach and Svk requirements

One of the main challenges in this project is the lack of clear guidelines from Svk for how to evaluate wind turbine performance based on grid frequency variations. The only formal reference is the predefined step-response test used in the prequalification of a wind farm. Since it was not possible to perform this test at Kronoberget within the scope of this project, the evaluation was based entirely on grid frequency events. The Chalmers wind turbine model was then used as a reference since the control structure is known and designed to meet Svk's minimum performance requirements. To support this comparison, a reference Svk droop line was included in the droop plots. Although not part of the formal evaluation procedure, it served as a benchmark to illustrate how the observed response to the grid frequency variations compares to the idealized step-response assumed in the prequalification testing. If the estimated droop lies above this reference line, it can be interpreted as an indication that the system is capable of meeting the response requirement. If it falls below, no direct conclusion can be drawn, since the test conditions differ from the formal procedure. However, if the response is steeper than that of the Chalmers wind turbine model, which was designed to meet Svk's requirements, it provides a strong indication that the evaluated system meets the requirements under the observed grid frequency variations. Conversely, if the response is weaker than that of the Chalmers model, it suggests that the system does not meet the requirement.

The evaluation method was structured to be easy to follow, starting from the selected day of interest, followed by identifying frequency events and estimating droop and ramp rate. This made it possible to compare the two systems using the same approach, even though only grid frequency was available as input. While this does not replace the formal prequalification test, it gives an indication of how well the turbines provide ancillary services, specifically FCR-D Down in this case, under grid frequency variations. However, since predefined step signals were not used, certain requirements such as endurance and steady-state accuracy could not be evaluated beyond showing good tracking of the frequency. To make the evaluation more complete, more days would need to be included, ideally covering both winter and summer conditions. The main difficulty is finding days where several factors align: clear FCR-D Down events, Chalmers wind turbine in operation, and active bids from Kronoberget. This limits which days can be included in the evaluation, which is a constraint in this study.

6.2 Interpretation of droop and ramp rate results

To compare the response of the two systems, droop and ramp rate were estimated using normalized values. For Chalmers, the maximum possible spilling was initially set to 10,000 W, but dynamically adjusted for each case to ensure that the normalized available regulation range remained smaller or equal to that of Kronoberget. For Kronoberget, it was defined as the accepted FCR-D Down bid for each hour. In both cases, the base level was taken as the spill power at the moment the frequency crossed 50.1 Hz, meaning the normalization was done relative to the available capacity range for that specific event. This approach was necessary to enable a fair comparison between systems with different capacities and control strategies.

In events such as those on 4 February, where the available regulation margin varied more due to changing wind conditions, the resulting slope of the normalized droop curve became steeper and the estimated droop value decreased. A similar effect was seen in the ramp rate estimation, where a lower regulation range led to higher normalized ramp values. This is due to how normalization is applied: when the available range is small, the same absolute change in power results in a larger normalized value. These results show how quickly each system responded relative to the available reserve, but the outcome depends on the operating point at the time of activation.

In this study, using the remaining regulation margin as the basis for normalization allowed a consistent evaluation of relative response behavior across different operating conditions. The lower droop values and faster ramp rates observed for Kronoberget reflect how effectively the system utilized its available capacity during each FCR-D Down activation, given the regulation range at the time of response.

6.3 Control strategy at Kronoberget

The evaluation suggests that Kronoberget wind farm applies two separate control strategies in parallel: one for frequency regulation and another for maintaining a relatively constant power output over time. This was particularly noticeable on the day when the turbines were operating close to rated power, where the total output remained nearly unchanged despite variations in available power. This behavior indicates that part of the available power may be held back rather than being fully used to support frequency deviations. According to information provided by SR Energy, such curtailment occurs only in response to limitations in the grid, which explains the presence of a base level of spilled power in the plots. Compared to the Chalmers wind turbine model, where the output is allowed to vary freely in response to frequency and no external limitations are present, the ability of Kronoberget to contribute to ancillary services may be constrained by these operating conditions.

6.4 Model testing and comparison limitations

The new frequency controller developed in this project has only been tested in simulation. Although the model represents Chalmers wind turbine closely at rated power, it would be valuable to apply the controller to the real turbine and use measured data to further evaluate its performance. This would help confirm how the control responds to grid frequency events and whether the simulated behavior reflects the actual response at both rated and medium wind speeds.

Although the possibility of implementing a faster controller was considered, no evaluation was conducted in this thesis to test more responsive tuning. Instead, the controller was configured to operate close to Svenska kraftnät's minimum droop threshold. This was done to provide a consistent reference that could be used to evaluate whether other wind farms deliver a response that is significantly faster or slower than what is required. An example of a stronger response is shown in Appendix A.2, where the droop constant in the simulation model of Chalmers wind turbine was decreased to 2% to illustrate the potential for a more responsive configuration. The results correspond to the frequency event between 01:55:49 and 01:56:04.

An additional constraint in the comparison is that the Chalmers wind turbine model was evaluated at rated power for both cases, while the commercial wind farm operated at rated power on 3 February and at medium or varying wind speeds on 4 February. This creates an imbalance in the evaluation, as the turbines were not operating under similar conditions. The difference in operating range affects how the frequency control can be compared between the two systems, particularly on 4 February when the available power varied.

In the simulation model, dynamic air density and filtering were included to improve the estimation of wind speed and available power. The difference from the standard air density value was small during the test period, so the effect on the results was barely noticeable. However, it was still useful to include, as the deviation can vary depending on the weather and season. Since air density affects the estimation of wind speed, available power, and mechanical torque, even small errors can propagate through the model and influence several parts of the control response, making it less accurate than it could be.

6.5 Summary of observed system behavior

When comparing the results, Kronoberget responded faster and stronger than Chalmers during the selected events. This was seen in two events on 3 February and two on 4 February. Kronoberget showed both a stronger droop response and a faster ramp rate, which indicates that it meets the requirements for FCR-D Down and performs well under the observed grid frequency variations. For most of the time during the evaluation days, only a small part of the accepted bids was needed due to limited frequency deviations. In some cases, especially when the bids were low and the wind speed varied, the wind farm delivered more than the accepted bid, as seen on 4 February, meaning that it overdelivered and provided more regulation than it was compensated for. The results also indicate that the control system is capable of holding a reserve in power, which could make the wind farm suitable for up-regulation as well. However, to be certain about compliance with formal requirements, the response would need to be verified against predefined step signals.

6.6 Future work

This study focused on evaluating ancillary service performance using a simulation model of Chalmers wind turbine and one commercial wind farm. Future work may extend this evaluation by including additional commercial wind farms operating under similar conditions. This would allow comparison of response, reserve activation, and dynamic behavior across different turbine types and control strategies, which

would support the problem statement in this thesis.

Further investigation should also include other ancillary services, such as FCR-N and FCR-D Up, based on the newly implemented frequency controller. This requires that the wind farm is prequalified to deliver these services, as defined by Svenska kraftnät. Since the current simulation model of Chalmers wind turbine is limited to high wind conditions, simulations under medium and low wind speeds would improve the comparison by covering a wider range of operating conditions. This would require updates to the model.

In the current study, the Chalmers wind turbine model was used as a reference for evaluating performance against Svenska kraftnät's requirements during frequency events. As an alternative, a different benchmarking approach may be considered to evaluate turbine behavior without relying on a specific reference model. To enable such an approach, clearer guidelines from Svenska kraftnät on how to evaluate turbine performance based on grid frequency variations would be necessary.

The evaluation in this study was also limited to two selected days. Including more days with active frequency events and available measurement data would strengthen the reliability of the results and allow more general conclusions to be drawn.

7 Conclusion

This thesis developed and applied a method to evaluate the ability of wind turbines to provide FCR-D Down services based on variations in grid frequency. The method was used to compare the performance of Chalmers wind turbine, represented through a simulation model with a known control structure, and a commercial wind farm, Kronoberget, where the internal control strategy was not known. The evaluation focused on selected frequency events and examined droop, ramp rate, available power, and how the response compared to the accepted bids.

The simulation model of Chalmers wind turbine was configured with a droop-based control strategy designed to meet the minimum requirements set by Svenska kraftnät. The turbine responded to frequency deviations by reducing power proportionally, using pitch-based de-loading to maintain reserve power when needed. These results served as a reference for evaluating how the control strategy influenced the frequency response, providing a baseline for comparison with commercial data.

Compared to Chalmers, Kronoberget showed stronger and faster responses in all of the selected events. Although the internal control system was not known, the results suggest that the wind farm applies effective control to manage reserve and respond quickly to frequency deviations. The differences in response between the two systems were influenced by the amount of available power and the regulation margin at the time of each event. Since the Chalmers wind turbine model is designed to meet Svk's minimum requirements for FCR-D Down services, its performance can be used as a reference for the expected response of wind turbines under grid conditions. Based on the comparison, Kronoberget consistently demonstrated a stronger response than Chalmers, both in terms of droop and ramp rate. This indicates that the wind farm is performing well and meeting the requirements for FCR-D Down, as evaluated using the developed method.

The evaluation method made it possible to compare both systems using the same approach, despite differences in scale and control design. By normalizing droop and ramp rate relative to the available regulation margin, the analysis captured how each system responded under different operating conditions. However, relying on grid frequency variation as input also meant that the test conditions were not consistent, which made it difficult to evaluate certain requirements, such as endurance and steady-state accuracy.

This method can be developed further by including more wind farms, additional evaluated days, and other services such as FCR-N and FCR-D Up. Expanding the evaluation in this way would make the method more robust and provide deeper insight into how different control strategies influence wind turbine behavior during frequency events. In this context, the method may serve as a useful tool for wind farm owners and developers when selecting and configuring turbines for participation in frequency control services.

References

[1] Svenska Kraftnät. Frekvensstabilitet - Om kraftsystemet, 2024. Accessed: 2025-01-27. URL: https://www.svk.se/om-kraftsystemet/om-systemansvaret/kraftsystemstabilitet/frekvensstabilitet/.

[2] Svenska Kraftnät. Kortsiktig marknadsanalys 2019, October 2019. Accessed: 2025-01-20. URL: https://www.svk.se/siteassets/om-oss/rapporter/2019/kortsiktig_marknadsanalys2019.pdf.

[3] Energiföretagen Sverige. Kraftläget i sverige - veckorapport vecka 52, 2024, 2024. Accessed: 2025-02-19. URL: https://www.energiforetagen.se/48cecf/globalassets/energiforetagen/statistik/kraftlaget/tidigare-kraftlagen/2024/kraftlaget-sverige-veckorapport-vecka-2024-52.pdf.

[4] Reuters. Wind power tops nuclear in sweden for first time, trade group says. January 2025. URL: https://www.reuters.com/business/energy/wind-power-tops-nuclear-sweden-first-time-trade-group-says-2025-01-09/.

[5] Erik Almqvist and Anton Johansson. Statistics and forecast q3 2024, October 2024. URL: https://swedishwindenergy.com/wp-content/uploads/2024/10/Statistics-and-Forecast-Q3-2024-1.pdf.

[6] M. Eriksson. Frekvensstyrning med vindkraft. Technical Report Report 2023:3, Chalmers University of Technology, Gothenburg, Sweden, 2022. URL: https://research.chalmers.se/publication/538917/file/538917_Fulltext.pdf.

[7] Frekvens och spänningsstyrning med chalmers vindkraftverk. Technical report, Chalmers University of Technology, Department of Electrical Engineering, Division of Electric Power Engineering, 2023. URL: https://odr.chalmers.se/items/fb2ad816-9fa8-4351-9679-7376fec80195.

[8] Naturvårdsverket. Vindval: The effects of wind power on human interests, 2013. Accessed: 2025-01-20. URL: https://www.naturvardsverket.se/4ac36d/globalassets/media/publikationer-pdf/ovriga-pub/vindval/978-91-620-6545-4.pdf.

[9] United Nations. Ensure access to affordable, reliable, sustainable, and modern energy for all, 2022. Accessed: 2025-01-20. URL: https://sdgs.un.org/goals/goal7.

[10] Naturvårdsverket. Vindval: The effect of wind power on birds and bats, 2012. Accessed: 2025-01-22. URL: https://www.naturvardsverket.se/4ac35d/globalassets/media/publikationer-pdf/ovriga-pub/vindval/978-91-620-6511-9.pdf.

[11] Naturvårdsverket. Vindval: The effects of wind power on marine life, 2012. Accessed: 2025-01-22. URL: https://www.naturvardsverket.se/4ac353/globalassets/media/publikationer-pdf/ovriga-pub/vindval/978-91-620-6512-6.pdf.

[12] Moses Peter Musau, Terry Lumbasi Chepkania, Abungu Nicodemus Odero, and Cyrus Wabuge Wekesa. Effects of renewable energy on frequency stability: A proposed case study of the kenyan grid. In *2017 IEEE PES PowerAfrica*, pages 12–15, 2017. doi:10.1109/PowerAfrica.2017.7991192.

[13] Svenska Kraftnät. Så kan du som privatperson bidra med stödtjänster, 2024. Accessed: 2025-01-27. URL: https://www.svk.se/om-kraftsystemet/om-systemansvaret/verktyg-for-systemdrift/stodtjanster-och-avhjalpande-atgarder/sa-kan-du-som-privatperson-bidra-med-stodtjanster/.

[14] Svenska kraftnät. Provide FCR, aFRR or mFRR, 2024. Accessed: 2025-02-10. URL: https://www.svk.se/en/stakeholders-portal/electricity-market/provision-of-ancillary-services/become-a-provider-of-ancillary-services/provide-fcr-afrr-or-mfrr/.

[15] Hassan Bevrani. *Robust power system frequency control*, volume 4. Springer, 2014. URL: https://link.springer.com/content/pdf/10.1007/978-0-387-84878-5.pdf.

[16] IEEE Power System Relaying and Control Committee, Working Group J20. Practices for generator synchronizing systems. Technical report, IEEE Power System Relaying and Control Committee, 2024. URL: https://www.pes-psrc.org/kb/report/119.pdf.

[17] ENTSO-E. *Policy 1: Load-Frequency Control and Performance*. European Network of Transmission System Operators for Electricity, 2004. Accessed: 2025-01-28. URL: https://www.entsoe.eu/fileadmin/user_upload/_library/publications/entsoe/Operation_Handbook/Policy_1_final.pdf.

[18] Svenska kraftnät. Om olika reserver, 2025. Accessed: 2025-01-28. URL: https://www.svk.se/aktorsportalen/bidra-med-reserver/om-olika-reserver/.

[19] ENTSO-E. Overview of frequency control in the nordic power system, 2024. Accessed: 2025-02-06. URL: https://eepublicdownloads.blob.core.windows.net/public-cdn-container/clean-documents/SOC%20documents/Nordic/2024/Overview_of_Frequency_Control_in_the_Nordic_Power_System.pdf.

[20] Jacob Aho, Andrew Buckspan, Jason Laks, Paul Fleming, Yunho Jeong, Fiona Dunne, Matthew Churchfield, Lucy Pao, and Kathryn Johnson. A tutorial of wind turbine control for supporting grid frequency through active power control. In *2012 American Control Conference (ACC)*, pages 3120–3131, 2012. doi:10.1109/ACC.2012.6315180.

[21] Energy Education. Betz limit. https://energyeducation.ca/encyclopedia/Betz_limit, 2025. [Accessed: Feb. 3, 2025].

[22] Ahmed A. Salem, Ali H. Kasem Alaboudy, and Hossam A. Gabbar. Realization of MPPT of PMSG-Based Wind Turbines Using New MPPT Indices. In

2019 IEEE 7th International Conference on Smart Energy Grid Engineering (SEGE), pages 315–320, 2019. doi:10.1109/SEGE.2019.8859935.

[23] Nivad Navid and Gary Rosenwald. Market Solutions for Managing Ramp Flexibility with High Penetration of Renewable Resource. *IEEE Transactions on Sustainable Energy*, 3(4):784–790, 2012. doi:10.1109/TSTE.2012.2203615.

[24] A. B. Attya, J. L. Domínguez-García, and O. Anaya-Lara. A review on frequency support provision by wind power plants: Current and future challenges. *Renewable and Sustainable Energy Reviews*, 81:2071–2087, 2017. URL: https://strathprints.strath.ac.uk/61464/, doi:10.1016/j.rser.2017.06.016.

[25] Guangdao Tan, Chao Xu, Fengzhi Wu, Chunfeng Qi, Dejun Wang, Peihao Yang, and Yangmin Feng. Research on primary frequency regulation of wind turbine based on new nonlinear droop control. In *2020 4th International Conference on HVDC (HVDC)*, pages 170–174, 2020. doi:10.1109/HVDC50696.2020.9292740.

[26] Panayiotis Moutis, Emmanouil Loukarakis, Stavros Papathanasiou, and Nikos D. Hatziargyriou. Primary load-frequency control from pitch-controlled wind turbines. In *2009 IEEE Bucharest PowerTech*, pages 1–7, 2009. doi:10.1109/PTC.2009.5281819.

[27] Fadi Kelada and Jérôme Buire. Contribution of power converters in frequency stability of low-inertia power systems. In *Conférence des Jeunes Chercheurs en Génie Electrique - Journées Couplées du GDR SEEDS*, Le Croisic, France, 2022. URL: https://hal.science/hal-03727208/document.

[28] Qunce Gao and Robin Preece. Improving frequency stability in low inertia power systems using synthetic inertia from wind turbines. In *2017 IEEE Manchester PowerTech*, pages 1–6, 2017. doi:10.1109/PTC.2017.7980836.

[29] Vahid Helac, Selma Hanjalic, Selma Grebovic, and Vedad Becirovic. Synthetic inertia in wind power plants: An overview. In *2023 22nd International Symposium INFOTEH-JAHORINA (INFOTEH)*, pages 1–6, 2023. doi:10.1109/INFOTEH57020.2023.10094115.

[30] Siyi Wang and Lihui Yang. Variable coefficient droop control strategy for optimal participation of wind farm in primary frequency regulation considering wake superposition effect. In *2021 4th International Conference on Energy, Electrical and Power Engineering (CEEPE)*, pages 483–488, 2021. doi:10.1109/CEEPE51765.2021.9475644.

[31] Cheng Yan, Yi Tang, Jianfeng Dai, Chenggen Wang, and Shengjun Wu. Uncertainty modeling of wind power frequency regulation potential considering distributed characteristics of forecast errors. *Protection and Control of Modern Power Systems*, 6(3):1–13, 2021. doi:10.1186/s41601-021-00200-3.

[32] Zhiwen Wang, Chen Shen, and Feng Liu. A conditional model of wind power forecast errors and its application in scenario generation. *Applied Energy*, 212:771–785, 2018. URL: https://www.sciencedirect.com/science/

article/pii/S0306261917317555, doi:10.1016/j.apenergy.2017.12.039.

[33] Anuj Banshwar, Naveen Kumar Sharma, Yog Raj Sood, and Rajnish Shrivastava. Renewable energy sources as a new participant in ancillary service markets. *Energy Strategy Reviews*, 18:106–120, 2017. doi:10.1016/j.esr.2017.09.009.

[34] Song Dongran. Kalman filter-based wind speed estimation for wind turbine control. *International Journal of Control Automation and Systems*, 15:1089–1096, 06 2017. doi:10.1007/s12555-016-0537-1.

[35] Shravana Musunuri and H. L. Ginn. Comprehensive review of wind energy maximum power extraction algorithms. In *2011 IEEE Power and Energy Society General Meeting*, pages 1–8, 2011. doi:10.1109/PES.2011.6039023.

[36] Zheren Ma, Zeyu Yan, Mohamed L. Shaltout, and Dongmei Chen. Optimal real-time control of wind turbine during partial load operation. *IEEE Transactions on Control Systems Technology*, 23(6):2216–2226, 2015. doi:10.1109/TCST.2015.2410735.

[37] Dongmyoung Kim, Taesu Jeon, Insu Paek, and Daeyoung Kim. A study on available power estimation algorithm and its validation. *Energies*, 15(7), 2022. URL: https://www.mdpi.com/1996-1073/15/7/2648, doi:10.3390/en15072648.

[38] Hyma Birudaraju, K. Sailaja, Vaitla Sreedevi, R. Viswanathan, and S. Vandaarkuzhali. Integrating machine learning (ml) and deep learning (dl) methods to produce reliable wind power predictions. In *2024 Second International Conference on Computational and Characterization Techniques in Engineering & Sciences (IC3TES)*, pages 1–5, 2024. doi:10.1109/IC3TES62412.2024.10877637.

[39] P. Louka, G. Galanis, N. Siebert, G. Kariniotakis, P. Katsafados, I. Pytharoulis, and G. Kallos. Improvements in wind speed forecasts for wind power prediction purposes using kalman filtering. *Journal of Wind Engineering and Industrial Aerodynamics*, 96(12):2348–2362, 2008. URL: https://www.sciencedirect.com/science/article/pii/S0167610508001074, doi:10.1016/j.jweia.2008.03.013.

[40] Chalmers University of Technology. Chalmers wind turbine, 2025. Accessed: 2025-04-08. URL: https://www.chalmers.se/en/departments/e2/resources-and-collaboration/chalmers-wind-turbine/.

[41] J. Jonkman, S. Butterfield, W. Musial, and G. Scott. Definition of a 5-mw reference wind turbine for offshore system development. Technical Report NREL/TP-500-38060, National Renewable Energy Laboratory (NREL), 2009. URL: https://www.nrel.gov/docs/fy09osti/38060.pdf.

[42] E. Rebello, S. L. H. Le, M. Kumar, and T. C. H. Chen. Performance analysis of a 10 mw wind farm in providing secondary frequency regulation. *IEEE Transactions on Power Systems*, 34(6):4595–4604, 2019. doi:10.1109/TPWRS.2019.2891962.

[43] P. Bousseau, P. C. M. Vassallo, and P. Hug. Contribution of wind farms to ancillary services, 2006. URL: https://www.researchgate.net/publication/229005248_Contribution_of_Wind_Farms_to_Ancillary_Services.

[44] M. Cole, B. Anderson, and J. Benson. A critical review of current and future options for wind farm participation in ancillary service provision. *Energies*, 16(3):1324, 2023. doi:10.3390/en16031324.

[45] SR Energy. Kronoberget Vindpark, 2025. Accessed: 2025-02-25. URL: https://srenergy.se/vindparker/kronoberget/.

[46] Länsstyrelserna and Energimyndigheten. Vindbrukskollen. Accessed: 2025-03-31. URL: https://vbk.lansstyrelsen.se/.

[47] Fingrid Oyj. Frequency - historical data, 2024. Accessed: 2025-04-08. URL: https://data.fingrid.fi/en/datasets/339.

[48] Richard Shelquist. An introduction to air density and density altitude calculations, 2023. Accessed: 2025-05-21. URL: https://wahiduddin.net/calc/density_altitude.htm.

[49] Xiankui Wen, Jiasheng Wang, and Qiang Fan. Impact of air humidity on wind power generator's output. *IOP Conference Series: Earth and Environmental Science*, 186(4):012067, September 2018. URL: https://dx.doi.org/10.1088/1755-1315/186/4/012067, doi:10.1088/1755-1315/186/4/012067.

[50] ENTSO-E. Technical requirements for frequency containment reserve provision in the nordic synchronous area. Technical report, ENTSO-E, Brussels, Belgium, March 2025. URL: https://www.svk.se/siteassets/aktorsportalen/bidra-med-reserver/om-olika-reserver/fcr/fcr-technical-requirements_v1.1_28_march_2025.pdf.

A Supplementary results and control data

A.1 Dynamic air density

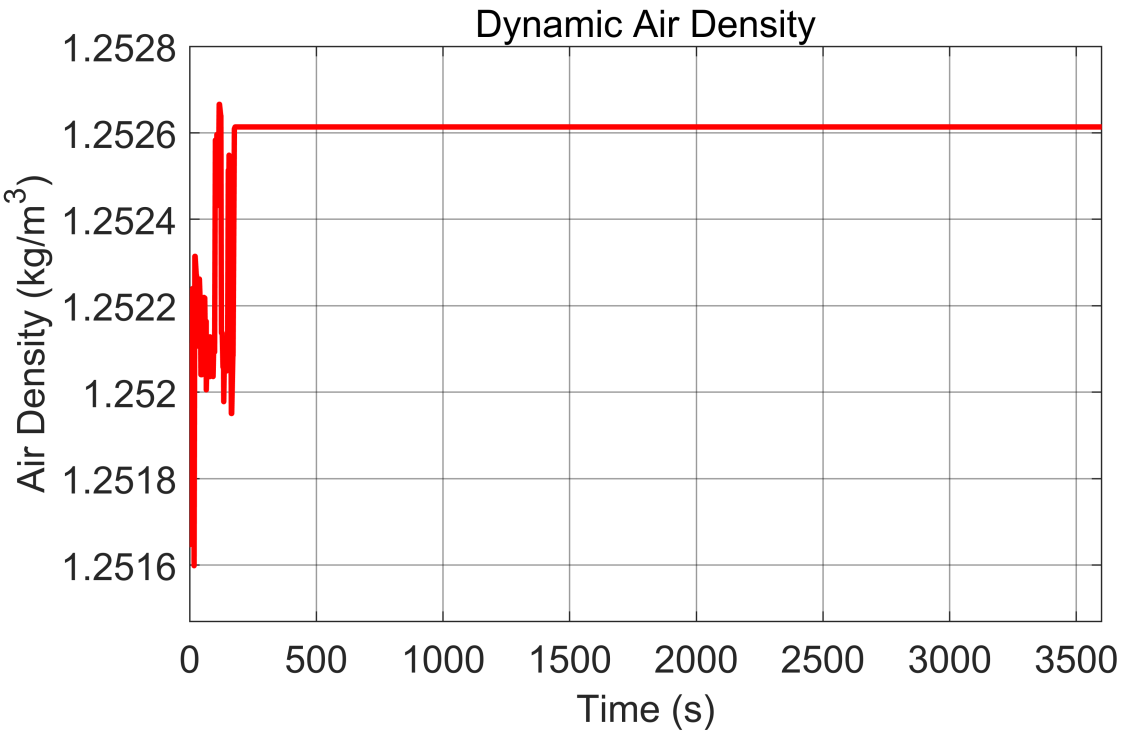

Figure A.1: Dynamic air density during the selected one-hour interval on 27 April 2023 for the Chalmers wind turbine model.

A.2 Test with faster frequency controller

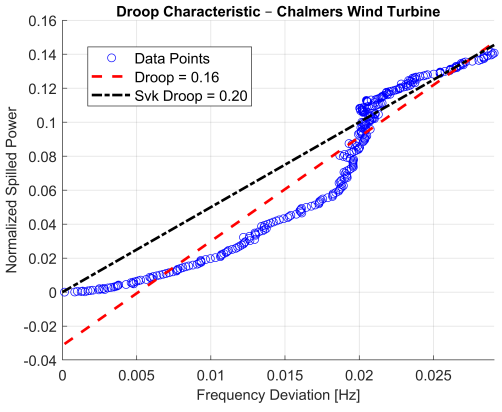

Figure A.2: Estimated droop response using a faster controller for the Chalmers wind turbine model with a 2% droop constant during the interval 01:55:49–01:56:04. Regulation range is 5 kW.

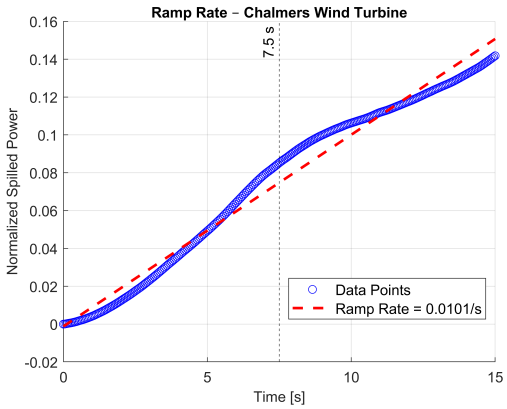

Figure A.3: Estimated ramp rate using a faster controller for the Chalmers wind turbine model with a 2% droop constant during the interval 01:55:49–01:56:04. Regulation range is 5 kW.

A.3 Ramp-down analysis

This section presents ramp-down responses for the Chalmers wind turbine model and Kronoberget wind farm. The samples correspond to the same frequency events analyzed in the main results chapter. A comparison between the two sites is also included at the end of the section.

A.3.1 Chalmers wind turbine model

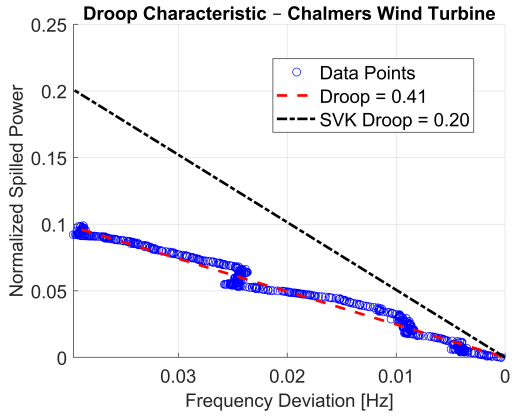

Figure A.4: Sample 1: Estimated droop response for the Chalmers wind turbine model during ramp-down on 3 February 2024, between 01:46:13 and 01:46:40.

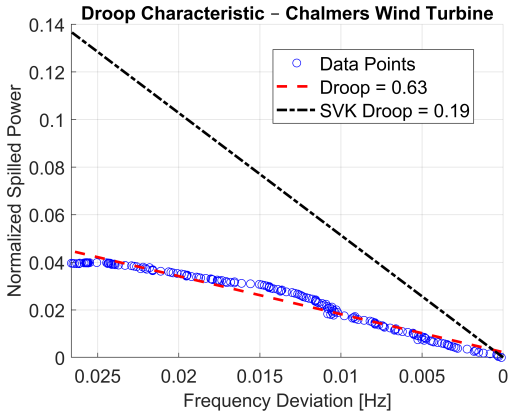

Figure A.5: Sample 2: Estimated droop response for the Chalmers wind turbine model during ramp-down on 3 February 2024, between 01:56:07 and 01:56:16.

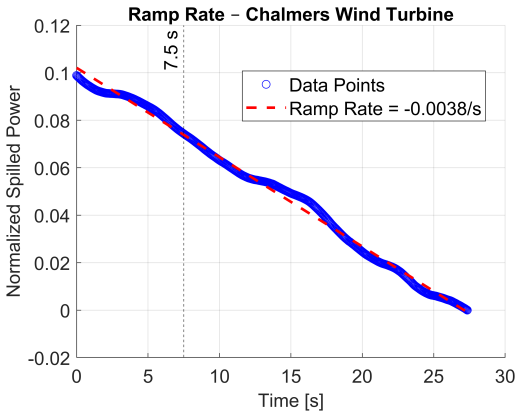

Figure A.6: Sample 1: Estimated ramp rate for the Chalmers wind turbine model during ramp-down on 3 February 2024, between 01:46:13 and 01:46:40.

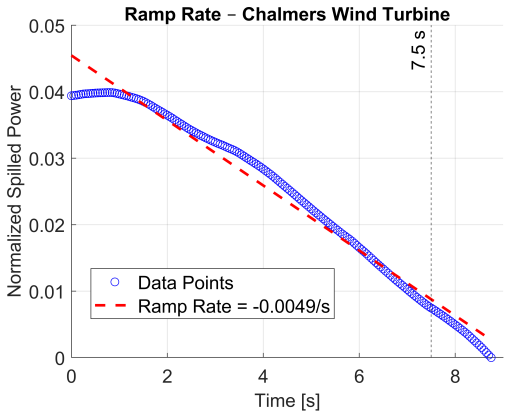

Figure A.7: Sample 2: Estimated ramp rate for the Chalmers wind turbine model during ramp-down on 3 February 2024, between 01:56:07 and 01:56:16.

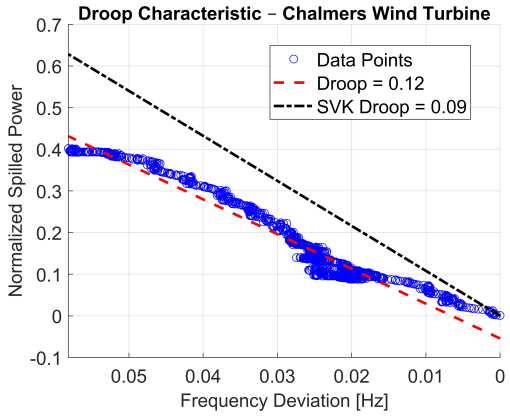

Figure A.8: Sample 1: Estimated droop response for the Chalmers wind turbine model during ramp-down on 4 February 2024, between 09:12:44 and 09:13:46.

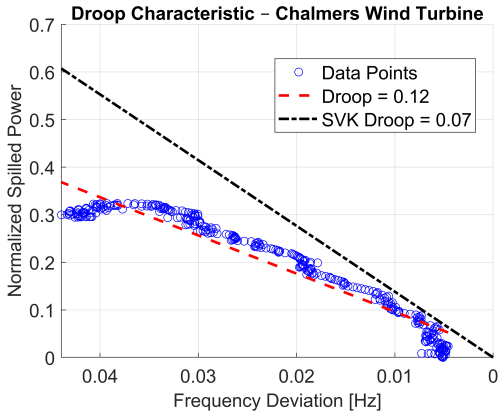

Figure A.9: Sample 2: Estimated droop response for the Chalmers wind turbine model during ramp-down on 4 February 2024, between 09:16:13 and 09:16:30.

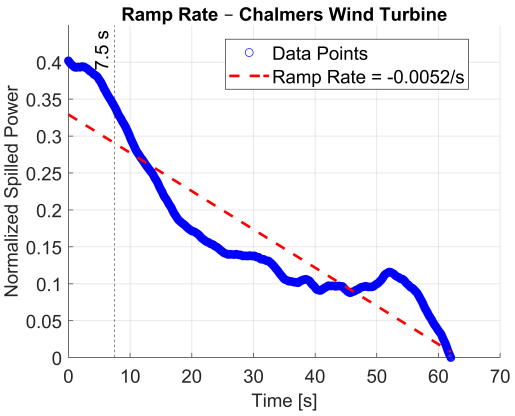

Figure A.10: Sample 1: Estimated ramp rate for the Chalmers wind turbine model during ramp-down on 4 February 2024, between 09:12:44 and 09:13:46.

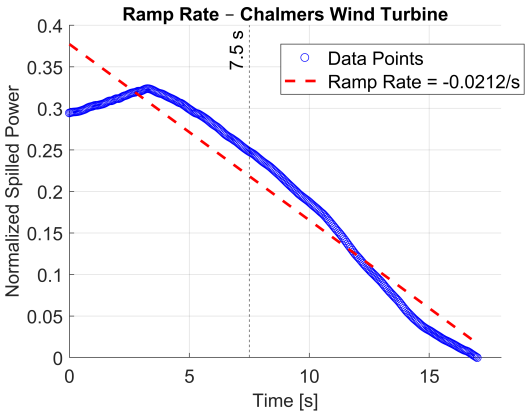

Figure A.11: Sample 2: Estimated ramp rate for the Chalmers wind turbine model during ramp-down on 4 February 2024, between 09:16:13 and 09:16:30.

A.3.2 Kronoberget wind farm

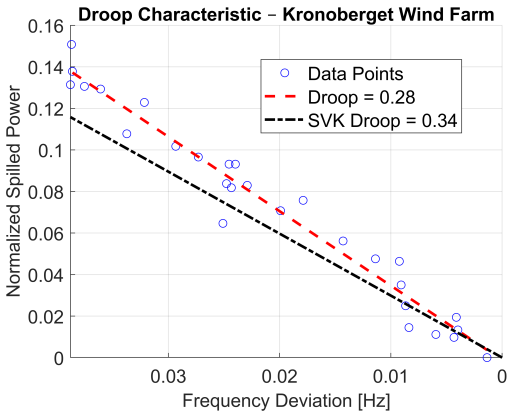

Figure A.12: Sample 1: Estimated droop response for Kronoberget wind farm between 01:46:13–01:46:40 on 3 February 2024.

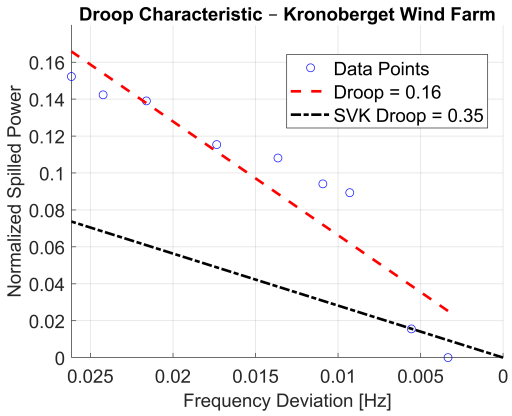

Figure A.13: Sample 2: Estimated droop response for Kronoberget wind farm between 01:56:07–01:56:16 on 3 February 2024.

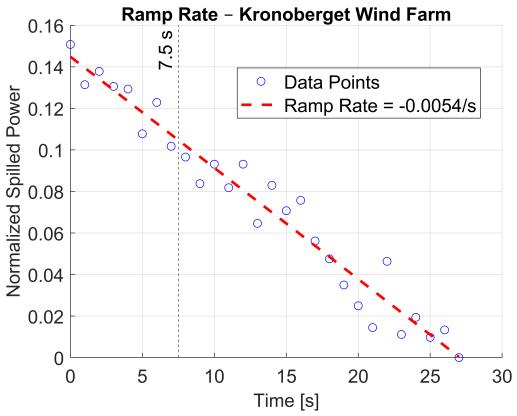

Figure A.14: Sample 1: Estimated ramp rate for Kronoberget wind farm between 01:46:13–01:46:40 on 3 February 2024.

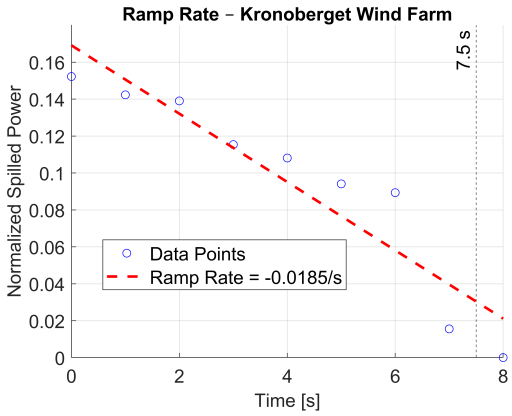

Figure A.15: Sample 2: Estimated ramp rate for Kronoberget wind farm between 01:56:07–01:56:16 on 3 February 2024.

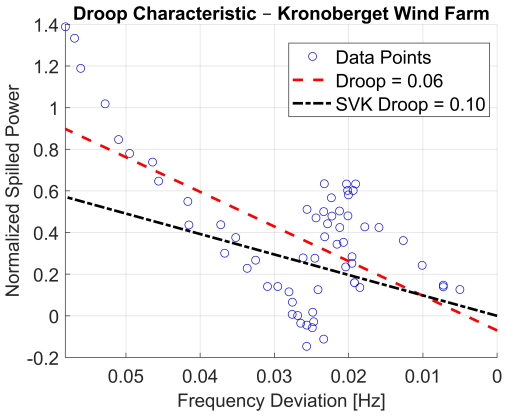

Figure A.16: Sample 1: Estimated droop response for Kronoberget wind farm between 09:12:44 and 09:13:46 on 4 February 2024.

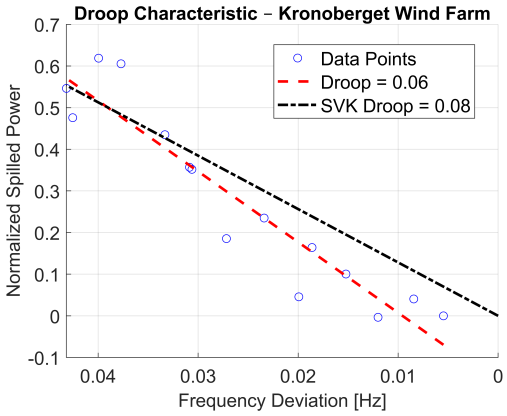

Figure A.17: Sample 2: Estimated droop response for Kronoberget wind farm between 09:16:13 and 09:16:27 on 4 February 2024.

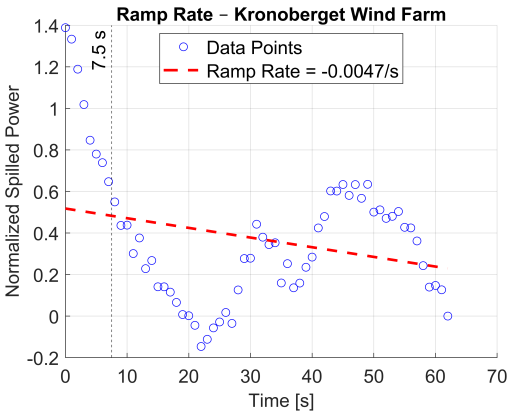

Figure A.18: Sample 1: Estimated ramp rate for Kronoberget wind farm between 09:12:44 and 09:13:46 on 4 February 2024.

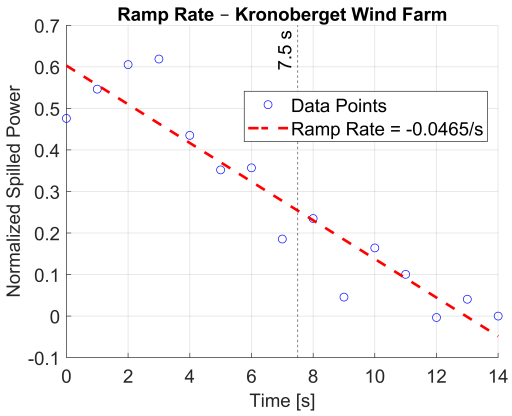

Figure A.19: Sample 2: Estimated ramp rate for Kronoberget wind farm between 09:16:13 and 09:16:27 on 4 February 2024.

A.3.3 Comparison between Chalmers and Kronoberget

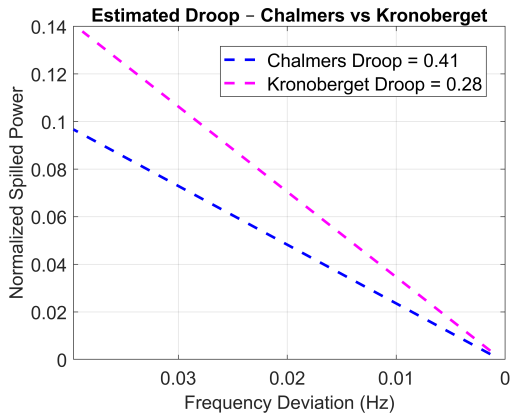

Figure A.20: Sample 1: Comparison of estimated droop response between the Chalmers wind turbine model and Kronoberget wind farm during ramp-down on 3 February 2024, between 01:46:13 and 01:46:40.

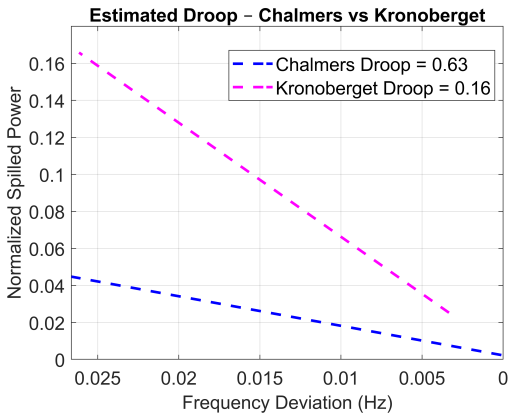

Figure A.21: Sample 2: Comparison of estimated droop response between the Chalmers wind turbine model and Kronoberget wind farm during ramp-down on 3 February 2024, between 01:56:07 and 01:56:16.

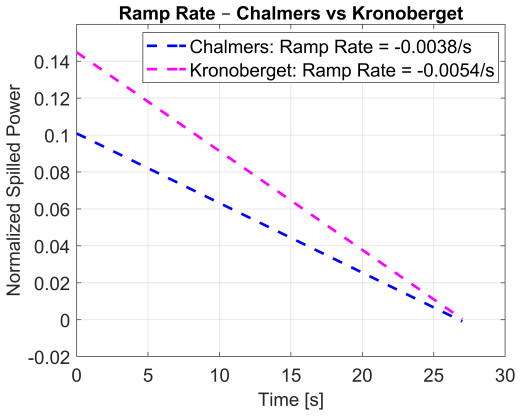

Figure A.22: Sample 1: Comparison of estimated ramp rate between the Chalmers wind turbine model and Kronoberget wind farm during ramp-down on 3 February 2024, between 01:46:13 and 01:46:40.

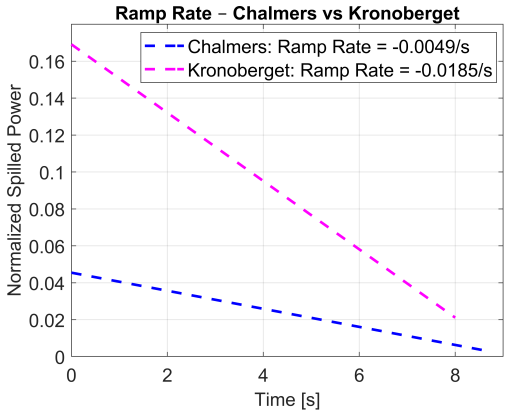

Figure A.23: Sample 2: Comparison of estimated ramp rate between the Chalmers wind turbine model and Kronoberget wind farm during ramp-down on 3 February 2024, between 01:56:07 and 01:56:16.

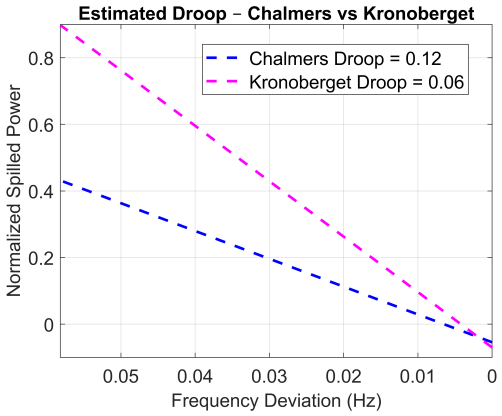

Figure A.24: Sample 1: Comparison of estimated droop response between the Chalmers wind turbine model and Kronoberget wind farm during ramp-down on 4 February 2024, between 09:12:44 and 09:13:46.

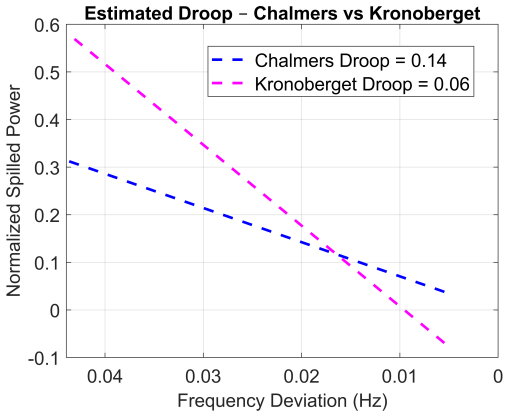

Figure A.25: Sample 2: Comparison of estimated droop response between the Chalmers wind turbine model and Kronoberget wind farm during ramp-down on 4 February 2024, between 09:16:13 and 09:16:27.

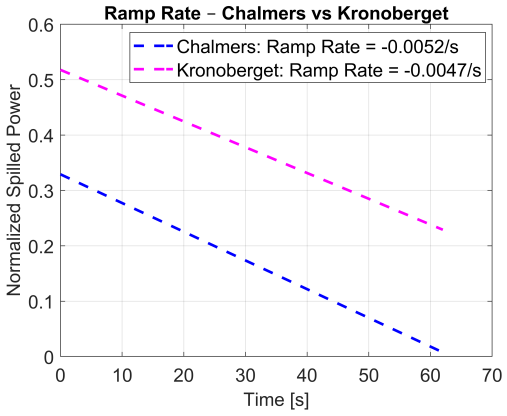

Figure A.26: Sample 1: Comparison of estimated ramp rate between the Chalmers wind turbine model and Kronoberget wind farm during ramp-down on 4 February 2024, between 09:12:44 and 09:13:46.

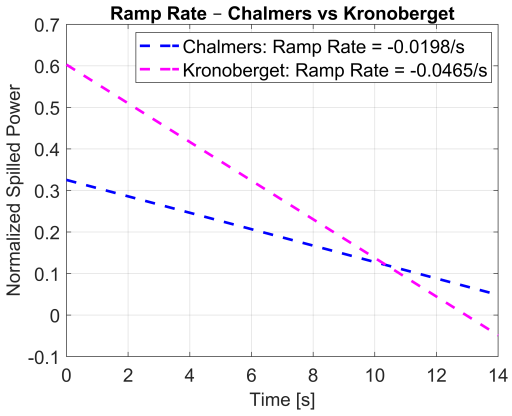

Figure A.27: Sample 2: Comparison of estimated ramp rate between the Chalmers wind turbine model and Kronoberget wind farm during ramp-down on 4 February 2024, between 09:16:13 and 09:16:27.

A.4 Turbine control data – 3 February 2024

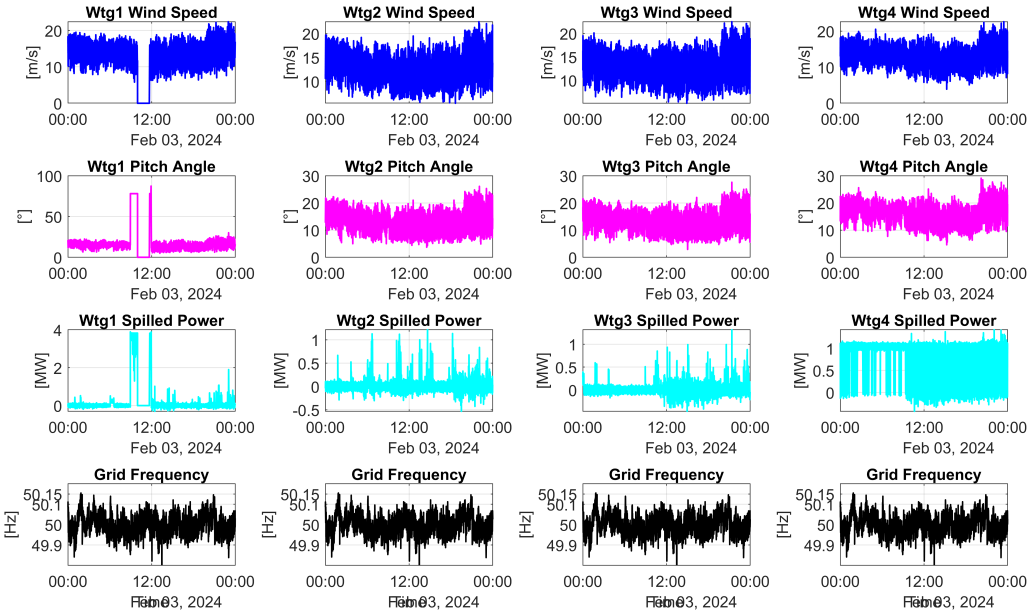

Figure A.28: Turbines 1–4: Wind Speed, Pitch Angle, Spilled Power, and Frequency.

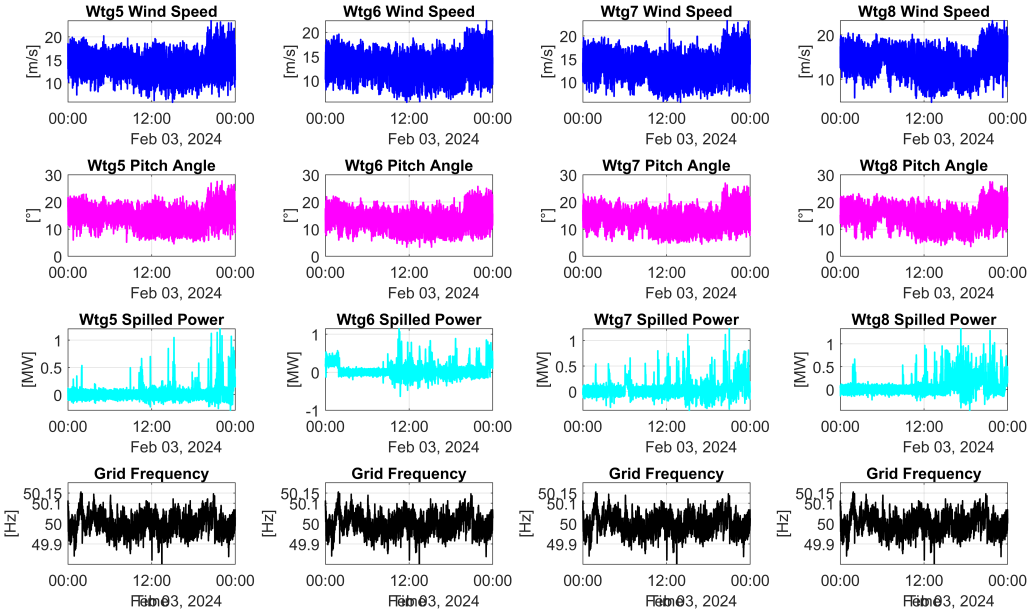

Figure A.29: Turbines 5–8: Wind Speed, Pitch Angle, Spilled Power, and Frequency.

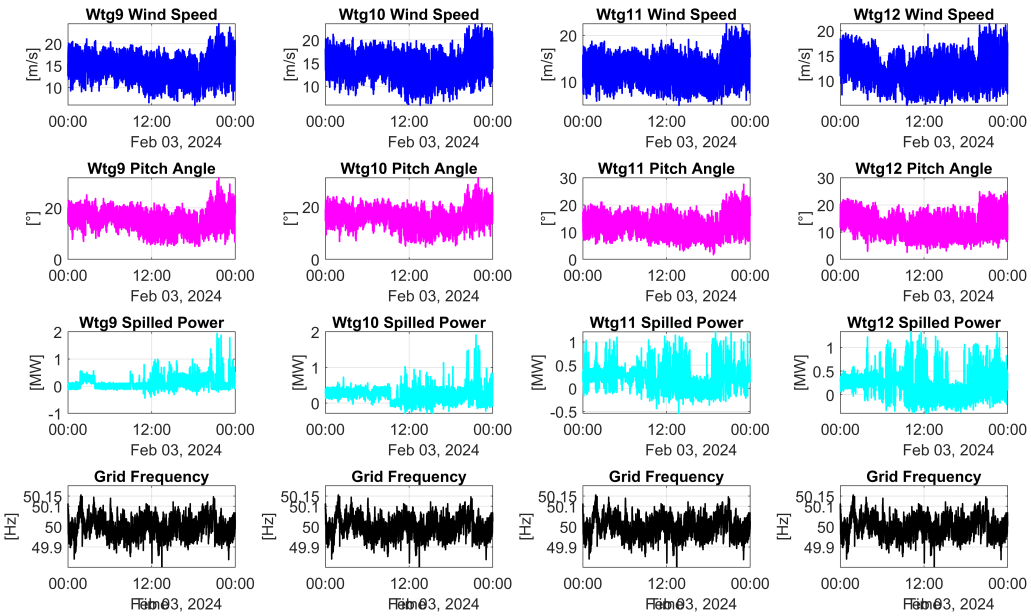

Figure A.30: Turbines 9–12: Wind Speed, Pitch Angle, Spilled Power, and Frequency.

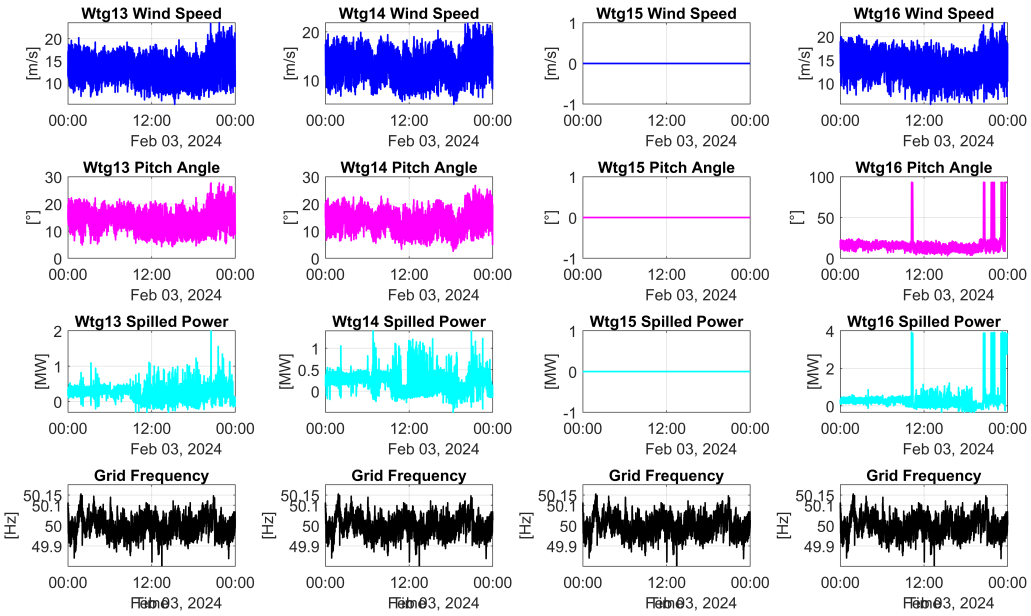

Figure A.31: Turbines 13–16: Wind Speed, Pitch Angle, Spilled Power, and Frequency.

A.5 Turbine control data – 4 February 2024

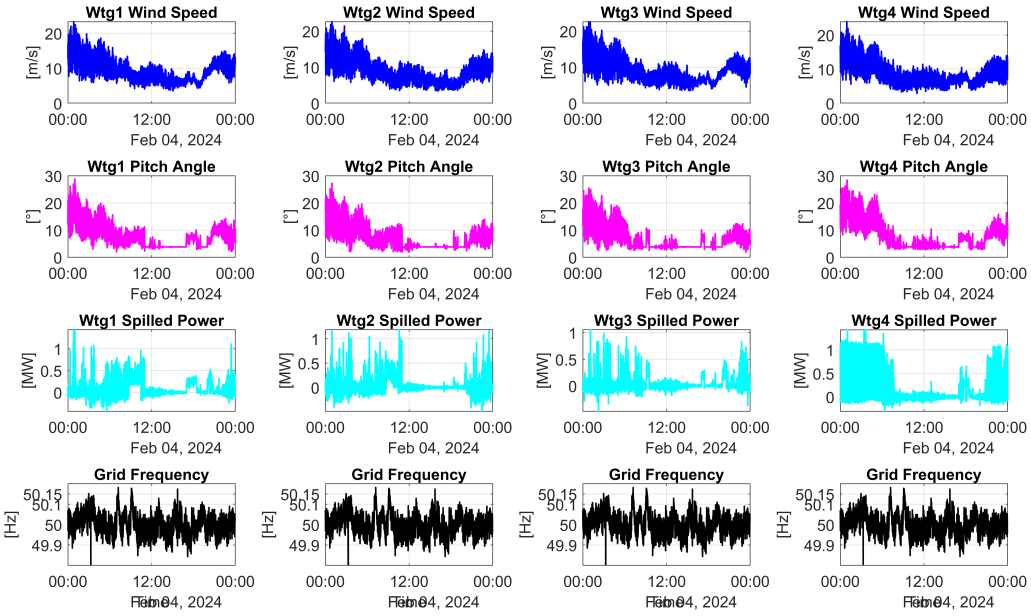

Figure A.32: Turbines 1–4: Wind Speed, Pitch Angle, Spilled Power, and Frequency.

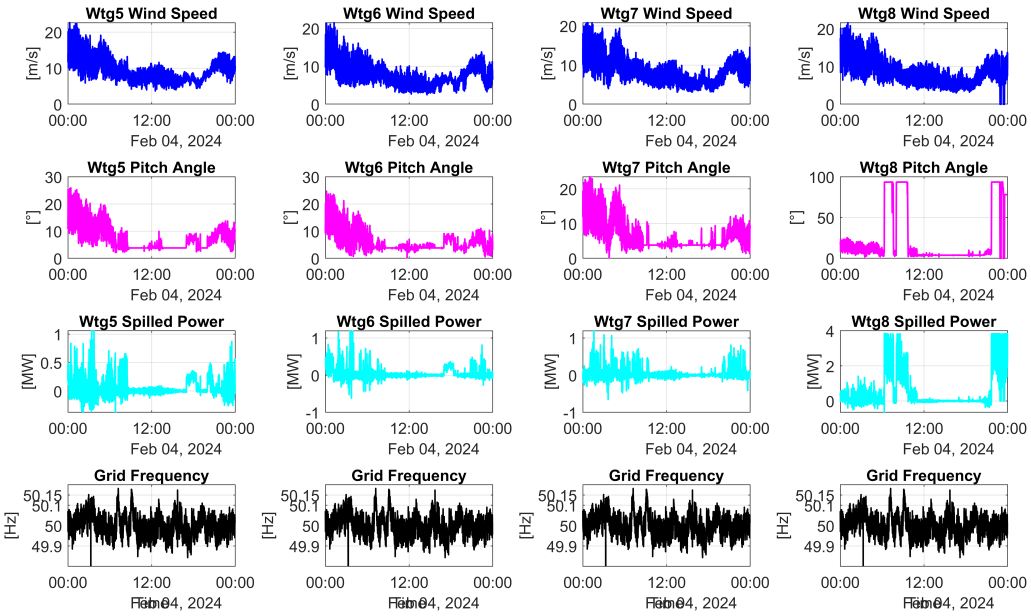

Figure A.33: Turbines 5–8: Wind Speed, Pitch Angle, Spilled Power, and Frequency.

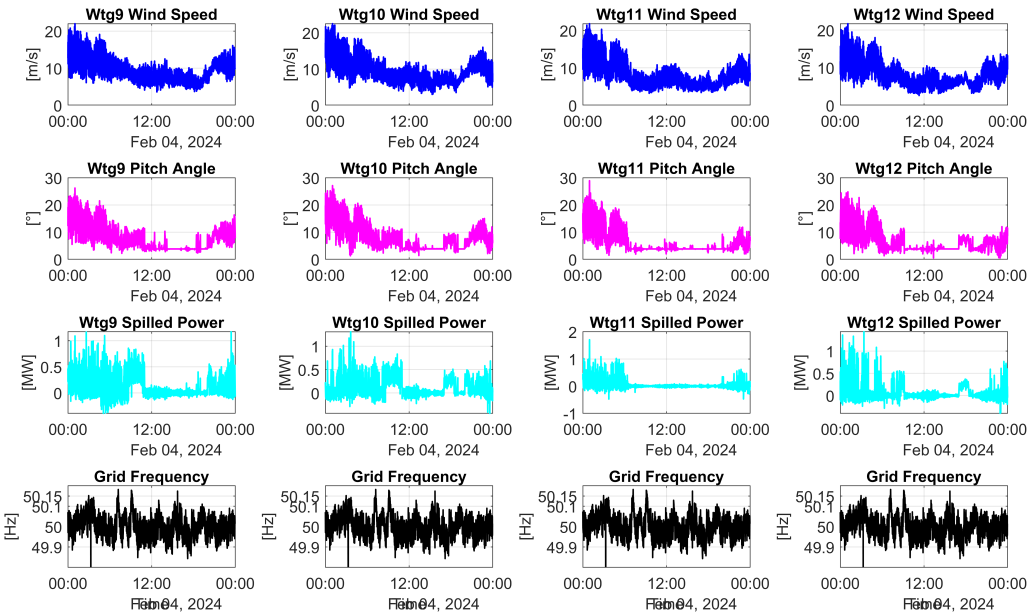

Figure A.34: Turbines 9–12: Wind Speed, Pitch Angle, Spilled Power, and Frequency.

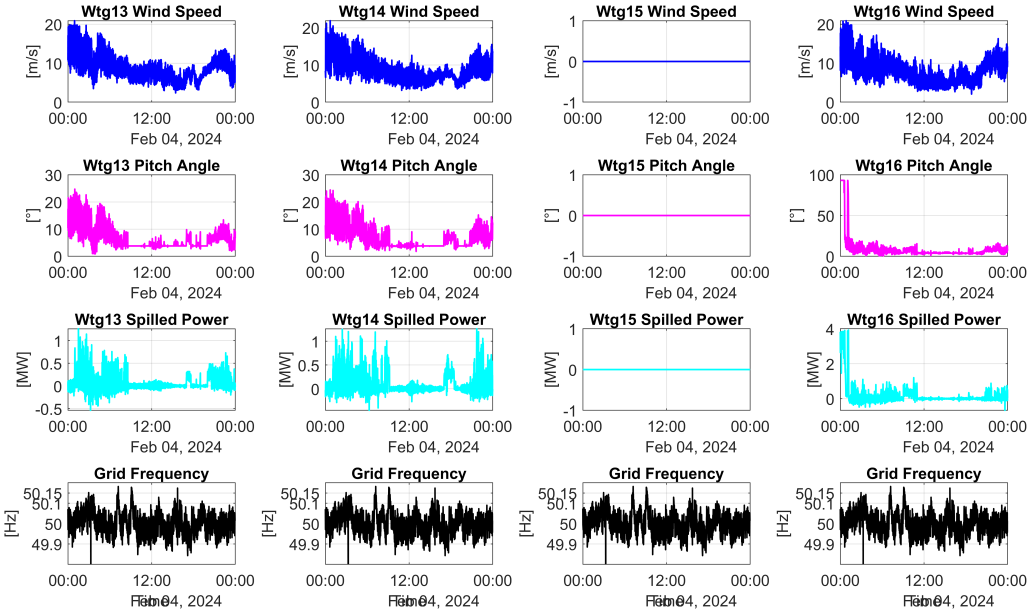

Figure A.35: Turbines 13–16: Wind Speed, Pitch Angle, Spilled Power, and Frequency.

B Matlab code for the simulation model

```
%======================== Reading measurement data ====================
delimiterIn = '\t';

% Load turbine data
%filename1 = ['B1_CL4_20_230427_08_19_16.txt'];
%measurements1 = importdata(filename1,delimiterIn);
filename2 = ['B1_CL4_20_230427_09_19_24.txt'];
measurements2 = importdata(filename2,delimiterIn);
filename3 = ['B1_CL4_20_230427_09_49_27.txt'];
measurements3 = importdata(filename3,delimiterIn);
% filename4 = ['B1_CL6_20_240604_08_35_30.txt'];
% measurements4 = importdata(filename4,delimiterIn);
% filename5 = ['B1_CL6_20_240604_08_42_29.txt'];
% measurements5 = importdata(filename5,delimiterIn);

measurements = [measurements2 ; measurements3 ];

%Include the following if a CL3 measurement file is studied:
%measurements(:,67:68) = zeros(length(measurements(:,1)),2);

input = measurements;

kanaluppdelning20220705; % The measurement data is split into power, wind
    speed, etc.

% Load weather data
file_weather = ['B1_MET_MCL1_1_230427_00_00_00.txt']; % load in weather
    data for a specific day

weather_data = importdata(file_weather, delimiterIn);

AIRTA22 = weather_data(:,4); % Column 4: Air Temperature (degrees celsius)
AIRHA22 = weather_data(:,5); % Column 5: Relative Humidity (%)
AIRPA22 = weather_data(:,6); % Column 6: Air Pressure (hPa)

% ================= De-loading Frequency Controllers ==================
f_nom = 50;        % Nominal frequency
R_FCRN = 0.06;     % Fixed droop constant for FCR-N (6%)
R_FCRD = 0.05;     % Fixed droop constant for FCR-D-UP/DOWN (5%)

% ================= DC-generator components: ====================
J          =  2600/(20^2);       % Moment of inertia [kgm^2]
b          =  0.1;               % Damping
Kp         =  3;                 % PI-reg
Ki         =  5;                 % PI-reg

% ================== NREL-reg: ============================
Sampl_t        = 0.05;       %  [s]         Sampling time of the controller
CornerFrequency = 10;        %  [rad/s]     Corner frequency of the
    generator speed low pass filter
VS_CtInSp      = 5.7;        %  [rad/s]     Cut-in generator speed
VS_RtPwr       = 25000;      %  [W]         Rated generator power
```

```
VS_RtGnSp       = 7.45;       % [rad/s]     Rated generator speed
VS_Rgn3MP       = 1.6;        % [rad]       Pitch angle to stay in Region 3
VS_Slope15      = 2600;       % [W/(rad/s)] Slope of torque curve in
    Region 1.5
VS_Rgn2Sp       = 6.2;        % [rad/s]     Lower generator speed limit for
     Region 2
VS_Rgn2K        = 35;         % [W/(rad/s)^2] Region 2 generator torque
    constant
VS_TrGnSp       = 7;          % [rad/s]     Lower generator speed limit for
     Region 2.5
VS_Slope25      = 3500;       % [W/(rad/s)] Slope of torque curve in
    Region 2.5
VS_SySp         = 6.5;        % [rad/s]     Generator speed where torque
    would be zero if in Region 2.5 (construction help point)
VS_MaxTq        = 225;        % [Nm]        Maximum generator torque
VS_MaxRat       = 500;        % [Nm/s]      Maximum generator torque rate
PC_MaxPit       = 1.5708;     % [rad]       Maximum allowed pitch angle (
    fully feathered position)
PC_MinPit       = 0.0349;     % [rad]       Minimum allowed pitch angle (
    fully fine position)
PC_KP           = 0.35;       % [rad/(rad/s)] Pitch controller
    Proportional gain
PC_KI           = 0.22;       % [rad/(rad/s)] Pitch controller Integral
    gain
PC_KK           = 0.4;        % [rad]       Pitch angle where pitch
    sensitivity is double that at pitch = 0 rad
PC_MaxRat       = 0.2;        % [rad/s]     Maximum allowed pitch rate
VS_SlPc         = 10;
StoppingPitchSpeed = 0.0349;  % Pitch rate when stopping the turbine
StartingPitchSpeed = -0.0249; % [rad/s] Pitch rate when starting the
    turbine
PC_RefSpd = 7.85;              % [rad/s] Reference generator speed
Run_Stop = 1;

%====================== Wind turbine parameters ==================
Lambda_opt=8.75;  % Optimal lambda
rho=1.225;        % [kg/m^3] Air density
d=16;             % [m] Turbine diameter
R = d/2;          % [m] Turbine radius
Cpmax=0.418;      % Maximum power coefficient of the turbine with MinPit
    at 2 deg
A=pi*R.^2;        % [m^2] Turbine area

%=== Stopping and Starting Pitch Speed Adjustment Near Feathered ===
SaS =  [PC_MinPit 1;
        PC_MaxPit*0.85 1;
        PC_MaxPit*0.98 0.15;
        PC_MaxPit*1.2 0.15;];

SaS_table = SaS(1:end,2:end);
SaS_BP = SaS(1:end,1)'; % Rad index for table

% ====================== Cp(lambda, Beta) table ====================
```

```
load('CP_data.mat');            % Data for the Cp table
breakpoints1 = data(2:end,1)';  % Row indices for table
breakpoints2 = data(1,2:end);   % Column indices for table
table_data = data(2:end,2:end); % Table output values

% ================== Max Cp for all angles over 2 degrees ==========
Cp_B0 = table_data;
Cp_B0(:,1) = 0;
Max_Cp = [breakpoints1' max(Cp_B0')'];
Vector_data = max(Cp_B0')';

%====================== Spill method count =====================
breakpoints3 = flip(table_data(32,1:7)); % Row index for blade angle table
Beta = flip(breakpoints2(1:7));       % Values for blade angle
Pspill = 0;                           % Number of watts spilled

%====================== Time and power ======================
time1=linspace(0,length(time)*Sampl_t,length(time))'; % [s] so that
    measurements
                                                      % start at t=0
Pel=(DCV.* DCC)./1000;  % [kW] Calculate electrical power (Pel) using
                        % DC-link voltage (DCV) and current (DCC)
Eleff=0.89;             % Generator efficiency
Pmec=Pel/Eleff;         % [kW] Mechanical power

%=============== Processing of frequency data ==================
load('FrekvensData.mat');           % Load frequency data
freq = Frekvens.freq_vector;        % Retrieve frequency vector
save('freq_data.mat', 'freq'); % Save the 'freq' variable to a MAT file
    named 'freq_data.mat'

%Find the position with the lowest frequency
min_freq = min(min(freq));
size_freq = size(freq);
for i = 1:size_freq(1)
    for j = 1:size_freq(2)
        if freq(i,j) == min_freq
            index=[i j];
        end
    end
end

% Create a 15 min long frequency and time vector around the lowest value
freq15 = freq(index(1),index(2)-4500:index(2)+3499);
time_freq=linspace(0,length(freq15)/10,length(freq15))'; % /10 because of
    10 Hz sampling of frequency

% ------------- Test signal for frequency from kronoberget measurements
    -------------------

% filename_kronoberget = 'SWPTC_Kronoberget_Server_FSRdata1sec_2025-01-27
    _23_59_00.csv';
%
```

```
% data = readtable(filename_kronoberget, 'PreserveVariableNames', true);
% column6 = data{:,6}; % Extract the 6th column
%
% time_vector = (0:length(column6)-1)' * Sampl_t; % Create a time vector based sampling time
%
% % Convert column6 into a timetable
% test_signal_freq = timetable(seconds(time_vector), column6);

% ======== Extract and Upsample Frequency Data for Simulink =========

filename_chalmers = 'grid_frequency_fingrid_2024-02-04.csv'; % Grid frequency for the specific day
grid_freq_data = readtable(filename_chalmers);

% Choose the time window for extraction (match time with weather data)
% This is the frequency that is fed into the model.
start_time = datetime('2024-02-04␣09:00:00'); % Set desired start time
end_time = start_time + hours(1);          % Extract exactly 1 hour

% Extract only rows within the selected time range
grid_freq_selected = grid_freq_data(grid_freq_data.Time_unix >= start_time & grid_freq_data.Time_unix <= end_time, :);

% Extract time and frequency values
original_time = seconds(grid_freq_selected.Time_unix - start_time); % Convert to seconds
freq_values = grid_freq_selected.Fgrid; % Extract frequency values

% Create new time vector matching Simulink's sampling (0.05 sec per step)
new_time_vector = (0:Sampl_t:(seconds(end_time - start_time)))';

% Interpolate frequency values to match Simulink's sampling rate
freq_upsampled = interp1(original_time, freq_values, new_time_vector, 'linear', 'extrap');

% Convert to timetable for Simulink
test_signal_freq = timetable(seconds(new_time_vector), freq_upsampled);

% ============== Weather Data ====================

% Define the start and end indices for the desired hour (01:40 - 02:40)
start_idx = 1 * 3600 + 40 * 60 + 1; % Start index at 01:40:00
end_idx = 2 * 3600 + 40 * 60;     % End index at 02:39:59

% Extract only this portion of the weather data
AIRTA22 = AIRTA22(start_idx:end_idx);
AIRHA22 = AIRHA22(start_idx:end_idx);
AIRPA22 = AIRPA22(start_idx:end_idx);

% Create a new time vector 'time2' for the extracted weather data
time2 = linspace(0, length(AIRTA22) * Sampl_t, length(AIRTA22))';

```

```
% ============== Input to Simulink ======================

% Generator speed
GenSpeed = timetable(seconds(time1),TurbSpeed2);

% Wind speed
Wind = timetable(seconds(time1), WS30);

% Tip speed
V_tip = timetable(seconds(time1), (2*pi*TurbSpeed2)/60*R);

% Mechanical power
P_mec = timetable(seconds(time1), Pmec*1000);

% Electrical power
P_el = timetable(seconds(time1), Pel*1000);

% Blade angle in degrees
Vinkel = timetable(seconds(time1), PAB1);

% Available power from the wind turbine
MPE = timetable(seconds(time1), MaxPwrEst);

% Frequency data
Frekvens = timetable(seconds(time_freq), freq15');

% FFR signal
FFR_sig = timetable(seconds(time1), Marker);

% P_Wasted
P_waste = timetable(seconds(time1), Pwaste);

% Grid frequency
Fgrid = timetable(seconds(time1), Fgrid);

% Air Temperature
Air_temp = timetable(seconds(time2), AIRTA22);

% Relative Humidity
Air_humidity = timetable(seconds(time2), AIRHA22);

% Air Pressure
Air_pressure = timetable(seconds(time2), AIRPA22);

%================= Retrieve parameters from model ===============
out = sim('Chalmers_wind_turbine_model_modified_our_own_model.slx'); % Run
     the model
open ('Chalmers_wind_turbine_model_modified_our_own_model.slx');  % Open
    the model

time_out = get(out,"tout");                % Retrieve time vector
Bladvinkel = get(out, 'Bladvinkel');       % Retrieve measured blade angle
```

```
Bladvinkel_sim = get(out, 'Bladvinkel_sim'); % Retrieve simulated blade
    angle
Varvtal = get(out, 'Vinkelhastighet');      % Retrieve measured rotational
    speed
Varvtal_sim = get(out, 'Vinkelhastighet_sim'); % Retrieve simulated
    rotational speed
Effekt = get(out, 'Effekt');                % Retrieve measured power
Effekt_sim = get(out, 'Effekt_sim');        % Retrieve simulated power
Tillganglig = get(out, "Tillganglig");      % Predicted available power
test_signal = get(out, "test_signal");
predicted_wind_speed = get(out, "predicted_wind_speed");
spilled_power_ref = get(out, "spilled_power_reference");
wind_speed_measured = get(out, "measured_wind_speed");
available_power_measured = get(out, "measured_available_power");

% Extract measured wind speed data
wind_speed_measured = wind_speed_measured.Data;

% Extract measured available power data
available_power_measured = available_power_measured.Data;

%================== Model fitting ======================
remove_t = 90*(1/Sampl_t); % Remove the first 90 seconds to avoid ramp-up
    of the model
%remove_t = 300*(1/Sampl_t); % Remove the first 300 seconds to avoid ramp-
    up of the model
time_out(1:remove_t) = [];
Varvtal(1:remove_t) = [];
Bladvinkel(1:remove_t) = [];
Effekt(1:remove_t) = [];
Varvtal_sim(1:remove_t) = [];
Bladvinkel_sim(1:remove_t) = [];
Effekt_sim(1:remove_t) = [];
Tillganglig(1:remove_t) = [];
test_signal(1:remove_t) = [];
predicted_wind_speed(1:remove_t) = [];
spilled_power_ref(1:remove_t) = []; % spilled power reference from
    controller
wind_speed_measured(1:remove_t) = [];
available_power_measured(1:remove_t) = [];
spilled_power = Tillganglig - Effekt_sim;

% ================= FCR MODE SELECTION ========================
options = {'FCR-N', 'FCR-D', 'FCRN␣+␣FCRD'}; % Updated options
[selection, ok] = listdlg('PromptString', 'Select␣FCR␣Mode:', ...
                          'SelectionMode', 'single', ...
                          'ListString', options, ...
                          'ListSize', [250, 150], ...
                          'Name', 'FCR␣Mode␣Selection');

if ok == 0
    selection = 1; % Default to FCR-N if the user cancels
end
```

```
283
284 % Update Simulink Constant Block with selected mode
285 set_param('Chalmers_wind_turbine_model_modified_our_own_model/Wind␣turbine
    ␣and␣control␣system/Spilled␣wind/Spilled␣power/FCR␣ACTIVATION/
    FCR_Mode_Selection', ...
286         'Value', num2str(selection));
287
288 % Display the selected mode in the chat
289 mode_names = ["FCR-N", "FCR-D", "FCRN + FCRD"];
290 disp(['Selected␣mode:␣', mode_names(selection)]);
```

The measurement files that have been used in the simulation:

- B1_CL4_20_230427_09_19_24.txt
- B1_CL4_20_230427_09_49_27.txt
- B1_MET_MCL1_1_230427_00_00_00.txt

C Python scripts used in the analysis

C.1 FCR-D Data Processing

```
# Import libraries
import numpy as np
import pandas as pd
import datetime
import matplotlib.pyplot as plt
import os

# Where to save the CSV files:
output_folder = r"Z:\Documents\Master␣thesis\Code␣for␣commercial␣wind␣
    turbines\commercial_wind_turbine_data"

# ---------------- READ & PROCESS CHALMERS WIND TURBINE DATA
    -----------------

# File paths to two half-day text files:
file_chalmers_1 = r'Z:\Documents\Master␣thesis\Code␣for␣commercial␣wind␣
    turbines\commercial_wind_turbine_data\B1_CL5_1_240501_00_00_00.txt' #
    From 00:00 - 12:00
file_chalmers_2 = r'Z:\Documents\Master␣thesis\Code␣for␣commercial␣wind␣
    turbines\commercial_wind_turbine_data\B1_CL5_1_240501_12_00_18.txt' #
    From 12:00 - 00:00

# Headers for the data from Chalmers wind turbine
headers_chalmers = [
    'Time', 'Torque_op', 'DCC_ref', 'Pitch_sp', 'Yaw_speed', '
        Yaw_damping_L',
    'Yaw_damping_R', 'Dig_IO', 'SysMode', 'DCC', 'DCV', 'RPM1', 'RPM2',
    'Blade1_pos', 'GTemp1', 'GTemp4', 'AirTempNA', 'HOP', 'HYMP1', 'HYMP2'
        ,
    'NAX1', 'NAX2', 'NAY1', 'NAY2', 'NAZ1', 'NAZ2', 'Yaw_pos', 'WD_NA',
    'AirHumNA', 'BRDTemp', 'PAB1', 'PAB2', 'PAB3', 'B1Pos', 'B2Pos', '
        B3Pos',
    'R24VMON', 'AirHum_hub1', 'AirTemp_hub1', 'RST2', 'B1EMR', 'B1FMR',
    'B2EMR', 'B2FMR', 'B3EMR', 'B3FMR', 'B1FM20A', 'B1FM20B', 'B1FM35A',
    'B1FM35B', 'B1FM50A', 'B1FM50B', 'B2FM20A', 'B2FM20B', 'B2FM35A',
    'TMBNS', 'TMBEW', 'WD30', 'WS30', 'WDN', 'WSN', 'PwrPercent', 'TMBTOR'
        ,
    'OptRpm', 'WindEst', 'MaxPwrEst', 'Fgrid', 'Pwaste', 'Method_f'
]

# Read both half-day files, separated with tabs
df_chalmers_1 = pd.read_csv(file_chalmers_1, delimiter='\t')
df_chalmers_2 = pd.read_csv(file_chalmers_2, delimiter='\t')

# This is required due to inconsistency in txt files
df_chalmers_1 = df_chalmers_1.iloc[:, :69] # Keep only the first 69
    columns
df_chalmers_2 = df_chalmers_2.iloc[:, :69] # Keep only the first 69
    columns

```

```
# Assign column names for both files
df_chalmers_1.columns = headers_chalmers
df_chalmers_2.columns = headers_chalmers

# Concatenate both files (vertical stack to get the full day of data)
df_chalmers = pd.concat([df_chalmers_1, df_chalmers_2], axis=0)

# Convert LabVIEW "Time" to Unix-based datetime in Swedish standard time
offset_labview_to_unix = 2082844800 # LabVIEW to Unix offset

# Time zone offset for Swedish standard time:
offset_swedish_time = 3600 # Time offset in seconds: 3600 for winter, 7200
    for summer had 7200 before here

# Convert LabVIEW time to Unix time and adjust for Swedish time zone
df_chalmers['Time_unix'] = df_chalmers['Time'] - offset_labview_to_unix +
    offset_swedish_time

# Convert Unix timestamp to a datetime format
df_chalmers['Time_unix'] = pd.to_datetime(df_chalmers['Time_unix'], unit='
    s')

# Set the DataFrame index to the corrected time
df_chalmers.set_index('Time_unix', inplace=True)

# Sort by time index in ascending order
df_chalmers.sort_index(inplace=True)

# Fill missing values with zeros
df_chalmers.fillna(0, inplace=True)

# ------------------ READ & PROCESS KRONOBERGET WIND TURBINE DATA
    ----------------------

# Read the data from the wind turbines
file_kronoberget = r'Z:\Documents\Master␣thesis\Code␣for␣commercial␣wind␣
    turbines\commercial_wind_turbine_data\
    SWPTC_Kronoberget_1s_data_Export_2024-06-29_23_59_00.csv'
df_kronoberget = pd.read_csv(file_kronoberget,
                          delimiter=';',
                          index_col=0,     # The first column is the
                              timestamp
                          parse_dates=True) # Parse as datetime (convert
                              to proper date format)

# Fill missing data with zeros
df_kronoberget.fillna(0, inplace=True)

# Rename columns for each turbine to shorter names (1 to 16)
for n in range(1, 17):
    df_kronoberget.rename(columns={
        f'Server_WTG{n:02d}_1Sec_HubDirection_Actual': f'wtg{n}_hubdir',
        f'Server_WTG{n:02d}_1Sec_kW_Actual':      f'wtg{n}_power',
```

```
        f'Server_WTG{n:02d}_1Sec_PitchAngle_Actual': f'wtg{n}_pitch',
        f'Server_WTG{n:02d}_1Sec_PossiblePower_Actual':f'wtg{n}_availpower',
        f'Server_WTG{n:02d}_1Sec_RotorRPM_Actual': f'wtg{n}_rpm',
        f'Server_WTG{n:02d}_1Sec_WindDir_Actual': f'wtg{n}_wd',
        f'Server_WTG{n:02d}_1Sec_Windspeed_Actual': f'wtg{n}_ws'
    }, inplace=True)

# Compute total output power and total available power across all turbines
df_kronoberget['wtg_power'] = df_kronoberget[[f'wtg{n}_power' for n in range(1, 17)]].sum(axis=1)   # sums the output power from all wind turbines
df_kronoberget['wtg_availpower'] = df_kronoberget[[f'wtg{n}_availpower' for n in range(1, 17)]].sum(axis=1) # sums the available power from all wind turbines

# Compute the total spilled power for all 16 turbines in kW and MW by subtracting actual output power from available power
df_kronoberget['Diff_kW'] = df_kronoberget['wtg_availpower'] - df_kronoberget['wtg_power'] # new column that shows spilled power in kW
df_kronoberget['Diff_MW'] = df_kronoberget['Diff_kW'] / 1000                               # new column that shows spilled power in MW

# Compute average wind speed across all 16 turbines
wind_speed_columns = [f'wtg{n}_ws' for n in range(1, 17)] # List of wind speed columns
df_kronoberget["Avg_WindSpeed"] = df_kronoberget[wind_speed_columns].mean(axis=1)

# Sort by time index in ascending order
df_kronoberget.sort_index(inplace=True)

# ------------ EXPORT DATAFRAMES TO CSV FOR PLOTTING IN MATLAB -------------

# --- CHALMERS WIND TURBINE ---
df_chalmers_reset = df_chalmers.reset_index()                                  # Move time index back to a column for the CSV file
df_chalmers_reset.rename(columns={'Time_unix': 'Time'}, inplace=True)   # Rename time column for clarity
df_chalmers_reset.to_csv(
    os.path.join(output_folder, "operation_chalmers_2024-05-01_processed.csv"), # Export to CSV
    date_format='%Y-%m-%d %H:%M:%S',                                           # Format datetime for readability
    index=False                                                                # Exclude default index from the file
)

# --- KRONOBERGET WIND TURBINES ---
```

```
df_kronoberget_reset = df_kronoberget.reset_index()
                                            # Move time index back to a
    column for the CSV file
df_kronoberget_reset.rename(columns={df_kronoberget_reset.columns[0]: '
    Time'}, inplace=True) # Rename first column to 'Time'
df_kronoberget_reset.to_csv(
    os.path.join(output_folder, "operation_kronoberget_2024-06-29
        _processed.csv"),         # Export to CSV
    date_format='%Y-%m-%d %H:%M:%S',
                                                                # Format
        datetime for readability
    index=False

        # Exclude default index from the file
)

# ------------- PLOTS TO VERIFY CODE ---------------

# Plot Chalmers grid frequency
plt.figure()
df_chalmers['Fgrid'].plot(title='Chalmers Fgrid')
plt.show()

# Plot Kronoberget total power (kW)
plt.figure()
df_kronoberget['wtg_power'].plot(title='Kronoberget Total Power (kW)')
plt.ylim(0, 60000) # Limit from 0 to 60,000 kW
plt.show()

print("First timestamp in Chalmers data:", df_chalmers.index[0])
print("First timestamp in Kronoberget data:", df_kronoberget.index[0])
```

C.2 Grid Frequency Fingrid

```
import pandas as pd
from datetime import timedelta

# File paths
file_3 = r'Z:\Documents\Master thesis\Code for commercial wind turbines\
    commercial_wind_turbine_data\Taajuusdata2024-02-03.csv'
file_4 = r'Z:\Documents\Master thesis\Code for commercial wind turbines\
    commercial_wind_turbine_data\Taajuusdata2024-02-04.csv'
file_5 = r'Z:\Documents\Master thesis\Code for commercial wind turbines\
    commercial_wind_turbine_data\Taajuusdata2024-02-05.csv'


# Load and combine data
df3 = pd.read_csv(file_3)
df4 = pd.read_csv(file_4)
df5 = pd.read_csv(file_5)
df = pd.concat([df3, df4, df5])

# Parse and shift time
```

```
df['Time'] = pd.to_datetime(df['Time']) # adjust column name if different
df['Time'] = df['Time'] - timedelta(hours=1)

# Extract data for 3 and 4 February
df_feb3 = df[(df['Time'] >= '2024-02-03 00:00:00') & (df['Time'] < '
    2024-02-04 00:00:00')]
df_feb4 = df[(df['Time'] >= '2024-02-04 00:00:00') & (df['Time'] < '
    2024-02-05 00:00:00')]

# Export paths
export_feb3 = r'Z:\Documents\Master thesis\Code for commercial wind
    turbines\commercial_wind_turbine_data\grid_frequency_fingrid_2024
    -02-03.csv'
export_feb4 = r'Z:\Documents\Master thesis\Code for commercial wind
    turbines\commercial_wind_turbine_data\grid_frequency_fingrid_2024
    -02-04.csv'

# Rename columns
df_feb3 = df_feb3.rename(columns={'Time': 'Time_unix', 'Value': 'Fgrid'})
df_feb4 = df_feb4.rename(columns={'Time': 'Time_unix', 'Value': 'Fgrid'})

# Save to CSV
df_feb3.to_csv(export_feb3, index=False)
df_feb4.to_csv(export_feb4, index=False)
```

C.3 Bid Data – Kronoberget 2024

```
import pandas as pd
import datetime
import os

# Define the file path to the Excel file
file_path = r"Z:\Documents\Master thesis\Code for commercial wind turbines
    \commercial_wind_turbine_data\SRKRONO_uppdaterad.xlsx"

# Read the sheet containing the bid data, skipping the first 5 rows
df = pd.read_excel(file_path, sheet_name='2024 och 2025', skiprows=5)

# Keep only the first three columns (assumed to be: Hour, Date, Bid)
df = df.iloc[:, :3]
df.columns = ['Hour', 'Date', 'Bid'] # Rename columns

# Keep only the first 8784 rows (full year of hourly data)
df = df.iloc[:8784, :]

# Convert "Date" column to datetime
df["Date"] = pd.to_datetime(df["Date"])

# Define output folder
output_folder = r"Z:\Documents\Master thesis\Code for commercial wind
    turbines\commercial_wind_turbine_data"
os.makedirs(output_folder, exist_ok=True)

```

```
# Save full year (2024) bid data
output_file_year = os.path.join(output_folder, "Bids_Kronoberget_2024.csv")
df[['Date', 'Bid']].to_csv(output_file_year, index=False)

# Extract and save data for a specific date
date_to_extract = datetime.date(2024, 6, 29) # Change to any desired day
df_day = df[df["Date"].dt.date == date_to_extract]

output_file_day = os.path.join(output_folder, f"Bids_Kronoberget_{date_to_extract}.csv")
df_day[['Date', 'Bid']].to_csv(output_file_day, index=False)

# Print confirmation
print(f"Saved Bids for 2024: {output_file_year}")
print(f"Saved Bids for {date_to_extract}: {output_file_day}")
```

C.4 SVK Demand – Kronoberget 2024

```
import pandas as pd
import datetime
import os

# Define file path
file_path = r"Z:\Documents\Master thesis\Code for commercial wind turbines\commercial_wind_turbine_data\SRKRONO_uppdaterad.xlsx"

# Read the correct sheet, skipping first 5 rows
df = pd.read_excel(file_path, sheet_name='Avropat', skiprows=5)

# Keep only necessary columns (1, 2, and 3)
df = df.iloc[:, :3]
df.columns = ['Hour', 'Date', 'FCRD_Demand'] # Rename columns

# Keep only rows up to 8784 (full year of hourly data)
df = df.iloc[:8784, :]

# Convert "Date" column to datetime format
df["Date"] = pd.to_datetime(df["Date"])

# Define output folder
output_folder = r"Z:\Documents\Master thesis\Code for commercial wind turbines\commercial_wind_turbine_data"
os.makedirs(output_folder, exist_ok=True)

# Save the full year (2024) data
output_file_year = os.path.join(output_folder, "SVK_Demand_Kronoberget_2024.csv")
df[['Date', 'FCRD_Demand']].to_csv(output_file_year, index=False)

# Extract and save data for a specific day
date_to_extract = datetime.date(2024, 6, 29) # year/month/day
df_day = df[df["Date"].dt.date == date_to_extract]
```

```
32
33 # Save only Date & FCRD_Demand for MATLAB
34 output_file_day = os.path.join(output_folder, f"SVK_Demand_Kronoberget_{
       date_to_extract}.csv")
35 df_day[['Date', 'FCRD_Demand']].to_csv(output_file_day, index=False)
36
37 # Print confirmation
38 print(f"Saved 2024 Data: {output_file_year}")
39 print(f"Saved FCR-D Demand for {date_to_extract}: {output_file_day}")
```

DEPARTMENT OF ELECTRICAL ENGINEERING
CHALMERS UNIVERSITY OF TECHNOLOGY
Gothenburg, Sweden
www.chalmers.se

CHALMERS
UNIVERSITY OF TECHNOLOGY